Fluctuation exchange calculations of Hubbard model: from a two-dimension lattice to a ladder

Yan Wang
Department of Physics and Astronomy, University of Tennessee, Knoxville, Tennessee 37996, USA
(Dated: June 26, 2017)

CONTENTS

I. THE PROJECT

We want to apply the conserving fluctuation exchange (FLEX) approximation[1–6] to study the self-consistent spin and charge susceptibility and the superconductivity in the two-dimensional one-orbital Hubbard model

$$H = H_0 + H_{\rm int}, \tag{1}$$

$$H_0 = -\sum_{i,j,\sigma} t_{ij} c^\dagger_{i\sigma} c_{j\sigma} - \mu \sum_{i,\sigma} \hat{n}_{i\sigma}, \tag{2}$$

$$H_{\rm int} = U \sum_i \hat{n}_{i\uparrow}\hat{n}_{i\downarrow}. \tag{3}$$

For a lattice with a periodic boundary condition, the lattice site sum in H_0 can be Fourier transformed to momentum space: $H_0 = \sum_{\mathbf{k},\sigma} \varepsilon_{\mathbf{k}} c^\dagger_{\mathbf{k}\sigma} c_{\mathbf{k}\sigma}$, where the band dispersion is

$$\varepsilon_{\mathbf{k}} = -2t(\cos k_x + \cos k_y) - 4t' \cos k_x \cos k_y - \mu, \tag{4}$$

where the nearest-neighbor hopping $t = t_{\langle ij\rangle}$ and next-nearest-neighbor $t' = t_{\langle\langle ij\rangle\rangle}$. Here, we set the lattice constant $a = 1$ for a square lattice. Because the FLEX interaction vertices have very simple form in momentum space, the equations for self-energies within FLEX are also written in momentum space. This (the Fourier transform from real to momentum space) implies a periodic boundary condition. To compare with DMRG calculations with an open boundary condition, it might be useful to consider a real space formulation for FLEX.

Next, by binding every two neighboring atomic sites into one site in the y-direction ("dimerization") and reducing the inter-site hopping in y-direction to zero, we obtain ladders running along x-direction, which is described by a one-dimensional two-orbital Hubbard model. A two-orbital FLEX calculation was done for layered organic superconductors by J. Schmalian.[7] The full fledged multiorbital extension of FLEX can be found in Ref. 8 and 9.

We will first introduce the FLEX equations for self-energies for the two-dimensional one-orbital Hubbard model and discuss the numerical method to solve them. Then, we will discuss the two-orbital extension.

II. FLEX FOR TWO-DIMENSIONAL ONE-ORBITAL HUBBARD MODEL

To treat the superconductivity, we use the Nambu 2-spinor notation. The dressed Green's function and self-energy are both matrices in particle-hole space:

$$\hat{G}(k) = \begin{pmatrix} G(k) & F(k) \\ F^\dagger(k) & -G(-k) \end{pmatrix}, \quad \hat{\Sigma}(k) = \begin{pmatrix} \Sigma(k) & \Phi(k) \\ \Phi^*(k) & -\Sigma(-k) \end{pmatrix}, \tag{5}$$

where $k = (\mathbf{k}, i\omega_n)$ and $\omega_n = (2n+1)\pi T$ is the fermionic Matsubara frequency. The matrix element $G(k)$ ($F(k)$) of the Green's function is called normal (anomalous) Green's function. They are defined as

$$G(\mathbf{k}, i\omega_n) = -\int_0^\beta d\tau e^{i\omega_n \tau} \langle T_\tau c_{\mathbf{k}\sigma}(\tau) c^\dagger_{\mathbf{k}\sigma} \rangle \tag{6}$$

$$F(\mathbf{k}, i\omega_n) = \int_0^\beta d\tau e^{i\omega_n \tau} \langle T_\tau c_{\mathbf{k}\uparrow}(\tau) c_{-\mathbf{k}\downarrow} \rangle \tag{7}$$

$$F^\dagger(\mathbf{k}, i\omega_n) = \int_0^\beta d\tau e^{i\omega_n \tau} \langle T_\tau c^\dagger_{-\mathbf{k}\downarrow}(\tau) c^\dagger_{\mathbf{k}\uparrow} \rangle, \tag{8}$$

where $\beta = 1/T$ and $c_{\mathbf{k}\sigma}(\tau) \equiv e^{\mathcal{H}\tau} c_{\mathbf{k}\sigma} e^{-\mathcal{H}\tau}$ and $c^\dagger_{\mathbf{k}\sigma}(\tau) \equiv e^{\mathcal{H}\tau} c^\dagger_{\mathbf{k}\sigma} e^{-\mathcal{H}\tau}$ with $\mathcal{H} \equiv H - \mu N$. Note that $[c_{\mathbf{k}\sigma}(\tau)]^\dagger = c^\dagger_{\mathbf{k}\sigma}(-\tau)$ by definition.

The bare Green's function $G_0(k) = \frac{1}{i\omega_n - \varepsilon_{\mathbf{k}}}$. By Dyson-Gor'kov equation, the dressed Green's function $\hat{G} = (\hat{G}_0^{-1} - \hat{\Sigma})^{-1}$. If $\Phi^*(k) = \Phi(k)$, we can simplify the matrix inversion by writing the self-energy in the form

$$\hat{\Sigma}(k) = i\omega_n [1 - Z(k)] \hat{\tau}_0 + X(k) \hat{\tau}_3 + \Phi(k) \hat{\tau}_1 \tag{9}$$

where

$$i\omega_n [1 - Z(k)] = [\Sigma(k) - \Sigma(-k)]/2, \tag{10}$$

$$X(k) = [\Sigma(k) + \Sigma(-k)]/2. \tag{11}$$

If there is an inversion symmetry ($\mathbf{k} \Leftrightarrow -\mathbf{k}$), the above becomes

$$i\omega_n [1 - Z(\mathbf{k}, i\omega_n)] = [\Sigma(\mathbf{k}, i\omega_n) - \Sigma(\mathbf{k}, -i\omega_n)]/2 = [\Sigma(\mathbf{k}, i\omega_n) - \Sigma^*(\mathbf{k}, i\omega_n)]/2, \tag{12}$$

$$X(\mathbf{k}, i\omega_n) = [\Sigma(\mathbf{k}, i\omega_n) + \Sigma(\mathbf{k}, -i\omega_n)]/2 = [\Sigma(\mathbf{k}, i\omega_n) + \Sigma^*(\mathbf{k}, i\omega_n)]/2. \tag{13}$$

In the last step we have used $\Sigma(\mathbf{k}, -i\omega_n) = \Sigma^*(\mathbf{k}, i\omega_n)$ that follows from the frequency Fourier transform and $G(\mathbf{k}, \tau)$ and $F(\mathbf{k}, \tau)$ being real. Therefore, $Z(k)$ and $X(k)$ are both even with respect to the frequency and real valued. These properties are used to speed up calculations. Last, after the matrix inversion, we have the Green's function

$$G(k) = \frac{i\omega_n Z(k) + [\varepsilon_{\mathbf{k}} + X(k)]}{[i\omega_n Z(k)]^2 - [\varepsilon_{\mathbf{k}} + X(k)]^2 - [\Phi(k)]^2}, \tag{14}$$

$$F(k) = \frac{\Phi(k)}{[i\omega_n Z(k)]^2 - [\varepsilon_{\mathbf{k}} + X(k)]^2 - [\Phi(k)]^2}. \tag{15}$$

The above is the basic formalism of the Green's functions and self-energies. Next, we use FLEX based on the perturbation theory to find the self-energies. The irreducible spin and charge susceptibilities are

$$\chi_0^s(q) = -\frac{T}{N} \sum_k [G(k+q)G(k) + F(k+q)F(k)], \tag{16}$$

$$\chi_0^c(q) = -\frac{T}{N} \sum_k [G(k+q)G(k) - F(k+q)F(k)], \tag{17}$$

where N is the total number of lattice sites and $k = (\mathbf{k}, i\omega_n)$ and $q = (\mathbf{q}, i\nu_m)$, where $\omega_n = (2n+1)\pi T$ is the fermionic Matsubara frequency and $\nu_m = 2m\pi T$ is the bosonic Matsubara frequency. The spin and charge fluctuation

interactions are given by

$$V_s(q) = \frac{3}{2}U^2\frac{\chi_0^s(q)}{1-U\chi_0^s(q)} - \frac{1}{2}U^2\chi_0^s(q), \tag{18}$$

$$V_c(q) = \frac{1}{2}U^2\frac{\chi_0^c(q)}{1+U\chi_0^c(q)} - \frac{1}{2}U^2\chi_0^c(q), \tag{19}$$

where the second terms are to remove the double counting in the second order, and the normal and anomalous effective interactions are

$$V_n(q) = V_s(q) + V_c(q), \tag{20}$$

$$V_a(q) = V_s(q) - V_c(q). \tag{21}$$

Finally, the self-energies are given by

$$\Sigma(k) = \frac{T}{N}\sum_{k'} V_n(k-k')G(k') + \Sigma_{\rm HF}, \tag{22}$$

$$\Phi(k) = \frac{T}{N}\sum_{k'} V_a(k-k')F(k') + \Phi_{\rm HF}, \tag{23}$$

where the Hartree-Fock self-energies are

$$\Sigma_{\rm HF} = \frac{T}{N}\sum_{k} UG(k)e^{i\omega_n 0^+} = \frac{T}{N}\sum_{k} UG(k) + \frac{U}{2}, \tag{24}$$

$$\Phi_{\rm HF} = \frac{T}{N}\sum_{k} UF(k). \tag{25}$$

For one-orbital case, $\Sigma_{\rm HF}$ can be absorbed into the chemical potential μ, but not for multi-orbital case. In the code we set $\Sigma_{\rm HF} = 0$. The chemical potential μ is chosen so that the filling (particle number density) n is a fixed value. Formally, we have $n = \frac{2}{N}\sum_{\mathbf{k}} G(\mathbf{k}, \tau = 0^-) = \frac{2T}{N}\sum_{\mathbf{k},n} G(\mathbf{k}, i\omega_n)e^{-i\omega_n 0^-} = \frac{2T}{N}\sum_{\mathbf{k},n} G(\mathbf{k}, i\omega_n)e^{i\omega_n 0^+} = 1 + \frac{2T}{N}\sum_{\mathbf{k},n} G(\mathbf{k}, i\omega_n)$. The last expression still has slow convergence with respect to the cut-off $|\omega_n| < \omega_c$ (meaning very large cut-off ω_c is needed to converge the filling). Instead, we use the following to calculate the filling

$$\begin{aligned} n &= 1 + \frac{2T}{N}\sum_{\mathbf{k},n} G(\mathbf{k}, i\omega_n) = 1 + \frac{2T}{N}\sum_{\mathbf{k},n}[G(\mathbf{k}, i\omega_n) - G_0(\mathbf{k}, i\omega_n)] + \frac{2T}{N}\sum_{\mathbf{k},n} G_0(\mathbf{k}, i\omega_n) \\ &= 1 + \frac{2T}{N}\sum_{\mathbf{k},|\omega_n|<\omega_c}[G(\mathbf{k}, i\omega_n) - G_0(\mathbf{k}, i\omega_n)] + \frac{2}{N}\sum_{\mathbf{k}} n_{\rm F}(\varepsilon_{\mathbf{k}}) - 1 \\ &= \frac{2T}{N}\sum_{\mathbf{k},|\omega_n|<\omega_c}[G(\mathbf{k}, i\omega_n) - G_0(\mathbf{k}, i\omega_n)] + \frac{2}{N}\sum_{\mathbf{k}} n_{\rm F}(\varepsilon_{\mathbf{k}}). \end{aligned} \tag{26}$$

Eqs. (12)–(25) together with the filling Eq. (26) constitute the set of FLEX equations we want to solve self-consistently by iterations. Since the momentum and frequency sum are in a convolution or cross-correlation form, using fast Fourier transform (FFT) can greatly speed up the computation than brutal force summation. The D-dimension spatial FFT is straightforward but the frequency FFT needs extreme care on the high frequency tail of the Green's function and accurately evaluating the Fourier integral over imaginary time τ when one Fourier transforms backward to frequency space, latter of which is an often overlooked problem (so called *anti-aliasing*, see Appendix A). There were a few endeavors in the literature on this $(D+1)$-dimension FFT method of solving the FLEX equations.[3,10–12] The reason to invest in a faster algorithm is that larger lattice size and higher energy cut-off can be afforded and lower temperature and larger coupling can be accessed. These are essential for investigating the subtle physics, for example, non-Fermi liquid behavior.[3]

A. Compare old and new code

As said above, I extend our FLEX code from using D-dimension FFT to $(D+1)$-dimension FFT by including frequency FFT. This kills two birds with one stone: much faster code and high frequency tail of Green's function is

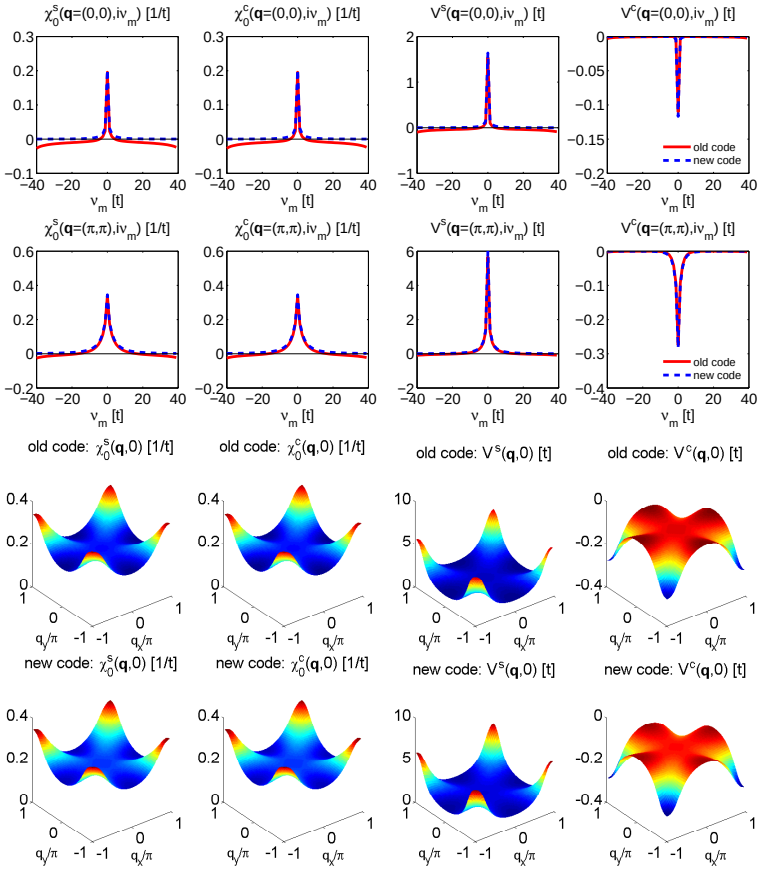

FIG. 1. Irreducible spin/charge susceptibilities $\chi_0^{s/c}(\mathbf{q}, i\nu_m)$ and spin/charge fluctuation interactions (RPA enhanced, but not so significant for this U and this temperature T).

easier to deal with. The high frequency problem was explained in detail in the section IIIB in Bickers and White.[4] My $(D+1)$-dimension FFT code follows the procedure from appendix B in Ref. 13, except that I use a higher order aliasing correction to FFT that has higher precision (see Appendix A).

I check the new implementation with $(D+1)$-dimension FFT by comparing new and old code for the same set of parameters in one-orbital Hubbard model: $U = 2t$, $T = 0.2t$, $t' = -0.15t$, k-grid 64×64 (lattice grid is the same), convergence threshold on the difference of the self-energies in successive iterations is $10^{-10}t$, and the frequency cut-off $\omega_c = 40t$. This comparison is done in the normal state since the old code is slow for $T < T_c$ and thus not viable in superconducting state calculation (within a few minutes). The results are shown in Fig. 1 and Fig. 2. First, it shows that the new code with $(D+1)$-dimension FFT is consistent with the old code with D-dimension FFT—new code is working. Second, the problem of having unphysical negative susceptibility $\chi_0^{s/c}(\mathbf{q} = (0,0), i\nu_m)$ at high frequency is now fixed in the new code.

B. FLEX calculation—preliminary results

Here, I try to reproduce Monthoux and Scalapino's result[6] using their parameters. I ran into the old problem of convergence at $U = 4t$ and $T < T_c$ and often hit the Stoner instability during the iterations. According to a few numerical tricks dealing with this problem mentioned in Ref. 2, I adiabatically increase U, and use the self-energies computed at lower U as the initial condition for next U. Currently, I managed converging at $U = 2.94t$ and $T = 0.015t$, with a frequency cut-off $\omega_c = 8t$. I haven't been able to reach $U = 4t$ yet. The results for $U = 2.94t$ are plotted in Fig. 3. A sizable gap $\Delta \sim 0.06t$ is seen, which has a $d_{x^2-y^2}$-wave momentum dependence. The static susceptibility is directly accessible from $\chi_0^s(\mathbf{q}, i\nu_m = 0)$, which is peaked near (π, π) with a value very close to $1/U$, indicating a strong RPA enhancement $1/[1 - U\chi_0^s(\mathbf{q}, i\nu_m)]$. The difference between spin and charge susceptibility manifests the nozero gap and anomalous Green's function $F(\mathbf{k}, i\omega_n)$ (see Eqs. (16) and (17)). In the normal state,

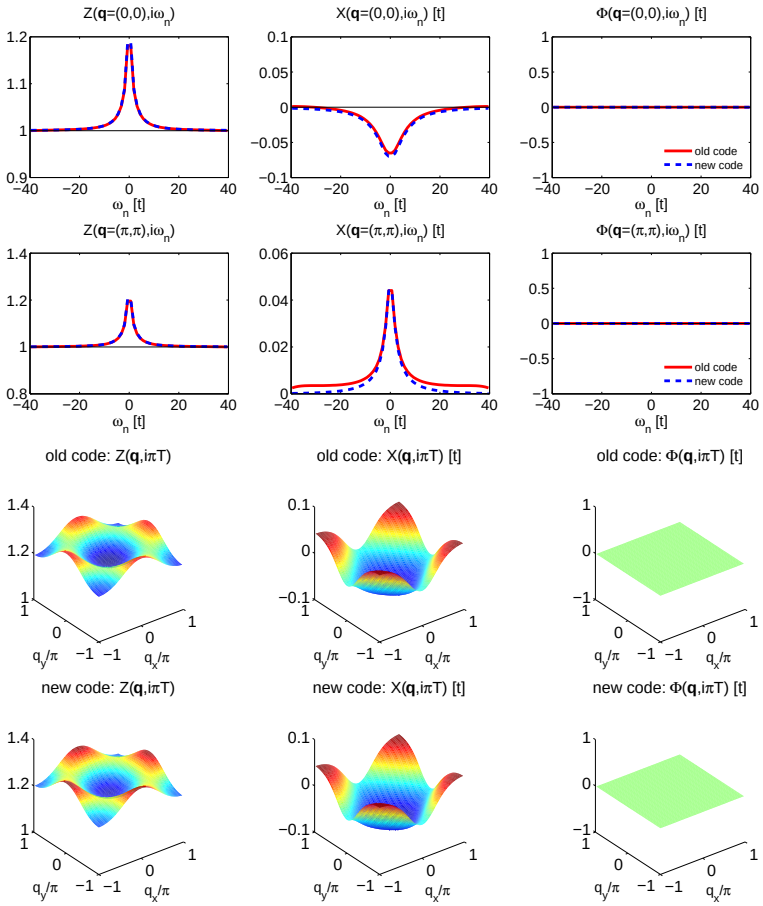

FIG. 2. Self-energies (Z, X, Φ) in the normal state ($T > T_c$).

$\chi_0^s = \chi_0^c$. Although along the nodal lines ($x = \pm y$) the gap and $F(\mathbf{k}, i\omega_n)$ are zero, $\chi_0^s(\mathbf{q}, i\nu_m) \neq \chi_0^c(\mathbf{q}, i\nu_m)$ because it involves a sum over the fermion momentum as in Eqs. (16) and (17). Nevertheless, if the gap function and anomalous self-energy has the exact $d_{x^2-y^2}$-wave symmetry, it is easy to see that $\chi_0^s(\mathbf{q} = X, 0) = \chi_0^c(\mathbf{q} = X, 0)$ and $\chi_0^s(\mathbf{q} = \Gamma, 0) - \chi_0^c(\mathbf{q} = \Gamma, 0) = -(\chi_0^s(\mathbf{q} = M, 0) - \chi_0^c(\mathbf{q} = M, 0)) < 0$. This is indeed consistent with our result in Fig. 3(b). Last we obtain the real axis spin susceptibility using Padé approximant.[14] For the $U = 2.94t$, $\mathrm{Im}\,\chi_0^s(\mathbf{q} = (\pi, \pi), \omega)$ has a visible peak, but not as strong as that in Ref. 6 for $U = 4t$.

C. FLEX calculation results for one-band Hubbard model

After overcoming the convergence problem at $U = 4t$ when solving the coupled FELX equations for the self-energies by iterations, I have finally reproduced all the results in Monthoux and Scalapino's work.[6] The results will be discussed below and I will focus on spin susceptibility measured by neutron scattering and compare the FLEX-RPA spin susceptibility with that calculated by simple RPA in Bulut and Scalapino's work.[15–17] The convergence problem is solved by using the following three tricks: (1) mix the Green's functions instead of self-energies; (2) use Anderson Acceleration in the mixing step;[18,19] (3) cut off the susceptibility $\chi_0^s(q)$ that passes the Stoner instability $U\chi_0^s(q) \geq 1$ at $U\chi_{0,\max}^s = 0.9999$ in first few iterations (but not in the final stable iterations). Here, "mixing" refers to the way of constructing new self-energies (or Green's functions) for the next iteration from old self-energies (or Green's functions) from the last iteration, which usually improves the convergence rate and radius comparing with the most common method—fixed-point iteration (Picard iteration). With the above three tricks, I can start the calculation directly at $U = 4t$ with zero self-energies and a constant s-wave gap function as initial conditions, the calculation can converge within 200 iterations and $d_{x^2-y^2}$-wave gap is obtained in the final iteration for the one-band Hubbard model with the chosen parameters. The convergence threshold is that the maximal difference of the self-energies (the norm $||\delta\Sigma(k)||_{+\infty}$) in the successive iterations is less by $10^{-7}t$. Near T_c ($T \sim T_c \pm 0.05T_c$), however, the convergence becomes

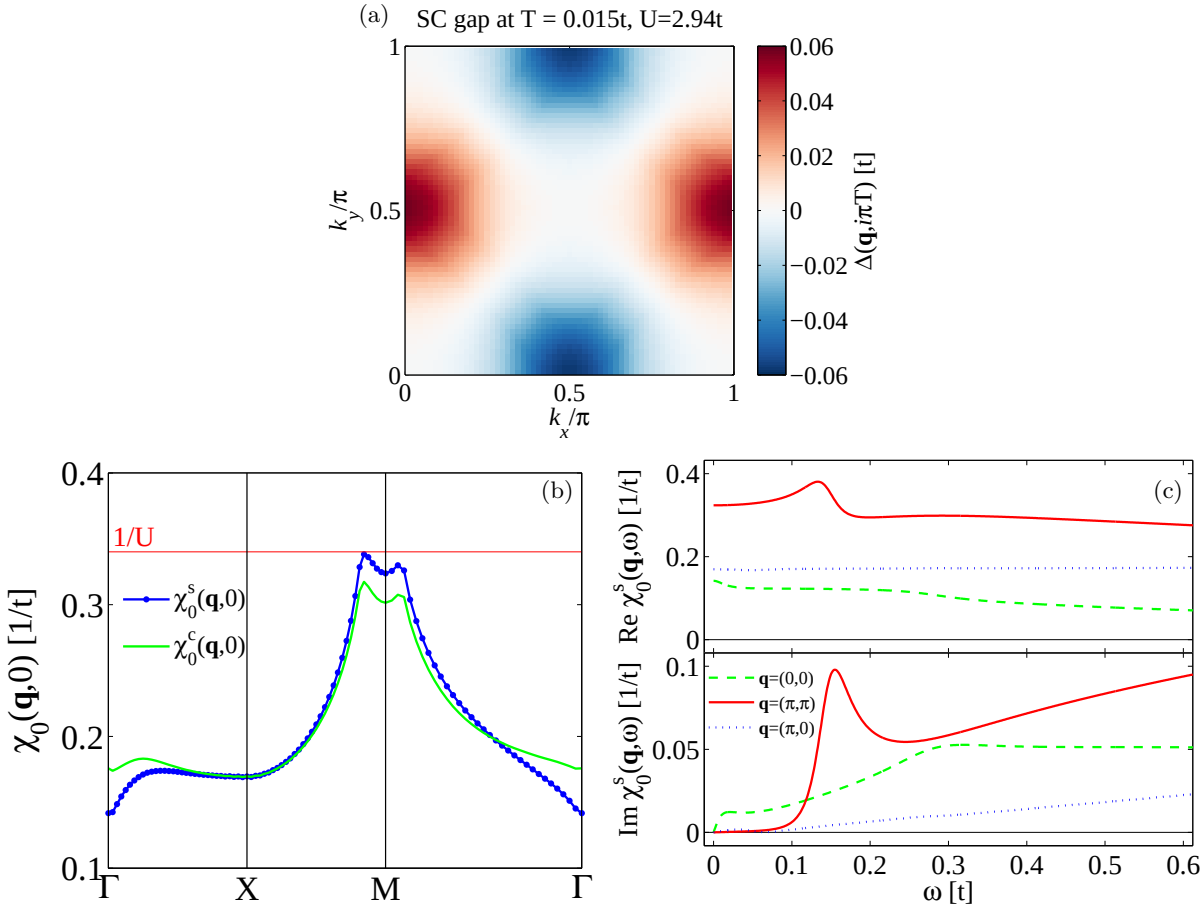

FIG. 3. (a) gap function $\Delta(\mathbf{k}, i\pi T) = \Phi(\mathbf{k}, i\pi T)/Z(\mathbf{k}, i\pi T)$. (b) static spin/charge susceptibilities $\chi_0^{s/c}(\mathbf{q}, i\nu_m = 0)$ obtained from imaginary axis result directly. (c) real and imaginary parts of the irreducible spin susceptibility $\chi_0^s(\mathbf{q}, \omega)$ from analytic continuation of $\chi_0^s(\mathbf{q}, i\nu_m)$ to real axis by Padé approximant. The values of real part at $\omega = 0$ are consistent with the values on the imaginary axis at $i\nu_m = 0$.

very difficult around $||\delta\Sigma(k)||_{+\infty} \sim 10^{-4}t$. Thus, the threshold is decreased to $10^{-5}t$ so the convergence can be reached within 1000 iterations near T_c. For $t' = -0.15t$ in the dispersion $\varepsilon_{\mathbf{k}} = -2t(\cos k_x + \cos k_y) - 4t' \cos k_x \cos k_y - \mu$, $U = 4t$, filling $n = 0.875$, a frequency energy cut-off $\omega_c = 5W$, band width $W = 8t$, and the 128×128 k-grid, I find $T_c = 0.0215t$. We will use t as units of energy below and T_c, as an important energy scale, will also be used as a measure in the spectrum of neutron scattering.

Gap Function. First, we show the gap vs temperature in Fig. 4. The gap on imaginary frequency axis is

$$\Delta(\mathbf{k}, i\omega_n) = \frac{\Phi(\mathbf{k}, i\omega_n)}{Z(\mathbf{k}, i\omega_n)}, \tag{27}$$

and on the real axis it is obtained by analytical continuation using Padé approximants[14]

$$\Delta(\mathbf{k}, \omega) = \Delta(\mathbf{k}, i\omega_n \to \omega + i\eta) = \frac{\Phi(\mathbf{k}, i\omega_n \to \omega + i\eta)}{Z(\mathbf{k}, i\omega_n \to \omega + i\eta)}. \tag{28}$$

Specifically, we use all $\omega_n > 0$ data to construct the Padé approximant and evaluate the approximant exactly on the real ω axis. An explicit value of η is not needed. The gap function is almost the same either from analytical continuation of $\Delta(\mathbf{k}, i\omega_n)$ or analytical continuation of $\Phi(\mathbf{k}, i\omega_n)$ and $Z(\mathbf{k}, i\omega_n)$ individually and then finding the ratio. On the real ω axis, the gap at the gap edge is defined as

$$\Delta(\mathbf{k}, \omega_0) = \mathrm{Re}\,\Delta\left(\mathbf{k}, \omega_0 = |\,\mathrm{Re}\,\Delta(\mathbf{k}, \omega_0)|\right). \tag{29}$$

This contortion in the definition is needed because in experiment, for example, for an s-wave gap, the density of states $N(\omega) = \mathrm{Re}\,\frac{\omega}{\sqrt{\omega^2 - \Delta^2(\omega)}}$ has a peak at the gap edge. Fig. 4(b) shows the pictorial way solving Eq. (29). The gap at the

gap edge is usually larger than the gap for the lowest Matsubara frequency, as shown in Fig. 4(a), (c), and (d). The maximal gap is located at X or Y point, not right on the Fermi surface, as shown in Fig. 4(c) and (d), so we show gap at X point in Fig. 4(a). The ratio $2\Delta(T=0)/T_c \sim 10$ is much larger than a BCS value, indicating a strong coupling feature. Furthermore, the $\mathrm{Re}\,\Delta(\mathbf{k},\omega)$ is still positive in high frequencies, which is opposite to the electron-phonon coupling case. The gap function has a $d_{x^2-y^2}$-wave symmetry [Fig. 4(c) and (d)].

Static spin susceptibility. Next, we show the results for the static irreducible spin susceptibility $\chi_0^s(\mathbf{q}, i\nu_m = 0)$ (the electron-hole bubble diagram) form FLEX calculation in Fig. 5. We notice the incommensurate peaks around $M = (\pi, \pi)$ point in the the static irreducible spin susceptibility $\chi_0^s(\mathbf{q}, i\nu_m = 0)$. This plot is very similar to the Fig. 3 in Ref. 6 as well as Fig. 2 in Ref. 15 where χ_0 is calculated with a nonselfconsistent BCS gap function (sometimes denoted χ_0^{BCS}) in the superconducting state. Comparing with Fig. 2 in Ref. 15, the selfconsistency within FLEX more strictly locks the value of χ_0 at $M = (\pi, \pi)$ point when temperature is decreased. We skip the analysis of $\mathrm{Im}\,\chi_0^s(\mathbf{q},\omega)/\omega|_{\omega\to 0}$, which is related to nuclear spin relaxation in NMR experiment.[15,20]

Dynamic spin susceptibility. To study the resonance peak in the magnetic susceptibility and compare with the neutron scattering experiment, we use the random-phase-approximation (RPA) form for the full spin susceptibility

$$\chi^s(\mathbf{q}, i\nu_m) = \frac{\chi_0^s(\mathbf{q}, i\nu_m)}{1 - U\chi_0^s(\mathbf{q}, i\nu_m)}, \tag{30}$$

where $\chi_0^s(\mathbf{q}, i\nu_m)$ is calculated from FLEX, so we call it FLEX-RPA susceptibility. The same RPA form is also used in the effective fluctuation interactions in the FLEX equations. This RPA susceptibility is *not* conserving[6] and thus leads to the violation of a few conservation laws in the FLEX results.[21,22] If χ_0^{BCS} is used on the right hand side in the above equation, we call it simple RPA susceptibility.

The plot of irreducible spin susceptibility $\mathrm{Im}\,\chi_0^s(\mathbf{q} = (\pi, \pi), \omega)$ in Fig. 6(a) is similar to Fig. 4(b) in Ref. 6; irreducible spin susceptibility $\mathrm{Im}\,\chi_0^s(\mathbf{q} = (\pi, \pi), \omega = 0.60T_c)$ and FLEX-RPA spin susceptibility $\mathrm{Im}\,\chi^s(\mathbf{q} = (\pi, \pi), \omega = 0.60T_c)$ in Fig. 8(a) is similar to Fig. 1 and Fig. 2 from simple RPA calculation in Ref. 17. From Fig. 8(a), we confirm the so called 45° rotation of the resonance peaks in $\mathrm{Im}\,\chi_0^s$ from $Q_\delta = 2\pi(0.5, 0.5 \pm \delta), 2\pi(0.5 \pm \delta, 0.5)$ to Q_γ along the diagonal line $q_x = q_y$; however, the resonance peaks in the enhanced FLEX-RPA susceptibility remain at Q_δ.

Although the irreducible and RPA spin susceptibility share similar behavior (enhanced resonance peak) when T decreases below T_c and $d_{x^2-y^2}$-wave gap opens, they follow quite different dispersion in the spectrum. As seen in Fig. 6(a) and (b), at M point, the peak of RPA spin susceptibility is much sharper than the irreducible one, and the resonance frequency $E_r^{\mathrm{RPA}} \lesssim 0.5E_r^0$, while $E_r^0 \approx 2\Delta(T) \sim 10T_c$. In Fig. 6(c) and (d), at the incommensurate vector $Q_\delta = 2\pi(0.5, 0.5 \pm \delta)$, the irreducible susceptibility is almost gapped out at low temperatures but the RPA one is greatly enhanced. The respective dispersion of the irreducible and RPA spin susceptibility can be seen in Fig. 7(a) and (b). While the irreducible susceptibility shows a "hourglass" dispersion [black line in Fig. 7(a)] with a commensurate resonance peak at M point and $\omega = E_r^0 \sim 0.2t$, the RPA susceptibility has a W-shaped dispersion with a commensurate resonance peak at M point and $\omega = E_r^{\mathrm{RPA}} \sim 0.1t$. It is easy to explain the difference between $\mathrm{Im}\,\chi_0^s$ and $\mathrm{Im}\,\chi^s$ since they are related as follows

$$\mathrm{Im}\,\chi^s(\mathbf{q},\omega) = \frac{\mathrm{Im}\,\chi_0^s(\mathbf{q},\omega)}{[1 - U\,\mathrm{Re}\,\chi_0^s(\mathbf{q},\omega)]^2 + [U\,\mathrm{Im}\,\chi_0^s(\mathbf{q},\omega)]^2}. \tag{31}$$

When $|1 - U\,\mathrm{Re}\,\chi_0^s(\mathbf{q},\omega)| \lesssim |U\,\mathrm{Im}\,\chi_0^s(\mathbf{q},\omega)|$, there is a large enhancement of susceptibility by a factor $[1 - U\,\mathrm{Re}\,\chi_0^s(\mathbf{q},\omega)]^{-2}$. The parabolic dispersion in Fig. 7(b) clearly matches the bottom portion of the black contour line in Fig. 7(c) for $\mathrm{Re}\,\chi_0^s(\mathbf{q},\omega) = 1/U$.

Although our calculation results are consistent with those in literature using simple RPA, the comparison of RPA spin susceptibility with neutron experiments on $\mathrm{Im}\,\chi^s(\mathbf{q},\omega)$ is not so straightforward—too many experiments and some are controversial in literature (see Ref. 23 and references therein). The model dispersion and the filling we use are for $La_{2-x}Sr_xCuO_4$ with $x \approx 0.14$. $\mathrm{Im}\,\chi_0^s(\mathbf{q},\omega)$ [Fig. 7(a)] and $\mathrm{Im}\,\chi^s(\mathbf{q},\omega)$ [Fig. 7(b)] both have some resemblance with Fig. 6.3 in Ref. 23 for a "hourglass" dispersion. Since we should compare RPA $\mathrm{Im}\,\chi^s(\mathbf{q},\omega)$ with the experiments, the resonance energy E_r at which the peaks become commensurate at M point is too low comparing with experiment: in experiment $E_r \sim 10T_c$ and in our calculation $E_r^{\mathrm{RPA}} \sim 5T_c$. If we neglect the difference in the energy scale (i.e., difference of the velocity of the spin-wave), the calculated RPA susceptibility in Fig. 8(a)–(d) [bottom right in each panel $\mathrm{Im}\,\chi^s$ for $T/T_c = 0.33$] are consistent with the experiment result in Fig. 1 in Ref. 24.

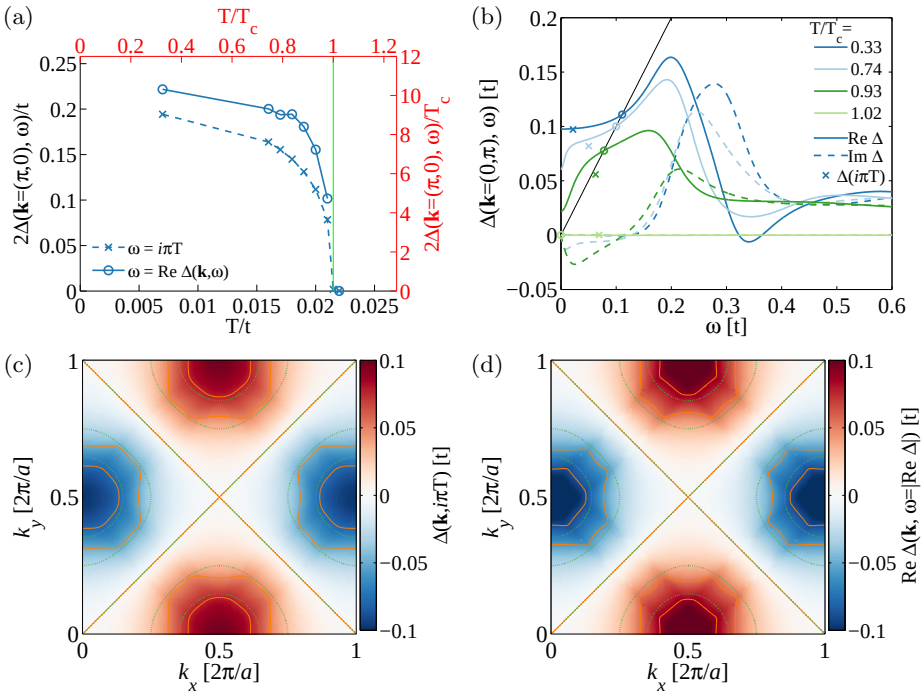

FIG. 4. (a) Gap function $\Delta(\mathbf{k},\omega)$ vs T. Here $\mathbf{k} = (\pi, 0)$, i.e., X point. The complex frequency is either pure imaginary $\omega = i\pi T$ (the lowest Matsubara frequency) or real $\omega = |\operatorname{Re}\Delta(\mathbf{k},\omega)|$, i.e., frequency at the gap edge. (b) Frequency dependence of the X point gap $\Delta(\mathbf{k},\omega)$ on the real frequency axis for various temperatures. The black line through the origin shows the pictorial way solving Eq. (29) and the circles indicate the gap value at the gap edge. (c) Momentum dependence of gap at $T = 0.007t \approx 0.33T_c$ for the lowest Matsubara frequency. (d) Momentum dependence of the gap at the gap edge on the real frequency axis at $T = 0.007t \approx 0.33T_c$. In (c) and (d), the orange solid contour lines are for the values of $0\Delta_{\max}$, $\pm 0.5\Delta_{\max}$, and $\pm 0.8\Delta_{\max}$; the green dotted contour lines are for the same set of values and a perfect $d_{x^2-y^2}$-wave function $-\Delta_{\max}(\cos k_x - \cos k_y)/2$.

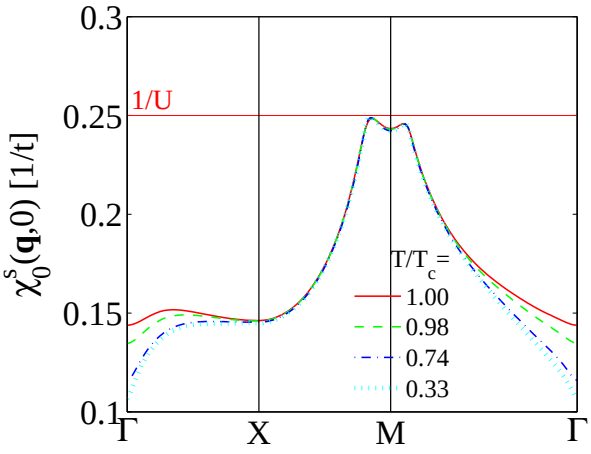

FIG. 5. The static spin susceptibility $\chi_0^s(\mathbf{q}, i\nu_m = 0)$ obtained from imaginary axis result directly.

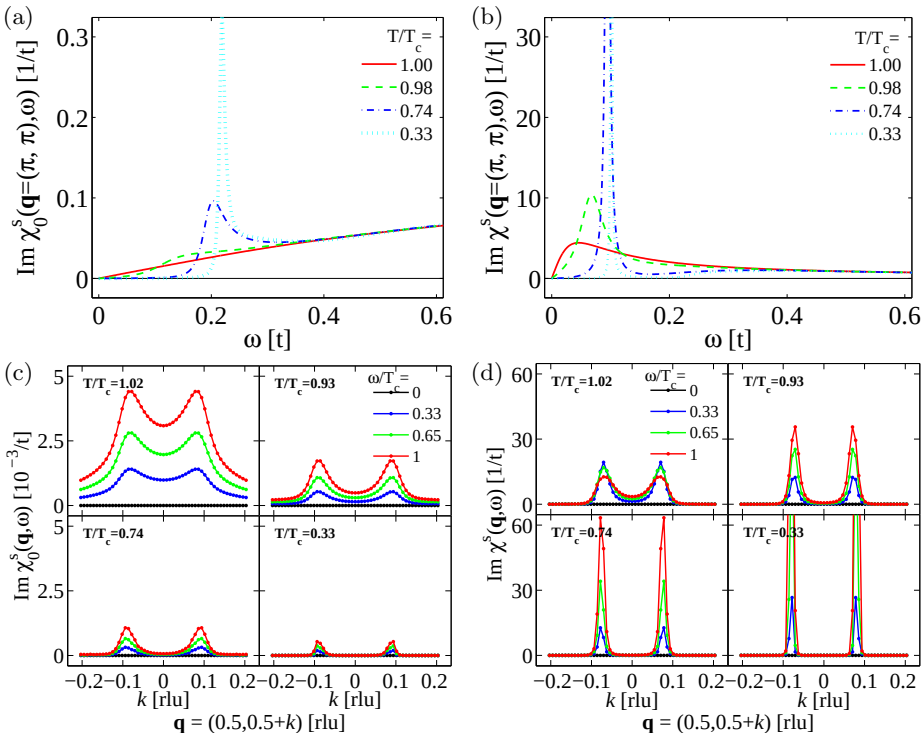

FIG. 6. Imaginary part of the irreducible spin susceptibility [(a) and (c)] and RPA spin susceptibility [(b) and (d)], at $M = (\pi, \pi)$ point [(a) and (b)] or along a high symmetry path X–M–X' [(c) and (d)]. Low frequency $\omega/T_c = 0$, 0.33, 0.65, and 1.0 data are plotted to show low energy excitations.

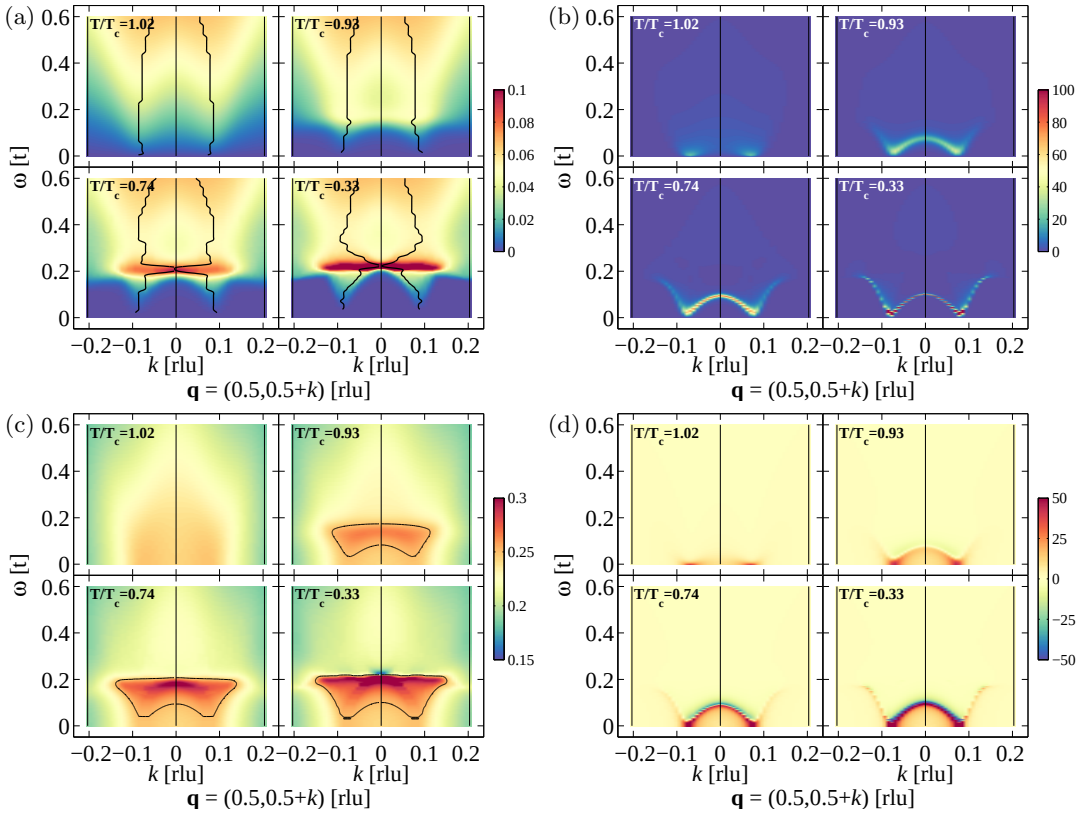

FIG. 7. (a) $\mathrm{Im}\,\chi_0^s(\mathbf{q},\omega)$ and (c) $\mathrm{Re}\,\chi_0^s(\mathbf{q},\omega)$ of the irreducible spin susceptibility. (b) $\mathrm{Im}\,\chi^s(\mathbf{q},\omega)$ and (d) $\mathrm{Re}\,\chi^s(\mathbf{q},\omega)$ of the RPA spin susceptibility. The high symmetry path is along X–M–X'. The black line in (a) traces the peak position in the spectrum along the high symmetry path for each individual frequency ω. The black contour line in (c) indicates $\mathrm{Re}\,\chi_0^s(\mathbf{q},\omega) = 1/U$.

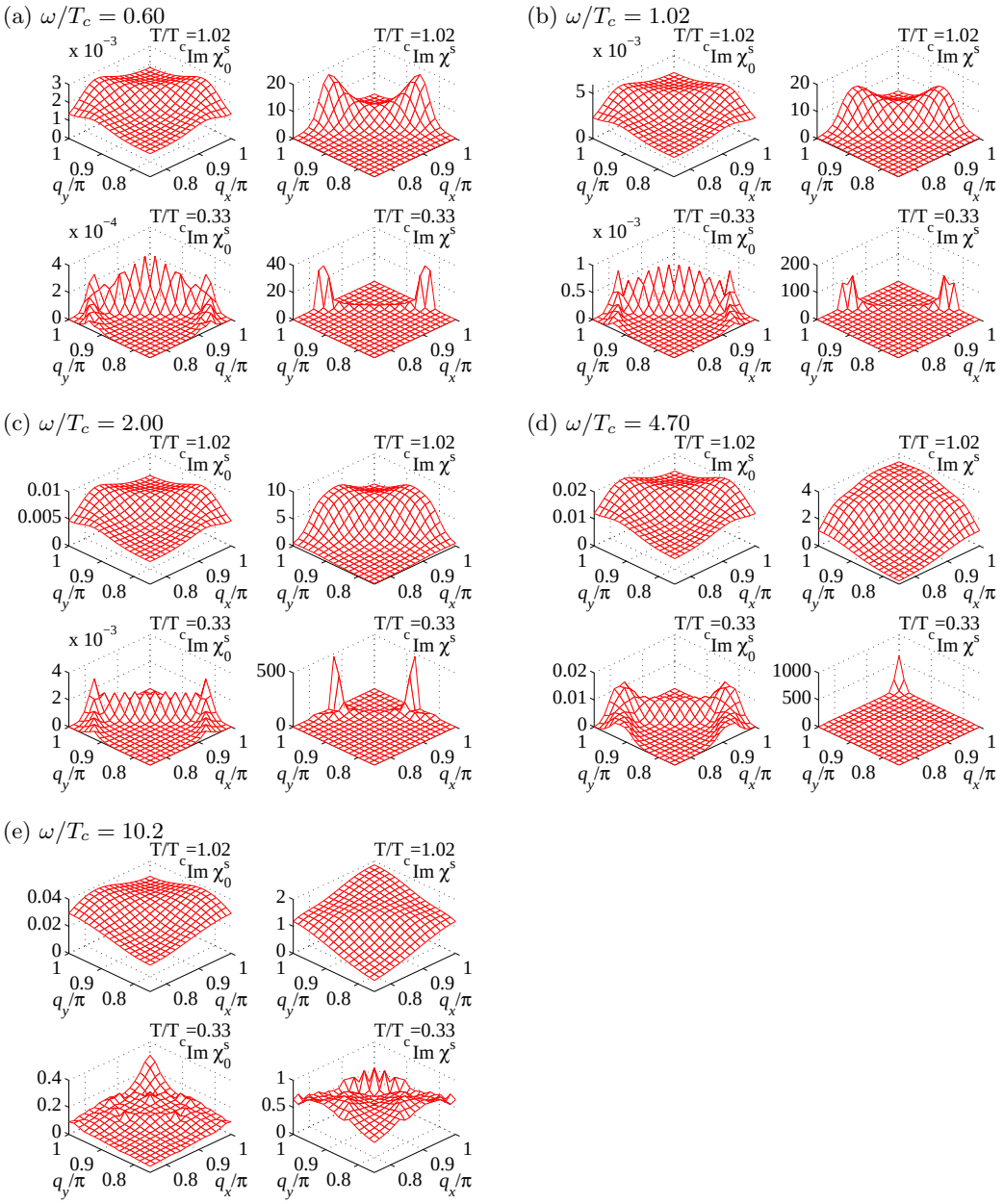

FIG. 8. (a)–(e) The spin susceptibility around $M = (\pi, \pi)$ point at different frequency $\omega/T_c = 0.60$–10.2. [C_4 symmetry is not imposed in the calculation (only C_2) so we symmetrize the data with respect to $q_x = q_y$ line to restore the C_4 symmetry. This doesn't affect the irreducible spin susceptibility and mainly makes the peaks in RPA spin susceptibility symmetric. The peaks in RPA susceptibility are too sharp to obtain as a symmetric value for our k-grid size and use of Padé approximant.] In each panel, there are four subplots for irreducible spin susceptibility (first column) and RPA spin susceptibility (second column) at two different temperatures $T/T_c = 1.02$ (first row) and $T/T_c = 0.33$ (second row). For the irreducible spin susceptibility, the resonance peaks become commensurate at $\omega = 10.2 \sim 2\Delta(T)$ [panel (e) bottom left]. For the RPA spin susceptibility, the resonance peaks become commensurate at $\omega = 4.70 \sim \Delta(T)$ [panel (d) bottom right].

III. FLEX FOR TWO-DIMENSIONAL MULTI-ORBITAL HUBBARD MODEL

A. Dyson's equation for matrix Green's function

To treat superconductivity, we adopt the Nambu 2-spinor notation. In a multi-orbital system with M orbitals, the Green's function $\hat{\underline{G}} = \hat{G}_{ab}$ is a $2M \times 2M$ matrix, which can be partitioned into 2×2 blocks, with each block being an $M \times M$ matrix in the orbital space. Here, the indices $a, b \in \{1, 2, \ldots, M\}$ denote the row and column of the matrix elements and the underscore $\underline{\ }$ denotes the whole matrix in the orbital space. The caret $\hat{\ }$ denotes the whole matrix in the Nambu space. Specifically, the matrix form for the Green's function is

$$\hat{G}_{ab} = -\langle T_\tau \begin{bmatrix} c_{\mathbf{k}a\sigma}(\tau) \\ c^\dagger_{-\mathbf{k}a\bar{\sigma}}(\tau) \end{bmatrix} \begin{bmatrix} c^\dagger_{\mathbf{k}b\sigma}(0) & c_{-\mathbf{k}b\bar{\sigma}}(0) \end{bmatrix} \rangle \tag{32}$$

$$= \begin{bmatrix} G^\sigma_{ab}(\mathbf{k},\tau) & F^{\sigma\bar{\sigma}}_{ab}(\mathbf{k},\tau) \\ \overline{F}^{\bar{\sigma}\sigma}_{ab}(\mathbf{k},\tau) & \overline{G}^{\bar{\sigma}}_{ab}(-\mathbf{k},\tau) \end{bmatrix}, \tag{33}$$

where the matrix elements for the four blocks in Nambu space are

$$G^\sigma_{ab}(\mathbf{k},\tau) = -\langle T_\tau c_{\mathbf{k}a\sigma}(\tau) c^\dagger_{\mathbf{k}b\sigma}(0)\rangle, \tag{34a}$$
$$\overline{G}^{\bar{\sigma}}_{ab}(-\mathbf{k},\tau) = -\langle T_\tau c^\dagger_{-\mathbf{k}a\bar{\sigma}}(\tau) c_{-\mathbf{k}b\bar{\sigma}}(0)\rangle, \tag{34b}$$
$$F^{\sigma\bar{\sigma}}_{ab}(\mathbf{k},\tau) = -\langle T_\tau c_{\mathbf{k}a\sigma}(\tau) c_{-\mathbf{k}b\bar{\sigma}}(0)\rangle, \tag{34c}$$
$$\overline{F}^{\bar{\sigma}\sigma}_{ab}(\mathbf{k},\tau) = -\langle T_\tau c^\dagger_{-\mathbf{k}a\bar{\sigma}}(\tau) c^\dagger_{\mathbf{k}b\sigma}(0)\rangle. \tag{34d}$$

Note $-\mathbf{k}$ in the definition for the hole Green's function $\overline{G}^{\bar{\sigma}}_{ab}$ and the order of spin indices $\bar{\sigma}\sigma$ in $\overline{F}^{\bar{\sigma}\sigma}_{ab}$; this is to be consistent with the general definitions below.

$$G^\sigma_{ab}(\mathbf{k},\tau) = -\langle T_\tau c_{\mathbf{k}a\sigma}(\tau) c^\dagger_{\mathbf{k}b\sigma}(0)\rangle, \tag{35a}$$
$$\overline{G}^{\sigma}_{ab}(\mathbf{k},\tau) = -\langle T_\tau c^\dagger_{\mathbf{k}a\sigma}(\tau) c_{\mathbf{k}b\sigma}(0)\rangle, \tag{35b}$$
$$F^{\sigma\sigma'}_{ab}(\mathbf{k},\tau) = -\langle T_\tau c_{\mathbf{k}a\sigma}(\tau) c_{-\mathbf{k}b\sigma'}(0)\rangle, \tag{35c}$$
$$\overline{F}^{\sigma\sigma'}_{ab}(\mathbf{k},\tau) = -\langle T_\tau c^\dagger_{-\mathbf{k}a\sigma}(\tau) c^\dagger_{\mathbf{k}b\sigma'}(0)\rangle. \tag{35d}$$

Using the above definitions, the definition of the time ordering operator T_τ, and the anticommutation relations we can prove the identity for the *particle-hole symmetry*

$$\overline{G}^{\sigma}_{ab}(\mathbf{k},\tau) = -G^\sigma_{ba}(\mathbf{k},-\tau), \tag{36a}$$
$$F^{\sigma\sigma'}_{ab}(\mathbf{k},\tau) = -F^{\sigma'\sigma}_{ba}(-\mathbf{k},-\tau), \tag{36b}$$

where the initial negative sign reflects Pauli principle. Using the relation between the adjoint of an operator and the complex conjugation of its matrix elements we can prove the identity for the *orbital symmetry*

$$G^\sigma_{ab}(\mathbf{k},\tau) = [G^\sigma_{ba}(\mathbf{k},\tau)]^*, \tag{37a}$$
$$F^{\sigma\sigma'}_{ab}(\mathbf{k},\tau) = [\overline{F}^{\sigma'\sigma}_{ba}(\mathbf{k},\tau)]^*. \tag{37b}$$

The above Eqs. (36) and (37) are fundamental symmetry relations, one due to the Pauli principle and the other due to the hermitian Hamiltonian, so they are always true.

Next, we consider the spin rational $SU(2)$ symmetry. In general, $F^{\sigma\sigma'}_{ab}(\mathbf{k},\tau)$ can be divided up into singlet and triplet sectors ($\sigma = \alpha$, $\sigma' = \beta$)

$$F^{\alpha\beta}_{ab}(\mathbf{k},\tau) = F^s_{ab}(\mathbf{k},\tau)(i\sigma_y)_{\alpha\beta} + \vec{F}^t_{ab}(\mathbf{k},\tau)\cdot(\vec{\sigma}i\sigma_y)_{\alpha\beta}. \tag{38}$$

Under the rotation of π degree about y-axis in spin space, $U^y(\pi) = \exp\left(-i\frac{S_y}{\hbar}\pi\right) = \exp\left(-i\frac{\sigma_y}{2}\pi\right) = -i\sigma_y$, $\sigma_{y'} \to \sigma_y$, $\sigma_{x'} \to -\sigma_x$, and $\sigma_{z'} \to -\sigma_z$, therefore the singlet component is invariant under this rotation. As a result, for singlet

pairing state and a paramagnetic system, we have the identity for the $SU(2)$ *symmetry*

$$G^{\sigma}_{ab}(\mathbf{k},\tau) = G^{\bar{\sigma}}_{ab}(\mathbf{k},\tau), \tag{39a}$$

$$F^{\sigma\sigma'}_{ab}(\mathbf{k},\tau) = \sigma\sigma' F^{\bar{\sigma}\bar{\sigma'}}_{ab}(\mathbf{k},\tau). \tag{39b}$$

Furthermore, the singlet and triplet components in Eq. (38) satisfy the following relation (under a transpose in spin space)

$$F^{\sigma\sigma'}_{ab}(\mathbf{k},\tau) = -F^{\sigma'\sigma}_{ab}(\mathbf{k},\tau), \quad \text{(for singlet)}, \tag{40a}$$

$$F^{\sigma\sigma'}_{ab}(\mathbf{k},\tau) = F^{\sigma'\sigma}_{ab}(\mathbf{k},\tau), \quad \text{(for triplet)}. \tag{40b}$$

Last, consider the time-reversal operator $T = U^y(\pi)K$, where K is the complex conjugation. From the above, we already see $[U^y(\pi)]^{-1}\sigma_y U^y(\pi) = \sigma_y$. Together with $K\sigma_y = -\sigma_y$, we obtain $T^{-1}\sigma_y T = -\sigma_y$. Similarly, $T^{-1}\sigma_x T = -\sigma_x$ and $T^{-1}\sigma_z T = -\sigma_z$. The general relation for angular momentum under time-reversal transformation is obtained $T^{-1}\vec{\sigma}T = -\vec{\sigma}$. Therefore, the singlet (triplet) component is even (odd) under the time-reversal transformation if we assume $F^{s}_{ab}(\mathbf{k},\tau)$ and $\vec{F}^{t}_{ab}(\mathbf{k},\tau)$ are real numbers. This leads to the identity for the *time-reversal symmetry* for singlet pairing state

$$G^{\sigma}_{ab}(\mathbf{k},\tau) = G^{\bar{\sigma}}_{ba}(-\mathbf{k},\tau), \tag{41a}$$

$$F^{\sigma\sigma'}_{ab}(\mathbf{k},\tau) = \sigma\sigma' \overline{F}^{\bar{\sigma'}\bar{\sigma}}_{ba}(-\mathbf{k},\tau). \tag{41b}$$

With the above symmetry identities we can reduce the number of independent blocks in the matrix Green's function, since

$$\begin{aligned}
&\overline{G}^{\bar{\sigma}}_{ab}(-\mathbf{k},\tau) \overset{\text{Eq. (36)}}{=} -G^{\bar{\sigma}}_{ba}(-\mathbf{k},-\tau) \overset{\text{Eq. (37)}}{=} -[G^{\bar{\sigma}}_{ab}(-\mathbf{k},-\tau)]^* \overset{\text{Eq. (39)}}{=} -[G^{\sigma}_{ab}(-\mathbf{k},-\tau)]^* \\
\Longrightarrow &\overline{G}^{\bar{\sigma}}_{ab}(-\mathbf{k},i\omega_n) = -[G^{\sigma}_{ab}(-\mathbf{k},i\omega_n)]^*. \\
&\overline{F}^{\bar{\sigma}\sigma}_{ab}(\mathbf{k},\tau) \overset{\text{Eq. (37)}}{=} [F^{\sigma\bar{\sigma}}_{ba}(\mathbf{k},\tau)]^* \overset{\text{Eq. (36)}}{=} [-F^{\bar{\sigma}\sigma}_{ab}(-\mathbf{k},-\tau)]^* \overset{\text{Eq. (39)}}{=} [F^{\sigma\bar{\sigma}}_{ab}(-\mathbf{k},-\tau)]^* \\
\Longrightarrow &\overline{F}^{\bar{\sigma}\sigma}_{ab}(\mathbf{k},i\omega_n) = [F^{\sigma\bar{\sigma}}_{ab}(-\mathbf{k},i\omega_n)]^*.
\end{aligned}$$

Another relations we will use later are

$$\begin{aligned}
&F^{\sigma\bar{\sigma}}_{ab}(\mathbf{k},\tau) \overset{\text{Eq. (36)}}{=} -F^{\bar{\sigma}\sigma}_{ba}(-\mathbf{k},-\tau) \overset{\text{Eq. (41)}}{=} \overline{F}^{\bar{\sigma}\sigma}_{ab}(\mathbf{k},-\tau) \\
\Longrightarrow &\overline{F}^{\bar{\sigma}\sigma}_{ab}(\mathbf{k},\tau) = F^{\sigma\bar{\sigma}}_{ab}(\mathbf{k},-\tau) &(42)\\
\Longrightarrow &\overline{F}^{\bar{\sigma}\sigma}_{ab}(\mathbf{k},i\omega_n) = F^{\sigma\bar{\sigma}}_{ab}(\mathbf{k},-i\omega_n). &(43)\\
&F^{\sigma\bar{\sigma}}_{ab}(\mathbf{k},\tau) \overset{\text{Eq. (36)}}{=} -F^{\bar{\sigma}\sigma}_{ba}(-\mathbf{k},-\tau) \overset{\text{Eq. (40)}}{=} \begin{Bmatrix} + \\ - \end{Bmatrix} F^{\sigma\bar{\sigma}}_{ba}(-\mathbf{k},-\tau) \overset{\mathbf{k}\text{ parity}}{=} F^{\sigma\bar{\sigma}}_{ba}(\mathbf{k},-\tau) \\
\Longrightarrow &F^{\sigma\bar{\sigma}}_{ab}(\mathbf{k},\tau) = F^{\sigma\bar{\sigma}}_{ba}(\mathbf{k},-\tau). &(44)
\end{aligned}$$

The signs in the curly brackets are for singlet (top) and triplet (bottom), respectively. Furthermore, using above, we have

$$\left.\begin{aligned} \overline{F}^{\bar{\sigma}\sigma}_{ab}(\mathbf{k},\tau) &= [F^{\sigma\bar{\sigma}}_{ba}(\mathbf{k},\tau)]^* \\ \overline{F}^{\bar{\sigma}\sigma}_{ab}(\mathbf{k},\tau) &= F^{\sigma\bar{\sigma}}_{ab}(\mathbf{k},-\tau) \end{aligned}\right\} \Longrightarrow F^{\sigma\bar{\sigma}}_{ab}(\mathbf{k},\tau) = [F^{\sigma\bar{\sigma}}_{ba}(\mathbf{k},-\tau)]^* = [F^{\sigma\bar{\sigma}}_{ab}(\mathbf{k},\tau)]^* \tag{45}$$

$$\Longrightarrow F^{\sigma\bar{\sigma}}_{ab}(\mathbf{k},\tau) \in \mathbb{R} \Longrightarrow F^{\sigma\bar{\sigma}}_{ab}(\mathbf{k},i\omega_n) = [F^{\sigma\bar{\sigma}}_{ab}(\mathbf{k},-i\omega_n)]^*. \tag{46}$$

If we combine the fact $F^{\sigma\bar{\sigma}}_{ab}(\mathbf{k},\tau) \in \mathbb{R}$ with $F^{\sigma\bar{\sigma}}_{ab}(\mathbf{k},\tau) = F^{\sigma\bar{\sigma}}_{ab}(-\mathbf{k},\tau)$ for singlet pairing state, we have $F^{\sigma\bar{\sigma}}_{ab}(\mathbf{r},\tau) \in \mathbb{R}$. Similarly, for $G^{\sigma}_{ab}(\mathbf{k},\tau)$, we have

$$\begin{aligned}
&G^{\sigma}_{ab}(\mathbf{k},\tau) \overset{\text{Eq. (41)}}{=} G^{\bar{\sigma}}_{ba}(-\mathbf{k},\tau) \overset{\text{Eq. (37)}}{=} G^{\bar{\sigma}}_{ab}(-\mathbf{k},\tau) \overset{\text{Eq. (39)}}{=} [G^{\sigma}_{ab}(-\mathbf{k},\tau)]^* \\
\Longrightarrow &G^{\sigma}_{ab}(\mathbf{r},\tau) \in \mathbb{R}. &(47)
\end{aligned}$$

In summary,

$$\begin{aligned}
&G_{ab}(\mathbf{r},\tau) = G_{ba}(\mathbf{r},\tau) \in \mathbb{R}, &(48)\\
\Longrightarrow &\underline{G}(\mathbf{r},\tau) = \underline{G}^t(\mathbf{r},\tau), \quad \underline{G}(\mathbf{k},i\omega_n) = \underline{G}^t(\mathbf{k},i\omega_n); &(49)\\
&F_{ab}(\mathbf{r},\tau) = F_{ba}(\mathbf{r},-\tau) \in \mathbb{R}, &(50)\\
\Longrightarrow &\underline{F}(\mathbf{r},\tau) = \underline{F}^t(\mathbf{r},-\tau), \quad \underline{F}(\mathbf{k},i\omega_n) = \underline{F}^{*,t}(\mathbf{k},i\omega_n) \equiv \underline{F}^{\dagger}(\mathbf{k},i\omega_n) &(51)
\end{aligned}$$

If we further assume all functions are even in $\mathbf{k}$ [$G^{\sigma}_{ab}(\mathbf{k}, i\omega_n)$ being even in $\mathbf{k}$ means that the system has inversion symmetry in real space; $F^{\sigma\bar{\sigma}}_{ab}(\mathbf{k}, i\omega_n)$ being even in $\mathbf{k}$ means singlet pairing state—also true for a system without inversion symmetry as long as there is time-reversal symmetry], the matrix form of the Green's function becomes

$$\begin{aligned}\hat{G}_{ab}(\mathbf{k}, i\omega_n) &= \begin{bmatrix} G^{\sigma}_{ab}(\mathbf{k}, i\omega_n) & F^{\sigma\bar{\sigma}}_{ab}(\mathbf{k}, i\omega_n) \\ \overline{F}^{\bar{\sigma}\sigma}_{ab}(\mathbf{k}, i\omega_n) & \overline{G}^{\bar{\sigma}}_{ab}(-\mathbf{k}, i\omega_n) \end{bmatrix} \\ &= \begin{bmatrix} G^{\sigma}_{ab}(\mathbf{k}, i\omega_n) & F^{\sigma\bar{\sigma}}_{ab}(\mathbf{k}, i\omega_n) \\ [F^{\sigma\bar{\sigma}}_{ab}(\mathbf{k}, i\omega_n)]^* & -[G^{\sigma}_{ab}(\mathbf{k}, i\omega_n)]^* \end{bmatrix}. \end{aligned} \tag{52}$$

In a full matrix form, this is

$$\hat{\underline{G}}(k) = \begin{bmatrix} \underline{G}(k) & \underline{F}(k) \\ \underline{F}^*(k) & -\underline{G}^*(k) \end{bmatrix}, \tag{53}$$

where the $k = (\mathbf{k}, i\omega_n)$. Note that the spin superscripts now have been dropped. Since

$$\hat{\underline{G}}_0(k) = \begin{bmatrix} \underline{G}_0(k) & 0 \\ 0 & -\underline{G}^*_0(k) \end{bmatrix}, \tag{54}$$

and due to the Dyson's equation, the self-energy must have the same form as $\hat{\underline{G}}(k)$

$$\hat{\underline{\Sigma}}(k) = \begin{bmatrix} \underline{\Sigma}(k) & \underline{\Phi}(k) \\ \underline{\Phi}^*(k) & -\underline{\Sigma}^*(k) \end{bmatrix}. \tag{55}$$

From Dyson's equation

$$\hat{\underline{G}}(k) = \hat{\underline{G}}_0(k) + \hat{\underline{G}}_0(k)\hat{\underline{\Sigma}}(k)\hat{\underline{G}}(k), \tag{56}$$

that is

$$\begin{bmatrix} \underline{G}(k) & \underline{F}(k) \\ \underline{F}^*(k) & -\underline{G}^*(k) \end{bmatrix} = \begin{bmatrix} \underline{G}_0(k) & 0 \\ 0 & -\underline{G}^*_0(k) \end{bmatrix} + \begin{bmatrix} \underline{G}_0(k) & 0 \\ 0 & -\underline{G}^*_0(k) \end{bmatrix} \begin{bmatrix} \underline{\Sigma}(k) & \underline{\Phi}(k) \\ \underline{\Phi}^*(k) & -\underline{\Sigma}^*(k) \end{bmatrix} \begin{bmatrix} \underline{G}(k) & \underline{F}(k) \\ \underline{F}^*(k) & -\underline{G}^*(k) \end{bmatrix},$$

we obtain four equations for each one of the $M \times M$ block (M is the number of orbitals), and the only two inequivalent ones are

$$\underline{G} = \underline{G}_0 + \underline{G}_0\underline{\Sigma}\underline{G} + \underline{G}_0\underline{\Phi}\underline{F}^*, \tag{57a}$$
$$\underline{F} = \underline{G}_0\underline{\Sigma}\underline{F} - \underline{G}_0\underline{\Phi}\underline{G}^*. \tag{57b}$$

The solution to the above equations are

$$\underline{G} = \left[\underline{G}_0^{-1} - \underline{\Sigma} - \underline{\Phi}\left(-\underline{G}_0^{*,-1} + \underline{\Sigma}^*\right)^{-1}\underline{\Phi}^*\right]^{-1} \tag{58a}$$
$$= \left\{[i\omega_n\mathbb{I} - (\underline{\varepsilon}_{\mathbf{k}} - \mu\mathbb{I}) - \underline{\Sigma}(k)] - \underline{\Phi}(k)\left[i\omega_n\mathbb{I} + (\underline{\varepsilon}_{\mathbf{k}} - \mu\mathbb{I}) + \underline{\Sigma}^*(k)\right]^{-1}\underline{\Phi}^*(k)\right\}^{-1}, \tag{58b}$$
$$\underline{F} = -\left(\underline{G}_0^{-1} - \underline{\Sigma}\right)^{-1}\underline{\Phi}\underline{G}^* = -\underline{G}\underline{\Phi}\left(\underline{G}_0^{*,-1} - \underline{\Sigma}^*\right)^{-1} \tag{58c}$$
$$= -\left[\left(\underline{G}_0^{*,-1} - \underline{\Sigma}^*\right)\underline{\Phi}^{-1}\left(\underline{G}_0^{-1} - \underline{\Sigma}\right) + \underline{\Phi}^*\right]^{-1} \tag{58d}$$
$$= \left\{[i\omega_n\mathbb{I} + (\underline{\varepsilon}_{\mathbf{k}} - \mu\mathbb{I}) + \underline{\Sigma}^*(k)]\,\underline{\Phi}^{-1}\,[i\omega_n\mathbb{I} - (\underline{\varepsilon}_{\mathbf{k}} - \mu\mathbb{I}) - \underline{\Sigma}] - \underline{\Phi}^*\right\}^{-1}. \tag{58e}$$

Note that $\underline{\Phi}$ is nearly singular near $T = T_c$ so one should avoid evaluating $\underline{\Phi}^{-1}$.

Remarks: the purpose of the above involved symmetry analysis is to simplify the matrix of Green's function in Nambu space. Note that in Eq. (52) the bottom two blocks are related to the top two blocks by a complex conjugation at the same 4-momentum point $k = (\mathbf{k}, i\omega_n)$. This expression is only valid for the singlet pairing state. Alternatively, using the following symmetries,

$$\begin{aligned}
&\overline{G}^{\bar{\sigma}}_{ab}(-\mathbf{k},\tau) \overset{\text{Eq. (36)}}{=} -G^{\bar{\sigma}}_{ba}(-\mathbf{k},-\tau) \overset{\text{Eq. (39)}}{=} -G^{\sigma}_{ba}(-\mathbf{k},-\tau)\\
\Longrightarrow &\overline{G}^{\bar{\sigma}}_{ab}(-\mathbf{k},i\omega_n) = -G^{\sigma}_{ba}(-\mathbf{k},-i\omega_n).\\
&\overline{F}^{\bar{\sigma}\sigma}_{ab}(\mathbf{k},\tau) \overset{\text{Eq. (?)}}{=} -F^{\bar{\sigma}\sigma}_{ba}(-\mathbf{k},\tau) \overset{\text{Eq. (40)}}{=} \left\{ \begin{smallmatrix} + \\ - \end{smallmatrix} \right\} F^{\sigma\bar{\sigma}}_{ba}(-\mathbf{k},\tau) \overset{\mathbf{k}\text{ parity}}{=} F^{\sigma\bar{\sigma}}_{ba}(\mathbf{k},\tau)\\
\Longrightarrow &\overline{F}^{\bar{\sigma}\sigma}_{ab}(\mathbf{k},i\omega_n) = F^{\sigma\bar{\sigma}}_{ba}(\mathbf{k},i\omega_n).
\end{aligned}$$

[**Red question mark means I cannot prove it for the triplet state but it should be true. The signs in the curly brackets are for singlet (top) and triplet (bottom), respectively. k parity of the singlet and triplet is also called orbital symmetry sometimes but it should be distinguished from the orbitals in our multiorbital model.**] we can write the matrix form of the Green's function

$$\begin{aligned}
\hat{G}_{ab}(\mathbf{k},i\omega_n) &= \begin{bmatrix} G^{\sigma}_{ab}(\mathbf{k},i\omega_n) & F^{\sigma\bar{\sigma}}_{ab}(\mathbf{k},i\omega_n) \\ F^{\sigma\bar{\sigma}}_{ba}(\mathbf{k},i\omega_n) & -G^{\sigma}_{ba}(-\mathbf{k},-i\omega_n) \end{bmatrix}\\
&= \begin{bmatrix} \underline{G}(k) & \underline{F}(k) \\ \underline{F}^t(k) & -\underline{G}^t(-k) \end{bmatrix},
\end{aligned}$$

where the superscript t means the transpose of the matrix in orbital space. The Dyson's equation becomes

$$\underline{G}(k) = \underline{G}_0(k) + \underline{G}_0(k)\underline{\Sigma}(k)\underline{G}(k) + \underline{G}_0(k)\underline{\Phi}(k)\underline{F}^t(k), \tag{59a}$$

$$\underline{F}(k) = \underline{G}_0(k)\underline{\Sigma}(k)\underline{F}(k) - \underline{G}_0(k)\underline{\Phi}(k)\underline{G}^t(-k). \tag{59b}$$

The above are two Eqs. (26) and (27) in Takimoto *et al.*[8] Although they apply to both singlet and triplet pairing states, the cost in numerical calculations is increased because the transpose of the matrix instead of the complex conjugation is used. For singlet pairing state, since $\underline{F}^t(k) = \underline{F}^*(k)$ and $\underline{G}^t(-k) = \underline{G}(-k) = \underline{G}^*(k)$, the above Dyson's equation is the same as the one I derived before. End of remarks.

B. Eliashberg equation with FLEX interaction

The Eliashberg equation with FLEX interaction for multiorbital system involves the Green's functions $G_{l_1l_2}, F_{l_1l_2}$, the self-energies $\Sigma_{l_1l_2}, \Phi_{l_1l_2}$, and the particle-hole susceptibility $\chi_{l_1l_2,l_3l_4}$, where the orbital index l_j $(j = 1,\ldots,4)$ takes the value from $\{1,\ldots,M\}$, where M is the total number of orbitals. Here, the Green's functions and the self-energies are $M \times M$ matrix in the orbital space. The four indices in $\chi_{l_1l_2,l_3l_4}$ can be grouped as $A = (l_1l_2)$ and $B = (l_3l_4)$ so $\chi_{A,B}$ becomes a $M^2 \times M^2$ matrix in the orbital space. I follow the notation of matrix form FLEX in Refs. 8, 25–27 and I will make proper adjustment and fix some typos in the equations from the above references.[28]

The interacting part of the Hamiltonian of the Hubbard model can be written in a symmetric form as follows.

$$H_{\text{int}} = \frac{1}{2}\sum_i \sum_{l\neq l',\sigma\sigma'} \left[U n_{i,l\sigma} n_{i,l\sigma'} + U' n_{i,l\sigma} n_{i,l'\sigma'} - J c^\dagger_{i,l\sigma} c_{i,l\sigma'} c^\dagger_{i,l'\sigma'} c_{i,l'\sigma} + J' c^\dagger_{i,l\sigma} c^\dagger_{i,l\sigma'} c_{i,l'\sigma'} c_{i,l'\sigma} \right] \tag{60}$$

$$= \frac{1}{4}\sum_i \sum_{\substack{l_1l_2l_3l_4 \\ \sigma_1\sigma_2\sigma_3\sigma_4}} U^{\sigma_1\sigma_2\sigma_3\sigma_4}_{l_1l_2l_3l_4} c^\dagger_{i,l_1\sigma_1} c^\dagger_{i,l_2\sigma_2} c_{i,l_3\sigma_3} c_{i,l_4\sigma_4}, \tag{61}$$

where the coupling constants U, U', J, J' are intraorbital Coulomb, interorbital Coulomb, exchange (Hund's rule coupling), and pair-hopping interactions, respectively; $\{l_j\}$ and $\{\sigma_j\}$ $(j = 1,\ldots,4)$ are the orbital and spin indices, respectively; i is the lattice site index; and the prefactor $\frac{1}{4}$ is to cancel the repeated terms from the sum due to the symmetry $1 \leftrightarrow 2$ and $3 \leftrightarrow 4$. The spin dependence of the interaction $U^{\sigma_1\sigma_2\sigma_3\sigma_4}_{l_1l_2l_3l_4}$ is parameterized as

$$U^{\sigma_1\sigma_2\sigma_3\sigma_4}_{l_1l_2l_3l_4} = -\frac{1}{2}U^s_{l_1l_2l_3l_4} \vec{\sigma}_{\sigma_1\sigma_4} \cdot \vec{\sigma}_{\sigma_2\sigma_3} + \frac{1}{2}U^c_{l_1l_2l_3l_4} \delta_{\sigma_1\sigma_4}\delta_{\sigma_2\sigma_3}, \tag{62}$$

where nonzero elements of the tensor $U^{s/c}_{l_1l_2l_3l_4}$ are

$$U^s_{l_1l_2l_3l_4} \equiv \begin{cases} U & (l_1=l_2=l_3=l_4) \\ U' & (l_1=l_3\neq l_2=l_4) \\ J & (l_1=l_4\neq l_2=l_3) \\ J' & (l_1=l_2\neq l_3=l_4) \end{cases}, \tag{63}$$

$$U^c_{l_1l_2l_3l_4} \equiv 2U^s_{l_1l_2l_4l_3} - U^s_{l_1l_2l_3l_4} = \begin{cases} U & (l_1=l_2=l_3=l_4) \\ 2J-U' & (l_1=l_3\neq l_2=l_4) \\ 2U'-J & (l_1=l_4\neq l_2=l_3) \\ J' & (l_1=l_2\neq l_3=l_4) \end{cases}. \tag{64}$$

We place the $M^2\times M^2$ elements of the tensor $U^{s/c}_{l_1l_2l_3l_4}$ into the matrix $U^{s/c}_{l_3l_2,l_1l_4}$, that is, we define the matrix $U^s_{l_3l_2,l_1l_4}\equiv U^s_{l_1l_2l_3l_4}$ and $U^c_{l_3l_2,l_1l_4}\equiv 2U^s_{l_1l_2l_4l_3}-U^s_{l_1l_2l_3l_4}$. Specifically,

$$U^s_{aa,aa}=U,\quad U^s_{ab,ab}=U',\quad U^s_{aa,bb}=J,\quad U^s_{ab,ba}=J'; \tag{65a}$$

$$U^c_{aa,aa}=U,\quad U^c_{ab,ab}=2J-U',\quad U^c_{aa,bb}=2U'-J,\quad U^c_{ab,ba}=J', \tag{65b}$$

where $a\neq b$.

The above definitions can be understood from the Feynman diagrams. Since $\vec{\sigma}_{\sigma_1\sigma_4}\cdot\vec{\sigma}_{\sigma_2\sigma_3}=2\delta_{\sigma_1\sigma_3}\delta_{\sigma_2\sigma_4}-\delta_{\sigma_1\sigma_4}\delta_{\sigma_2\sigma_3}$[29] and $U^c_{l_1l_2l_3l_4}\equiv 2U^s_{l_1l_2l_4l_3}-U^s_{l_1l_2l_3l_4}$, the interacting Hamiltonian becomes

$$\begin{aligned} H_{\rm int} &= \frac{1}{4}\sum_i \sum_{\substack{l_1l_2l_3l_4\\ \sigma_1\sigma_2\sigma_3\sigma_4}} \left[-\frac{1}{2}U^s_{l_1l_2l_3l_4}(2\delta_{\sigma_1\sigma_3}\delta_{\sigma_2\sigma_4}-\delta_{\sigma_1\sigma_4}\delta_{\sigma_2\sigma_3})+\frac{1}{2}U^c_{l_1l_2l_3l_4}\delta_{\sigma_1\sigma_4}\delta_{\sigma_2\sigma_3}\right] c^\dagger_{i,l_1\sigma_1}c^\dagger_{i,l_2\sigma_2}c_{i,l_3\sigma_3}c_{i,l_4\sigma_4} \\ &= \frac{1}{4}\sum_i \sum_{\substack{l_1l_2l_3l_4\\ \sigma\sigma'}} \left[U^s_{l_1l_2l_3l_4}c^\dagger_{i,l_1\sigma}c^\dagger_{i,l_2\sigma'}c_{i,l_4\sigma'}c_{i,l_3\sigma}+\frac{1}{2}(U^s_{l_1l_2l_3l_4}+U^c_{l_1l_2l_3l_4})c^\dagger_{i,l_1\sigma}c^\dagger_{i,l_2\sigma'}c_{i,l_3\sigma'}c_{i,l_4\sigma}\right] \\ &= \frac{1}{2}\sum_i \sum_{\substack{l_1l_2l_3l_4\\ \sigma\sigma'}} U^s_{l_1l_2l_3l_4}c^\dagger_{i,l_1\sigma}c^\dagger_{i,l_2\sigma'}c_{i,l_4\sigma'}c_{i,l_3\sigma} \\ &= \frac{1}{2}\sum_i \sum_{\substack{l_1l_2l_3l_4\\ \sigma\sigma'}} U^s_{l_3l_2,l_1l_4}c^\dagger_{i,l_1\sigma}c^\dagger_{i,l_2\sigma'}c_{i,l_4\sigma'}c_{i,l_3\sigma}. \end{aligned} \tag{66}$$

Thus, the four interaction terms U, U', J, and J' in Eq. (60) can be represented by the diagrams in Eq. (67); $U^{\sigma_1\sigma_2\sigma_3\sigma_4}_{l_1l_2l_3l_4}$ in Eq. (61) can be represented by the diagrams in Eq. (68). Switching the bottom two legs in Eq. (68), we obtain the matrix elements for particle-hole scattering as shown in Eq. (69), which gives matrix elements defined in Eq. (65), following our rule to populate the matrix $U^s_{l_3l_2,l_1l_4}=U^s_{l_1l_2l_3l_4}$. (Changing from particle-particle to particle-hole scattering, the interaction should acquire a negative sign. We do not, however, add this sign since we will preserve the normal ordering of the Hamiltonian.) The diagrams in Eq. (69) are building blocks for the ladder diagrams giving the FLEX-RPA spin susceptibility $\underline{\chi}^s=(1-\underline{\chi}^{0,s}\underline{U}^s)^{-1}\underline{\chi}^{0,s}$. (An extra negative sign has already been included in this ladder sum because in the self-energy diagram the two ends of one of the legs of the ladder diagram is connected by an internal fermion line, resulting in a fermion loop and thus a negative sign.) Our convention to populate the matrix $\underline{U}^s=U^s_{ll',nn'}$ makes the matrix multiplication equivalent to the necessary summation of orbital indices. Furthermore, if we switch l_3 and l_4 index in Eq. (69) and then, using the crossing symmetry, move l_3 (l_4) leg for an out-going hole (in-coming particle) to the left (right) as an in-coming particle (out-going hole), we obtain the diagrams for $U^s_{l_1l_2l_4l_3}$ in Eq. (70), which is a part of $U^c_{l_3l_2,l_1l_4}$. [The crossing symmetry changes the particle-hole scattering in t channel in Eq. (69) to the particle-hole scattering in s channel in Eq. (70).] The diagrams in Eq. (70) are building blocks for the bubble diagrams giving the FLEX-RPA charge susceptibility $\underline{\chi}^c=(1+\underline{\chi}^{0,c}\underline{U}^c)^{-1}\underline{\chi}^{0,c}$. The above is an intuitive understanding of the matrix FLEX formalism from the diagrammatic point of view.

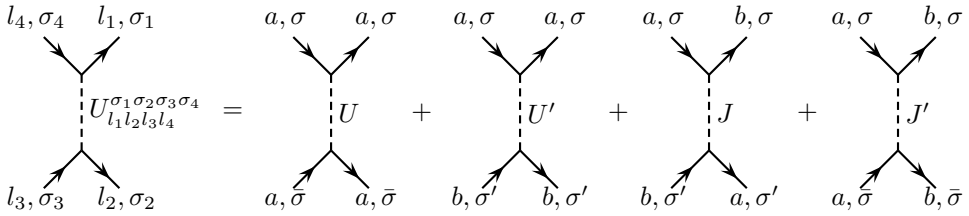

(67)

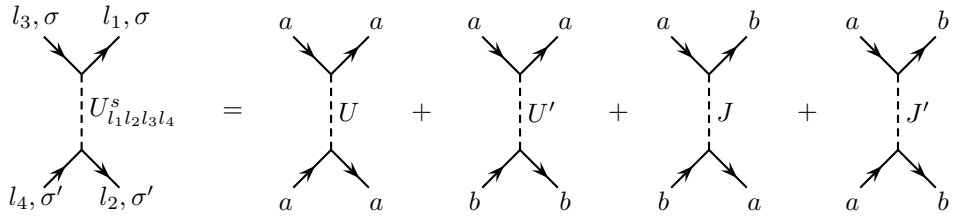

(68)

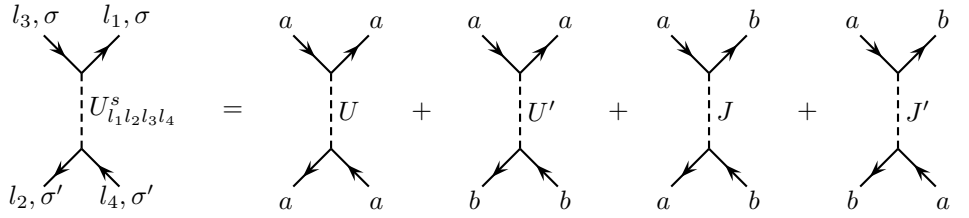

(69)

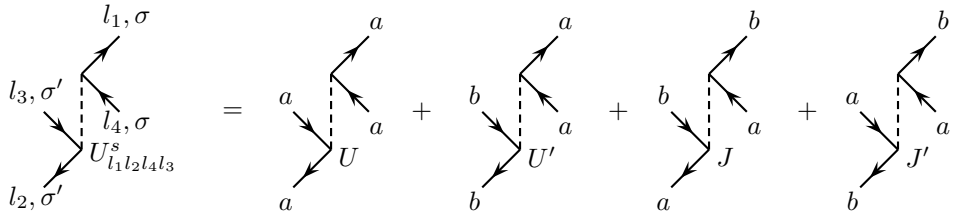

(70)

According to the above discussion, the irreducible spin and charge susceptibilities (in a proper matrix form) are defined as

$$\chi^{0,s}_{l_1l_2,l_3l_4}(q) = -\frac{T}{N}\sum_k [G_{l_1l_3}(k+q)G_{l_4l_2}(k) + F_{l_1l_4}(k+q)F^*_{l_3l_2}(k)], \tag{71a}$$

$$\chi^{0,c}_{l_1l_2,l_3l_4}(q) = -\frac{T}{N}\sum_k [G_{l_1l_3}(k+q)G_{l_4l_2}(k) - F_{l_1l_4}(k+q)F^*_{l_3l_2}(k)], \tag{71b}$$

where $F^*_{l_3l_2}$ means complex conjugation of $F_{l_3l_2}$, N is the total number of lattice sites, and $k = (\mathbf{k}, i\omega_n)$ and $q = (\mathbf{q}, i\nu_m)$, where $\omega_n = (2n+1)\pi T$ is the fermionic Matsubara frequency and $\nu_m = 2m\pi T$ is the bosonic Matsubara frequency.

The spin- and charge-fluctuation interactions are given by

$$\underline{V}^s(q) = \frac{3}{2}\underline{U}^s\left[\underline{\chi}^s(q) - \underline{\chi}^{0,s}(q)\right]\underline{U}^s, \tag{72a}$$

$$\underline{V}^c(q) = \frac{1}{2}\underline{U}^c\left[\underline{\chi}^c(q) - \underline{\chi}^{0,c}(q)\right]\underline{U}^c, \tag{72b}$$

where the RPA susceptibilities are

$$\underline{\chi}^s(q) = [\mathbb{I} - \underline{\chi}^{0,s}(q)\underline{U}^s]^{-1}\underline{\chi}^{0,s}(q), \tag{73a}$$

$$\underline{\chi}^c(q) = [\mathbb{I} + \underline{\chi}^{0,c}(q)\underline{U}^c]^{-1}\underline{\chi}^{0,c}(q). \tag{73b}$$

In the expression for the interaction $\underline{V}^s(q)$ and $\underline{V}^c(q)$, the second term in the brackets is to prevent the double counting in the second order. Since in the second order, the ladder and bubble diagram for the interaction gives the same self-energy diagram (see below), we subtract the second order and then calculate the second order by perturbation theory and add in the correct form explicitly. The normal and anomalous effective interactions are

$$\underline{V}^n(q) = \underline{V}^s(q) + \underline{V}^c(q) + \underline{V}^{n,(2)}(q) + \underline{V}^{n,\mathrm{HF}}, \tag{74a}$$

$$\underline{V}^a(q) = \underline{V}^s(q) - \underline{V}^c(q) + \underline{V}^{a,(2)}(q) + \underline{V}^{n,\mathrm{HF}}. \tag{74b}$$

The second order terms are[13]

$$\underline{V}^{n,(2)}(q) - \frac{3}{2}\underline{U}^s\underline{\chi}^{0,s}(q)\underline{U}^s - \frac{1}{2}\underline{U}^c\underline{\chi}^{0,c}(q)\underline{U}^c = -\frac{3}{4}\underline{U}^s\underline{\chi}^{0,G}(q)\underline{U}^s - \frac{1}{4}\underline{U}^c\underline{\chi}^{0,G}(q)\underline{U}^c, \tag{75a}$$

$$\underline{V}^{a,(2)}(q) - \frac{3}{2}\underline{U}^s\underline{\chi}^{0,s}(q)\underline{U}^s + \frac{1}{2}\underline{U}^c\underline{\chi}^{0,c}(q)\underline{U}^c = -\frac{3}{4}\underline{U}^s\underline{\chi}^{0,F}(q)\underline{U}^s - \frac{1}{4}\underline{U}^c\underline{\chi}^{0,F}(q)\underline{U}^c, \tag{75b}$$

where

$$\underline{\chi}^{0,G}(q) = \frac{1}{2}\left[\underline{\chi}^{0,s}(q) + \underline{\chi}^{0,c}(q)\right], \tag{76a}$$

$$\underline{\chi}^{0,F}(q) = \frac{1}{2}\left[\underline{\chi}^{0,s}(q) - \underline{\chi}^{0,c}(q)\right]. \tag{76b}$$

The first order Hartree-Fock terms are

$$\underline{V}^{n,\mathrm{HF}} = \frac{1}{2}(3\underline{U}^s - \underline{U}^c), \tag{77a}$$

$$\underline{V}^{a,\mathrm{HF}} = \frac{1}{2}(\underline{U}^s + \underline{U}^c), \tag{77b}$$

where the form given for $\underline{V}^{a,\mathrm{HF}}$ is only for the singlet pairing state. The Hartree-Fock terms need to be dealt with care because of the rule for the "same-time" Feynman diagram that when the fermion line is a closed loop or connected by the bare (instaneous) interaction line, a convergence factor $e^{-i\omega_n 0^-} = e^{i\omega_n 0^+}$ must be added.

To sum up, the FLEX interactions are

$$\underline{V}^n(q) = \frac{3}{2}\underline{U}^s\underline{\chi}^s(q)\underline{U}^s + \frac{1}{2}\underline{U}^c\underline{\chi}^c(q)\underline{U}^c - \frac{3}{4}\underline{U}^s\underline{\chi}^{0,G}(q)\underline{U}^s - \frac{1}{4}\underline{U}^c\underline{\chi}^{0,G}(q)\underline{U}^c + \frac{1}{2}(3\underline{U}^s - \underline{U}^c), \tag{78a}$$

$$\underline{V}^a(q) = \frac{3}{2}\underline{U}^s\underline{\chi}^s(q)\underline{U}^s - \frac{1}{2}\underline{U}^c\underline{\chi}^c(q)\underline{U}^c - \frac{3}{4}\underline{U}^s\underline{\chi}^{0,F}(q)\underline{U}^s - \frac{1}{4}\underline{U}^c\underline{\chi}^{0,F}(q)\underline{U}^c + \frac{1}{2}(\underline{U}^s + \underline{U}^c). \tag{78b}$$

Note that the above expression is given by Yada and Kontani[25] and Zhang *et al.*[13,26] but it is different from Takimoto *et al.*[8] in the second order correction term. In many studies,[30,31] only the interaction $\underline{V}^a(q)$ for the anomalous self-energy is given near $T = T_c$ and $\underline{\chi}^{0,F}(q)$ is neglected, and thus the correct form of the second order correction is irrelevant for $\underline{V}^a(q)$ at $T = T_c$.

Finally, the self-energies are given by

$$\Sigma_{lm}(k) = \frac{T}{N}\sum_q\sum_{l'm'} V^n_{ll',mm'}(q)G_{l'm'}(k-q), \tag{79a}$$

$$\Phi_{lm}(k) = \frac{T}{N}\sum_q\sum_{l'm'} V^a_{ll',m'm}(q)F_{l'm'}(k-q). \tag{79b}$$

Eqs. (58), (71), (73), (76), (78), (79) constitute the self-consistent Eliashberg equations for the self-energies and Green's functions from FLEX approximation of a multiorbital system. As a conserving approximation, in principle, the chemical potential should remain the same as the non-interacting case at the same temperature. [**Need refs here!**] In reality, due to the neglected vertex correction, we must fix the electron filling n (for two spins) by adjusting the chemical potential according to the following equation

$$n = \frac{2}{N}\sum_l\sum_{\mathbf{k}} G_{ll}(\mathbf{k}, \tau = 0^-) = \frac{2T}{N}\sum_l\sum_{\mathbf{k},n} G_{ll}(\mathbf{k}, i\omega_n)e^{-i\omega_n 0^-} = \frac{2T}{N}\sum_l\sum_{\mathbf{k},n} G_{ll}(\mathbf{k}, i\omega_n)e^{i\omega_n 0^+}. \tag{80}$$

Note that, while Eq. (58) follows the $M \times M$ matrix algebra, Eq. (79) involves two types of matrices of dimension $M \times M$ and $M^2 \times M^2$. The summation of index for normal (Σ_{lm}) and anomalous (Φ_{lm}) self-energies can be understood

from diagrams. We use the one-band Hubbard model to explain this. The FLEX diagrams are shown in Fig. 9, where the diagrams for $V^a(q)$ are for the singlet pairing state. (Again, they are called FLEX diagrams because they are derived from the conservation approximation proposed by Baym and Kadanoff, and the self-energy calculated using the effective interaction vertex obeys the conservation laws.) The numeral labels of the external legs of the effective interactions are placed according to the flow of the momenta and the matrix subscript notation for $V^n_{12,34}$ and $V^a_{12,34}$ are chosen so that the flow of the momenta is consistent between them. This results in the summation of different pair of indices as in Eq. (79) for multi-orbital case.

Last, we can write down directly the FLEX interaction for one-band model from Fig. 9. Assuming near T_c and $\chi^{0,s}(q) = \chi^{0,c}(q) \equiv \chi_0(q)$, we have

$$\begin{aligned} V^n(q) &= -(-U) - \frac{(-U)^2(-\chi_0)}{1-(-U)(-\chi_0)} + \frac{(-U)^2\chi_0}{1-(-U)^2\chi_0^2} - U^2\chi_0 \\ &= U + \frac{U^2\chi_0}{1-U\chi_0} + \frac{U^2\chi_0}{2}\left[\frac{1}{1-U\chi_0} + \frac{1}{1+U\chi_0}\right] - U^2\chi_0 \\ &= U + \frac{3}{2}\frac{U^2\chi_0}{1-U\chi_0} + \frac{1}{2}\frac{U^2\chi_0}{1+U\chi_0} - U^2\chi_0 \end{aligned} \tag{81}$$

$$\begin{aligned} V^s(q) &= -(-U) - \frac{(-U)^2(-\chi_0)}{1-(-U)(-\chi_0)} - \frac{(-U)^3\chi_0^2}{1-(-U)^2\chi_0^2} \\ &= U + \frac{U^2\chi_0}{1-U\chi_0} + \frac{U^2\chi_0}{2}\left[\frac{1}{1-U\chi_0} - \frac{1}{1+U\chi_0}\right] \\ &= U + \frac{3}{2}\frac{U^2\chi_0}{1-U\chi_0} - \frac{1}{2}\frac{U^2\chi_0}{1+U\chi_0} \end{aligned} \tag{82}$$

The minus sign in $(-U)$ is from the rule of Fynman diagram. The minus sign in $-\chi_0$ for the ladder diagrams is from the definition of the susceptibility $\chi_0 = -\frac{T}{N}\sum_q G(k+q)G(k)$, which includes a fermion loop sign as in the bubble diagrams. The two minus signs (in red color) in $V^n(q)$ are from the fact that, in the ladder diagrams, when we make the contraction for the term $\langle T_\tau c_{1'}(\tau)\ c_1(\tau_1)\ c_2(\tau_1)^\dagger \dots c_4(\tau_2)\ c_3(\tau_2)^\dagger c_{4'}(0)^\dagger\rangle$ (from the perturbation expansion of the Green's function), the ordering (1243) of the four operators from interaction is different from the normal ordering (3241) and it takes an odd number of permutations to change 1243 to 3241. (Another way to explain it is that when self-energy is constructed from these ladder diagrams, an extra fermion loop is created so the definition of the effective interaction includes this minus sign from the fermion loop.) Similarly, the last minus sign (in red color) in $V^a(q)$ for the bubble diagrams is due the odd number of permutations to change 1234 to 3214. The first two minus signs (in red color) in $V^a(q)$ are from the opposite spin in the definition of the interaction and in the ladder diagrams (see the caption of Fig. 9).

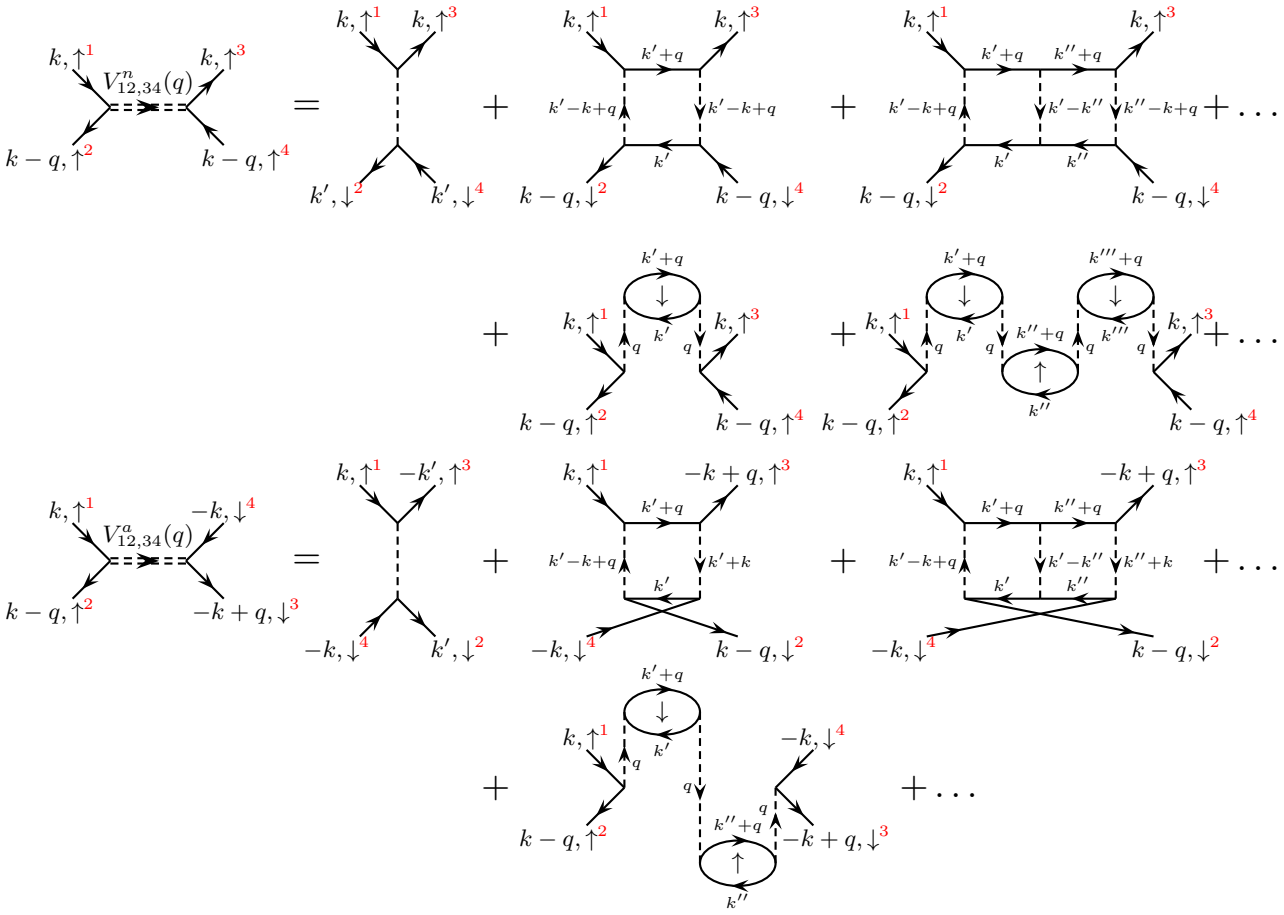

FIG. 9. The effective interaction $V^n_{12,34}(q)$ for the normal self-energy and $V^a_{12,34}(q)$ (for singlet pairing state) for the anomalous self-energy, in terms of the ladder and bubble diagrams derived from the fluctuation-exchange (FLEX) approximation to the one-band Hubbard interaction. The effective interaction includes the necessary extra minus signs that are not defined by Feynman diagrams shown on the right-hand side of the equation, so that the self-energy $\Sigma(1_\uparrow 3_\uparrow) = V^n(1_\uparrow \bar{2}_\uparrow, 3_\uparrow \bar{4}_\uparrow) G(\bar{2}_\uparrow \bar{4}_\uparrow)$ and $\Phi(1_\uparrow 4_\downarrow) = V^a(1_\uparrow \bar{2}_\uparrow, \bar{3}_\downarrow 4_\downarrow) F(\bar{2}_\uparrow \bar{3}_\downarrow)$, where the bar symbol over the numerals indicates an integration over that variable. Therefore, there is an extra negative sign in the first three diagrams for $V^a_{12,34}(q)$ due to the opposite spin and the relation $F(\bar{2}_\downarrow \bar{3}_\uparrow) = -F(\bar{2}_\uparrow \bar{3}_\downarrow)$ for the singlet pairing state. In $V_n^{12,34}(q)$, the first ladder diagram (the second term) and the first bubble diagram (the fourth term) contribute to the same self-energy diagram (hence the double counting), one of them must be subtracted from the $V_n^{12,34}(q)$ in the end.

IV. FLEX FOR COUPLED LADDER SYSTEM

A. Model and FLEX equations

In Fig. 10 we show the physical model of the coupled ladder system we consider. The non-interacting part Hamiltonian H_0 is

$$H_0 = -\sum_{\substack{i,j\\ \sigma,l,l'}} t_{ll'}^{ij} c_{i,l,\sigma}^{\dagger} c_{j,l',\sigma}, \tag{83}$$

where the minus is a matter of convention and its Fourier transform $H_0(\mathbf{k})$ is

$$H_0(\mathbf{k}) = \sum_{\mathbf{k}\sigma} \sum_{ll'} \varepsilon_{ll'}^{\mathbf{k}\sigma} c_{\mathbf{k},l,\sigma}^{\dagger} c_{\mathbf{k},l',\sigma}, \tag{84}$$

where the dispersion $\varepsilon_{ll'}^{\mathbf{k}\uparrow}$ and $\varepsilon_{ll'}^{\mathbf{k}\downarrow}$ are related by the time-reversal symmetry (in a time-reversal invariant system) $\varepsilon_{ll'}^{\mathbf{k}\downarrow} = (\varepsilon_{ll'}^{-\mathbf{k},\uparrow})^*$.

If we assume the coupled ladder system is in 2D-space with the rungs along the b direction as shown in Fig. 10(a), the matrix $\varepsilon_{ll'}^{\mathbf{k}\uparrow}$ in orbital space $l, l' \in \{\alpha, \beta\}$ due to only the nearest-neighbor hoppings (t, $t_\perp$, $t_{\alpha\beta}$ and $t_{\beta\alpha}$) is

$$[\varepsilon^{\mathbf{k}\uparrow}]_{ll'} = \begin{array}{c} \\ \alpha \\ \beta \end{array} \begin{array}{c} \begin{array}{cc} \alpha & \beta \end{array} \\ \begin{pmatrix} -2t\cos(k_x a) & -t_{\alpha\beta} e^{-ik_y b} - t_\perp \\ -t_{\beta\alpha} e^{ik_y b} - t_\perp & -2t\cos(k_x a) \end{pmatrix} \end{array}. \tag{85}$$

This is the lattice model studied in Ref. 32. It is easy to verify that $\varepsilon_{ll'}^{\mathbf{k}\downarrow} = (\varepsilon_{ll'}^{-\mathbf{k}\uparrow})^* = \varepsilon_{ll'}^{\mathbf{k}\uparrow}$. This is due to the fact that all hoppings are real. So we drop the spin index and denote $\varepsilon_{ll'}^{\mathbf{k}} \equiv \varepsilon_{ll'}^{\mathbf{k}\uparrow} = \varepsilon_{ll'}^{\mathbf{k}\downarrow}$ and denote the full matrix as $[\varepsilon^{\mathbf{k}}]_{ll'} = \underline{\varepsilon}_{\mathbf{k}}$. However, the elements of this matrix in orbital space does not have a simple parity relation in momentum space since $\underline{\varepsilon}_{\mathbf{k}} \neq \underline{\varepsilon}_{-\mathbf{k}}$. This leads us to consider the other coupled ladder system in 3D-space with the rungs along the c direction as shown in Fig. 10(b). This quasi-2D system is periodic in the a and b directions but not in the c direction. The matrix $\underline{\varepsilon}_{\mathbf{k}}$ due to only the nearest-neighbor hoppings (t, $t_\perp$, $t_{\alpha\alpha}$ and $t_{\beta\beta}$) now becomes

$$\underline{\varepsilon}_{\mathbf{k}} = \begin{array}{c} \\ \alpha \\ \beta \end{array} \begin{array}{c} \begin{array}{cc} \alpha & \beta \end{array} \\ \begin{pmatrix} -2t\cos(k_x a) - 2t_{\alpha\alpha}\cos(k_y b) & -t_\perp \\ -t_\perp & -2t\cos(k_x a) - 2t_{\beta\beta}\cos(k_y b) \end{pmatrix} \end{array}. \tag{86}$$

A few special cases of this model have been extensively studied. For instance, when lattice parameter $a = b$, and the hopping $t_{\alpha\alpha} = t_{\beta\beta} = t$ and $t_{\alpha\beta} = t_{\beta\alpha} = 0$, it becomes the so-called bilayer Hubbard model. A great amount of theoretical studies on this model with various methods for different ratios of $t_\perp/t$ exist and it is found that the pairing symmetry depends on this ratio. See Scalapino's review Ref. 33 and the references therein. Kuroki *et al.*[34] studied the bilayer Hubbard model with FLEX method.

We wish to study the case with $a = c$, $t_\perp = t$, and $t_{\alpha\alpha}/t = t_{\beta\beta}/t \to 0$ when the length of b lattice parameter is increased. In the limit $t_{\alpha\alpha}/t = t_{\beta\beta}/t = 0$, the ladders completely decouple, and we will compare the FLEX result with that from a numerically exact method, the density matrix renormalization group (DMRG) method, which is suitable for an isolated two-leg ladder. (Three- or more-leg ladder system can also be studied with the current multiorbital FLEX method by increasing the dimension of the orbital space. Physically, this corresponds to decouple a ladder system consisting of more Hubbard layers than the bilayer system.)

For the bilayer system in Fig. 10(b), the matrix FLEX formalism involves the Hubbard interaction matrix and the susceptibility matrix in a two-orbital basis. We denote the two orbitals as $\alpha = 1$ and $\beta = 2$ as shown in Fig. 10(b). As defined in Eq. (65), the spin (charge) interaction matrices $U^s_{l_1 l_2, l_3 l_4}$ ($U^c_{l_1 l_2, l_3 l_4}$) is a 4×4 matrix in the two-orbital basis, $(l_1 l_2) = (11, 22, 12, 21)$ for the rows and $(l_3 l_4) = (11, 22, 12, 21)$ for the columns, respectively. They have the following matrix form

$$\underline{U}^s = \begin{array}{c} \\ 11 \\ 22 \\ 12 \\ 21 \end{array} \begin{array}{c} \begin{array}{cccc} 11 & 22 & 12 & 21 \end{array} \\ \begin{pmatrix} U & J & 0 & 0 \\ J & U & 0 & 0 \\ 0 & 0 & U' & J' \\ 0 & 0 & J' & U' \end{pmatrix} \end{array}, \quad \underline{U}^c = \begin{array}{c} \\ 11 \\ 22 \\ 12 \\ 21 \end{array} \begin{array}{c} \begin{array}{cccc} 11 & 22 & 12 & 21 \end{array} \\ \begin{pmatrix} U & 2U' - J & 0 & 0 \\ 2U' - J & U & 0 & 0 \\ 0 & 0 & 2J - U' & J' \\ 0 & 0 & J' & 2J - U' \end{pmatrix} \end{array}. \tag{87}$$

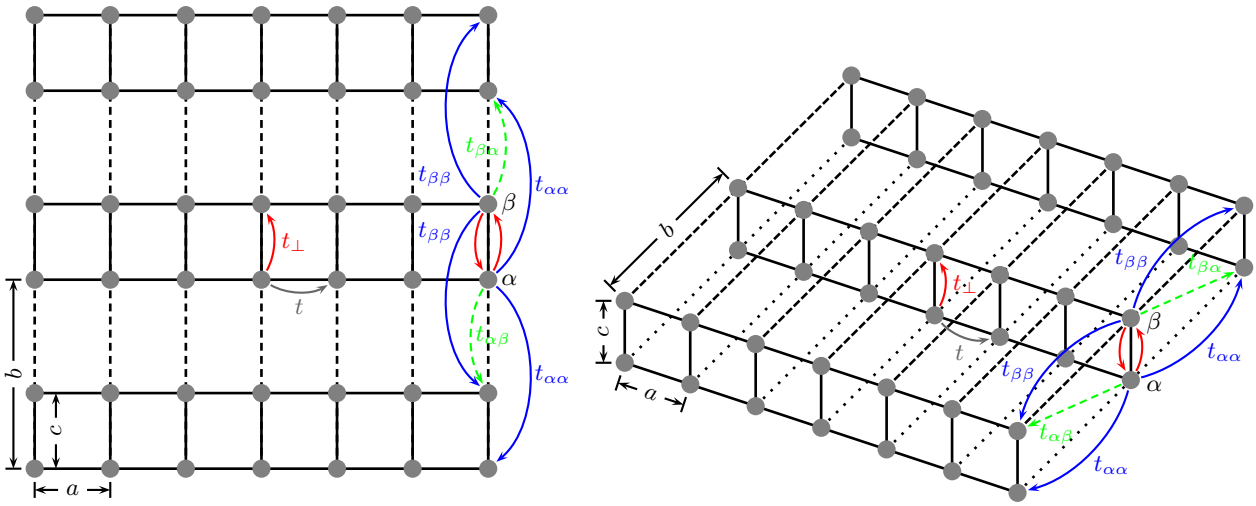

FIG. 10. Two types of coupled ladder system with two equivalent orbitals α and β in each unit cell. (a) Coupled ladder system in 2D-space with the rungs along the b direction. This 2D system is periodic in the a and b directions. (b) Coupled ladder system in 3D-space with the rungs along the c direction. This quasi-2D system is periodic in the a and b directions but not in the c direction.

The dispersion $\underline{\varepsilon}_{\mathbf{k}}$ and the non-interacting Green's function $\underline{G}_0(\mathbf{k}, i\omega_n)$ are

$$\underline{\varepsilon}_{\mathbf{k}} = \begin{array}{c} \\ 1 \\ 2 \end{array}\begin{array}{c} \begin{array}{cc} 1 & 2 \end{array} \\ \begin{pmatrix} \varepsilon^{\mathbf{k}}_{11} & \varepsilon^{\mathbf{k}}_{12} \\ \varepsilon^{\mathbf{k}}_{21} & \varepsilon^{\mathbf{k}}_{22} \end{pmatrix} \end{array}, \quad \underline{G}_0(\mathbf{k}, i\omega_n) = [i\omega_n \mathbb{I} - (\underline{\varepsilon}_{\mathbf{k}} - \mu\mathbb{I})]^{-1} = \frac{\begin{pmatrix} i\omega_n - (\varepsilon^{\mathbf{k}}_{22} - \mu) & \varepsilon^{\mathbf{k}}_{12} \\ \varepsilon^{\mathbf{k}}_{21} & i\omega_n - (\varepsilon^{\mathbf{k}}_{11} - \mu) \end{pmatrix}}{[i\omega_n - (\varepsilon^{\mathbf{k}}_{11} - \mu)][i\omega_n - (\varepsilon^{\mathbf{k}}_{22} - \mu)] - \varepsilon^{\mathbf{k}}_{12}\varepsilon^{\mathbf{k}}_{21}}, \tag{88}$$

where $\varepsilon^{\mathbf{k}}_{11} = -2t\cos(k_x a) - 2t_{\alpha\alpha}\cos(k_y b)$ and $\varepsilon^{\mathbf{k}}_{22} = -2t\cos(k_x a) - 2t_{\beta\beta}\cos(k_y b)$, and $\varepsilon^{\mathbf{k}}_{12} = \varepsilon^{\mathbf{k}}_{21} = -t_\perp$.

The susceptibility matrix has the form

$$\underline{\chi}^p = \begin{array}{c} \\ 11 \\ 22 \\ 12 \\ 21 \end{array}\begin{array}{c} \begin{array}{cccc} 11 & 22 & 12 & 21 \end{array} \\ \begin{pmatrix} \chi^p_{11,11} & \chi^p_{11,22} & \chi^p_{11,12} & \chi^p_{11,21} \\ \chi^p_{22,11} & \chi^p_{22,22} & \chi^p_{22,12} & \chi^p_{22,21} \\ \chi^p_{12,11} & \chi^p_{12,22} & \chi^p_{12,12} & \chi^p_{12,21} \\ \chi^p_{21,11} & \chi^p_{21,22} & \chi^p_{21,12} & \chi^p_{21,21} \end{pmatrix} \end{array}. \tag{89}$$

where $p = 0, s$ ($p = 0, c$) for irreducible spin (charge) susceptibility $\underline{\chi}^{0,s}$ ($\underline{\chi}^{0,c}$), and $p = s$ ($p = c$) for RPA spin $\underline{\chi}^s = (\mathbb{I} - \underline{\chi}^{0,s}\underline{U}^s)^{-1}\underline{\chi}^{0,s}$ [charge $\underline{\chi}^c = (\mathbb{I} + \underline{\chi}^{0,c}\underline{U}^c)^{-1}\underline{\chi}^{0,c}$] susceptibility. Fortunately, if we only consider the on-site intraorbital Coulomb interaction U and set $U' = J = J' = 0$, the spin (charge) interaction matrices become

$$\underline{U}^s = \begin{array}{c} \\ 11 \\ 22 \\ 12 \\ 21 \end{array}\begin{array}{c} \begin{array}{cccc} 11 & 22 & 12 & 21 \end{array} \\ \begin{pmatrix} U & 0 & 0 & 0 \\ 0 & U & 0 & 0 \\ 0 & 0 & 0 & 0 \\ 0 & 0 & 0 & 0 \end{pmatrix} \end{array}, \quad \underline{U}^c = \begin{array}{c} \\ 11 \\ 22 \\ 12 \\ 21 \end{array}\begin{array}{c} \begin{array}{cccc} 11 & 22 & 12 & 21 \end{array} \\ \begin{pmatrix} U & 0 & 0 & 0 \\ 0 & U & 0 & 0 \\ 0 & 0 & 0 & 0 \\ 0 & 0 & 0 & 0 \end{pmatrix} \end{array}. \tag{90}$$

Therefore, $\underline{U}^s = \underline{U}^c$, and the FLEX interactions in Eq. (78) take a much simpler form as follows.

$$\underline{V}^n(q) = \frac{3}{2}U^2\underline{\chi}^s(q) + \frac{1}{2}U^2\underline{\chi}^c(q) - U^2\underline{\chi}^{0,G}(q) + U\mathbb{I}, \tag{91a}$$

$$\underline{V}^a(q) = \frac{3}{2}U^2\underline{\chi}^s(q) - \frac{1}{2}U^2\underline{\chi}^c(q) - U^2\underline{\chi}^{0,F}(q) + U\mathbb{I}, \tag{91b}$$

where each matrix is 2×2 dimension instead of 4×4 dimension. Here, $\underline{\chi}^s = (\mathbb{I}-\underline{\chi}^{0,s}U)^{-1}\underline{\chi}^{0,s}$, $\underline{\chi}^c = (\mathbb{I}+\underline{\chi}^{0,c}U)^{-1}\underline{\chi}^{0,c}$, $\underline{\chi}^{0,G} = (\underline{\chi}^{0,s}+\underline{\chi}^{0,c})/2$, $\underline{\chi}^{0,F} = (\underline{\chi}^{0,s}-\underline{\chi}^{0,c})/2$, and

$$\underline{\chi}^p = \begin{array}{c} \\ 11 \\ 22 \end{array}\begin{array}{c} \begin{array}{cc} 11 & 22 \end{array} \\ \begin{pmatrix} \chi^p_{11,11} & \chi^p_{11,22} \\ \chi^p_{22,11} & \chi^p_{22,22} \end{pmatrix} \end{array} \equiv \begin{array}{c} \\ 11 \\ 22 \end{array}\begin{array}{c} \begin{array}{cc} 11 & 22 \end{array} \\ \begin{pmatrix} \chi^p_{1,1} & \chi^p_{1,2} \\ \chi^p_{2,1} & \chi^p_{2,2} \end{pmatrix} \end{array}, \tag{92}$$

where $p = 0, s$ ($p = 0, c$) for irreducible spin (charge) susceptibility, which are defined by Eq. (71) as follows.

$$\chi^{0,s}_{l,m}(q) \equiv \chi^{0,s}_{ll,mm}(q) = -\frac{T}{N}\sum_k [G_{lm}(k+q)G_{ml}(k) + F_{lm}(k+q)F^*_{ml}(k)], \tag{93a}$$

$$\chi^{0,c}_{l,m}(q) \equiv \chi^{0,c}_{ll,mm}(q) = -\frac{T}{N}\sum_k [G_{lm}(k+q)G_{ml}(k) - F_{lm}(k+q)F^*_{ml}(k)]. \tag{93b}$$

We use the short notation $\chi_{l,m}$ for $\chi_{ll,mm}$. Other types of susceptibilities $\chi_{l_1l_2,l_3l_4}$ for $l_1 \neq l_2$ or $l_3 \neq l_4$ do not enter the FLEX effective interactions so they are not calculated. Furthermore, we have the symmetry $\chi_{ll,mm}(q) = \chi_{mm,ll}(q) = \chi_{mm,ll}(-q) = [\chi_{mm,ll}(q)]^* = [\chi_{ll,mm}(q)]^*$ so every matrix element of the susceptibilities and the interactions is real. If we further assume $t_{\alpha\alpha} = t_{\beta\beta}$, that is, $G_{11}(k) = G_{22}(k)$ and $F_{11}(k) = F_{22}(k)$, we have $\chi_{11,11}(q) = \chi_{22,22}(q)$. Therefore, we only need to calculate two out of four matrix elements of each of the irreducible susceptibilities $\chi^{0,s}_{l,m}(q)$ and $\chi^{0,c}_{l,m}(q)$ for $l, m \in \{\alpha = 1, \beta = 2\}$. Similarly, the Hartree-Fock normal self-energy $\Sigma^{\rm HF}_{11} = \Sigma^{\rm HF}_{22} = Un^\sigma_{11} = Un^\sigma_{22}$, which can be absorbed into the chemical potential.

Since the interactions $V^n_{ll',mm'}(q) = V^n_{l,m}(q)\delta_{ll'}\delta_{mm'}$ and $V^n_{ll',m'm}(q) = V^n_{l,m}(q)\delta_{ll'}\delta_{mm'}$, the self-energy Eq. (79) becomes

$$\Sigma_{lm}(k) = \frac{T}{N}\sum_q V^n_{l,m}(q)G_{lm}(k-q),$$

$$\Phi_{lm}(k) = \frac{T}{N}\sum_q V^a_{l,m}(q)F_{lm}(k-q).$$

Without any summation over the orbital index in the self-energy equation, different matrix element in the orbital space only couple to each other through the Dyson's Eq. (58) as follows.

$$\begin{aligned} \underline{G} &= \left[\underline{G}_0^{-1} - \underline{\Sigma} - \underline{\Phi}\left(-\underline{G}_0^{*,-1} + \underline{\Sigma}^*\right)^{-1}\underline{\Phi}^*\right]^{-1} \\ &= \left\{[i\omega_n\mathbb{I} - (\underline{\varepsilon}_{\mathbf{k}} - \mu\mathbb{I}) - \underline{\Sigma}(k)] - \underline{\Phi}(k)\left[i\omega_n\mathbb{I} + (\underline{\varepsilon}_{\mathbf{k}} - \mu\mathbb{I}) + \underline{\Sigma}^*(k)\right]^{-1}\underline{\Phi}^*(k)\right\}^{-1}, \\ \underline{F} &= -\underline{G}\underline{\Phi}\left(\underline{G}_0^{*,-1} - \underline{\Sigma}^*\right)^{-1} = \underline{G}\underline{\Phi}\left[i\omega_n\mathbb{I} + (\underline{\varepsilon}_{\mathbf{k}} - \mu\mathbb{I}) + \underline{\Sigma}^*\right]^{-1}. \end{aligned}$$

As discussed in the Appendix C, the chemical potential is determined from the FLEX Green's function using Eq. (C21) as follows.

$$\frac{2T}{N}\sum_{\mathbf{k}}\sum_{n=-N_c}^{N_c-1}\sum_l \left[G_{ll}(\mathbf{k}, i\omega_n; \mu) - \frac{1}{i\omega_n - \xi}\right] = 0,$$

where

$$\xi = T\ln\left(\frac{2M}{n} - 1\right),$$

where $M = 2$ is the total number of orbitals.

B. Numerical results

In this section we show the anomalous self-energies (superconducting gap) and susceptibilities self-consistently calculated from the bilayer model illustrated in Fig. 10(b), which can be viewed as coupled ladders (meaning electrons

can hop between different two-leg ladders) when $t_{\alpha\alpha} = t_{\beta\beta} \neq 0$ or decoupled ladders when $t_{\alpha\alpha} = t_{\beta\beta} = 0$. Note that we always set $t_{\alpha\beta} = t_{\beta\alpha} = 0$. Note again that we use the hopping $t = 1$ along the legs of the ladder as the units of energy.

Since the superconducting gap (the spectral gap) is only well defined in the band space as the energy gap in the single-electron spectral function, the anomalous self-energies $\Phi_{ll'}$ ($l, l' \in \{\alpha, \beta\}$) is strictly speaking not the superconducting gap. Because we are considering two equivalent orbitals (α and β denote the two legs of the ladder, respectively), we can easily perform an unitary transformation on the normal and anomalous self-energies and find the superconducting gap defined in band space as follows. Due to the symmetry and the equivalent orbitals, even in the interacting case ($U \neq 0$), the unitary transformation is a matrix consisting of the two eigenvectors: $(1, 1)/\sqrt{2}$ for the bonding band (denoted by a plus "+" sign) and $(1, -1)/\sqrt{2}$ for the antibonding band (denoted by a minus "−" sign). Specifically, for the normal self-energy

$$\begin{pmatrix} \Sigma_{++} & \Sigma_{+-} \\ \Sigma_{-+} & \Sigma_{--} \end{pmatrix} = \frac{1}{\sqrt{2}} \begin{pmatrix} 1 & 1 \\ 1 & -1 \end{pmatrix} \begin{pmatrix} \Sigma_{\alpha\alpha} & \Sigma_{\alpha\beta} \\ \Sigma_{\beta\alpha} & \Sigma_{\beta\beta} \end{pmatrix} \frac{1}{\sqrt{2}} \begin{pmatrix} 1 & 1 \\ 1 & -1 \end{pmatrix} = \begin{pmatrix} \Sigma_{\alpha\alpha} + \Sigma_{\alpha\beta} & 0 \\ 0 & \Sigma_{\alpha\alpha} - \Sigma_{\alpha\beta} \end{pmatrix},$$

where the last step is because of $\Sigma_{\alpha\alpha} = \Sigma_{\beta\beta}$ and $\Sigma_{\alpha\beta} = \Sigma_{\beta\alpha}$. A similar transformation is done for the anomalous self-energy $\Phi_{ll'}$. Defined in the band space, the mass renormalization $Z_{jj}(\mathbf{k}, i\omega_n) = 1 - [\Sigma_{jj}(\mathbf{k}, i\omega_n) - \Sigma_{jj}(\mathbf{k}, -i\omega_n)]/(2i\omega_n)$ ($j = +$ or $-$) and the gap function $\Delta_{jj}(\mathbf{k}, i\omega_n) = \Sigma_{jj}(\mathbf{k}, i\omega_n)/Z_{jj}(\mathbf{k}, i\omega_n)$. At low temperature, the gap function at lowest Matsubara frequency $\Delta_{jj}(\mathbf{k}, i\pi T)$ is a very good approximation of the gap at the gap edge in the spectral function. Last, if needed, the gap in orbital space can be found by the inverse of the unitary transformation, which gives $\Delta_{\alpha\alpha} = \Delta_{\beta\beta} = (\Delta_{++} + \Delta_{--})/2$ and $\Delta_{\alpha\beta} = \Delta_{\beta\alpha} = (\Delta_{++} - \Delta_{--})/2$.

1. *a bilayer of Hubbard planes*

In this section, we show the results for a bilayer of Hubbard planes, i.e., the coupled ladders, for a *dimerised* case where the hopping is relatively large between the planes, i.e., along the vertical rungs of the ladder. The results shown in this section can be compared with that in Ref. 34. All hopping parameters and U are the same upon a rescale of energy units. The difference is that we solve the FLEX equations in the superconducting state ($T < T_c$), while in Ref. 34, the self-energies are solved self-consistently in the normal state ($T > T_c$) and a linearized gap equation is used to find T_c and the eigen vector for the gap function but the gap magnitude is inaccessible in that method. In short, we have done a slightly more complicated calculation (by including the anomalous self-energy) to find the properties in the superconducting state.[6,8] We set the filling $n = 0.95$, $t \equiv t_x = 1$, $t_\perp \equiv t_z = 1.625$, $U = 10$, and $t_{\alpha\alpha} = t_{\beta\beta} \equiv t_y = 1,\ 0.8,\ 0.6,\ 0.5,\ 0.4$. The results are plotted in Fig. 11. The T_c is determined from the temperature at which the anomalous self-energy (or the gap) changing from zero to finite. We find that T_c decreases for decreasing t_y. The trend shown in Fig. 11(a, b) indicates the T_c will go to zero before t_y reaches zero. In this strongly dimerised case and near half filling, the pairing is suppressed when the ladders decouple.

Another remarkable fact is that due to the interaction U, the Fermi pocket from the antibonding band is already removed in the normal state. This is shown in Fig. 11(c, d). The band structure is obtained by diagonalizing the following matrix

$$\begin{pmatrix} \varepsilon_{\alpha\alpha}(\mathbf{k}) + \mu + \Sigma_{\alpha\alpha}(\mathbf{k}, i\pi T) & \varepsilon_{\alpha\beta}(\mathbf{k}) + \Sigma_{\alpha\beta}(\mathbf{k}, i\pi T) \\ \varepsilon_{\beta\alpha}(\mathbf{k}) + \Sigma_{\beta\alpha}(\mathbf{k}, i\pi T) & \varepsilon_{\beta\beta}(\mathbf{k}) + \mu + \Sigma_{\beta\beta}(\mathbf{k}, i\pi T) \end{pmatrix}.$$

The band structure defined in this way (with self-energy at lowest Matsubara frequency) is a good approximation to that defined by the spectral function at low T and low energy (near the Fermi level). The gaps for the two bands have the opposite sign, and thus it is usually denoted as $s_\pm$ pairing.

Next, we show magnetic response function, i.e., the spin susceptibility. We have calculated the irreducible spin susceptibility in orbital space $\begin{pmatrix} \chi^{0,s}_{\alpha\alpha} & \chi^{0,s}_{\alpha\beta} \\ \chi^{0,s}_{\beta\alpha} & \chi^{0,s}_{\beta\beta} \end{pmatrix}$. Since $\chi^{0,s}_{\alpha\beta} = \chi^{0,s}_{\beta\alpha} < 0$ and $\chi^{0,s}_{\alpha\alpha} = \chi^{0,s}_{\beta\beta}$, this matrix has two eigen values $\chi^{0,s}_{+} = \chi^{0,s}_{\alpha\alpha} + \chi^{0,s}_{\alpha\beta}$ (bonding band) and $\chi^{0,s}_{-} = \chi^{0,s}_{\alpha\alpha} - \chi^{0,s}_{\alpha\beta}$ (antibonding band). The transformation coincides with the unitary transformation of the Hamiltonian from orbital to band space. The two eigen vectors of the unitary matrix can also be written as $(1, e^{iq_z})/\sqrt{2}$ for $q_z = 0$ and π, so we also denote the χ_+ (χ_-) as $q_z = 0$ ($q_z = \pi$) component. The RPA spin susceptibility is $\chi^s_\pm = \chi^s_\pm/(1 - U\chi^{0,s}_\pm)$. We plot the sum of these two RPA spin susceptibilities $\chi^s_+ + \chi^s_-$ in Fig. 12(a,b) for $\mathbf{q} = (\pi, \pi)$ vs real frequency. The analytic continuation from Matsubara frequency to real frequency is done by the Padé approximants. A noticeable difference between the strongly coupled ladder and weakly coupled

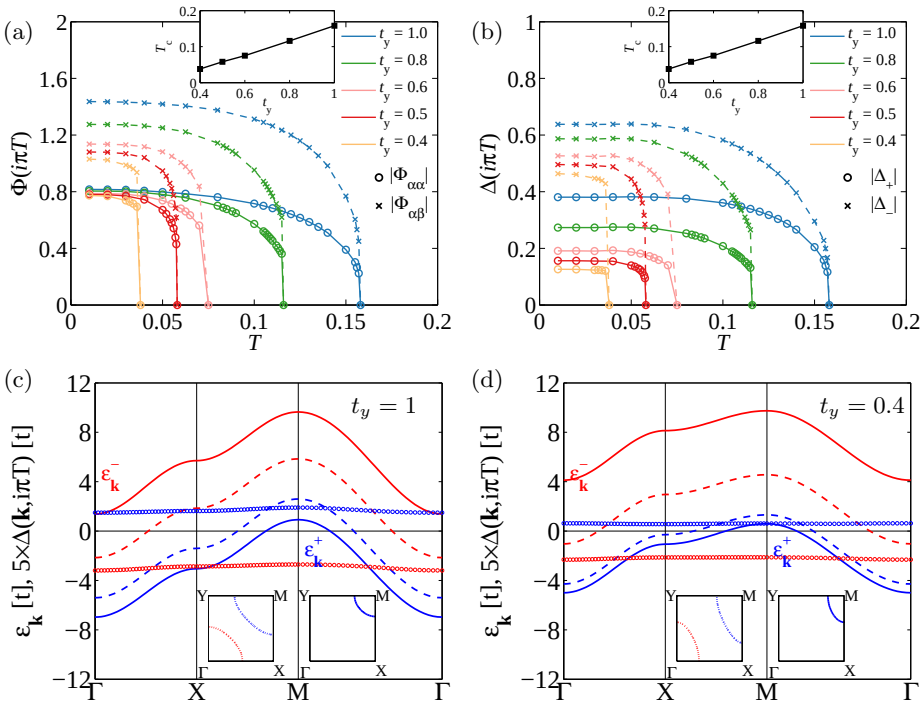

FIG. 11. (a) Anomalous self-energy in orbital space $\max_{\mathbf{k}\in \mathrm{BZ}} |\Phi(\mathbf{k}, i\pi T)|$ vs T, for different values of t_y, at a filling $n = 0.95$ and $U = 10$. (b) Superconducting gap function in band space $\max_{\mathbf{k}\in \mathrm{BZ}} |\Delta(\mathbf{k}, i\pi T)|$ vs T, for different values of t_y, at a filling $n = 0.95$ and $U = 10$. (c) Energy dispersions $\varepsilon_{\mathbf{k}}$ (lines) and superconducting gap function (circles) in band space along a high symmetry path for $t_y = 1$, $n = 0.95$, and $U = 10$ at $T = 0.01$. The dashed lines are the non-interacting bands and the solid lines are the interacting bands. The insets show the noninteracting Fermi surface (dashed lines) and interacting Fermi surface (solid lines), respectively. Blue: bonding band; red: antibonding band. (d) Similar to (c) but with $t_y = 0.4$.

ladder is the spin susceptibility is gapped at low frequency. The individual χ^s_+ and χ^s_- are plotted in Fig. 12(c)–(f). Since $\chi^{0,s}_{\alpha\beta} = \chi^{0,s}_{\beta\alpha} < 0$, the antibonding band spin susceptibility $\chi^{0,s}_- = \chi^{0,s}_{\alpha\alpha} - \chi^{0,s}_{\alpha\beta}$ is dominant. As a result, the energy gap in the normal state in the total spin susceptibility for $t_y = 0.4$ at M point [Fig. 12(b)] is clearly caused by the gap in antibonding band spin susceptibility [see Fig. 12(e) and (f)].

2. *a single ladder*

In this section, we show computation results for a single ladder ($t_y = 0$ case). We still use $t \equiv t_x = 1$ as the energy units. The hopping along the vertical rungs of the ladder is reduced to $t_\perp \equiv t_z = 1$. We study the system by (a) varying U value; (b) varying filling n; (c) coupling ladders with nonzero t_y hopping.

a. ***varying*** U ***value.*** We set $U = 4,\ 6,\ 8,\ 10$ and $n = 0.95$. The results are plotted in Fig. 13. The gaps for the two bands also have the opposite sign, and thus it is also $s_\pm$ pairing as in the bilayer case. However, the gaps in the ladder system change sign and have nodes in the momentum space. When Fourier transformed to real space, we see the nearest-neighbor pairing is strongest and has the oppositive sign in the x and y direction, representing a B_{1g}-like symmetry.[35] The RPA spin susceptibilities are plotted in Fig. 14. In the ladder system, near the half filling, the peak of the spin susceptibility is much shaper than the bilayer system, but peak position is at much lower energy and accordingly the energy gap in the susceptibility is smaller than the bilayer system.

b. ***varying filling*** n***.*** We set $U = 6$ and $n = 0.5$–1. In this part, we focus on the magnetic response function at low temperature $T = 0.01$. The RPA spin susceptibilities are plotted in Fig. 15(b). The noninteracting irreducible susceptibilities are plotted in Fig. 15(a) as a reference to the doping effect on the noninteracting band structure. Here, $q_z = 0$ ($q_z = \pi$) denotes the bonding (antibonding) band.

The low energy part $0 \le \omega \le 1$ of Fig. 15(b) is plotted in Fig. 16(a) (color map scale changed) to compare with the results by the computational method of density matrix renormalization group (DMRG). These two methods, FLEX and DMRG, give spin susceptibilities that agree quite well, especially for the $q_z = \pi$ component.

For the FLEX result in Fig. 16(a), $q_z = \pi$ (antibonding component), the three cases $n = 0.96$, $n = 0.92$, and

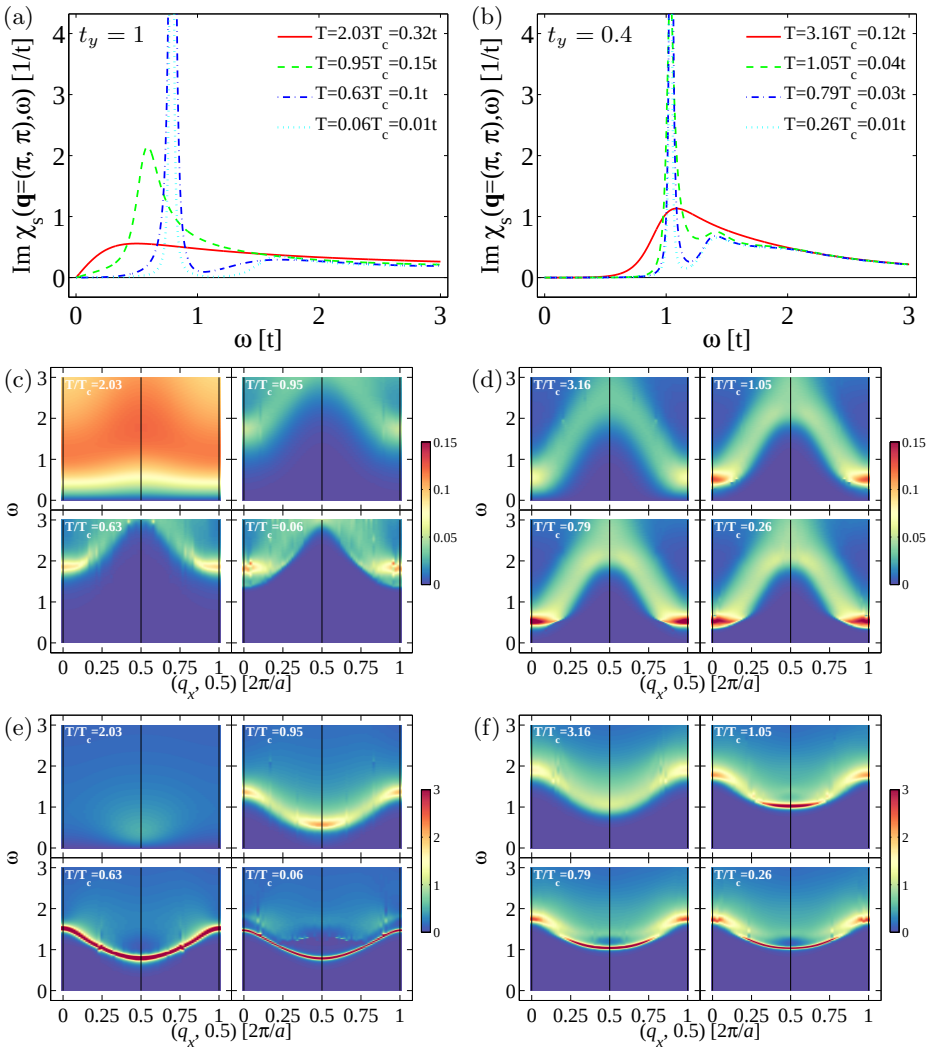

FIG. 12. (a) The RPA spin susceptibility $\chi^s_+(\mathbf{q},\omega) + \chi^s_-(\mathbf{q},\omega)$ at different temperatures in the normal and superconducting states at $\mathbf{q} = (\pi,\pi)$ point for $t_y = 1$, $n = 0.95$, and $U = 10$. (b) Similar to (a) but with $t_y = 0.4$. (c) and (e): RPA spin susceptibility $\chi^s_+(\mathbf{q},\omega)$ (bonding band) and $\chi^s_-(\mathbf{q},\omega)$ (antibonding band) along a path $\mathbf{q} = (q_x, q_y)$ where $q_y = \pi/a$ for $t_y = 1$, $n = 0.95$, and $U = 10$. (d) and (f): Similar to (c) and (e) but with $t_y = 0.4$

$n = 0.67$, are relatively different with others. We find these three cases are in the superconducting state while the others are in the normal state after inspecting the anomalous self-energies plotted in Fig. 17. The gap function is rather different near half filling and at low filling. We plot the momentum and real space gap in Fig. 18 for $n = 0.96$ (a, c) and $n = 0.67$ (b, d). The gap changes sign in momentum space near half filling and not at low filling. In real space, the nearest-neighbor pairing are equally strong in both x and y direction near half filling, but nearest-neighbor pairing is much weaker in x than in y direction at low filling.

c. ***coupling ladders.*** Finally, we set $t_y = 0,\ 0.1,\ 0.2,\ 0.3$ to study the influence of weak coupling between ladders on the magnetic response function. The results are plotted in Fig. 19. The energy gap in the RPA spin susceptibility tends to close at M point when t_y increases. Otherwise, in the energy range $0 \leq \omega \leq 3$, the effect of weak coupling ($t_y \leq 0.3$) between ladders is quite small.

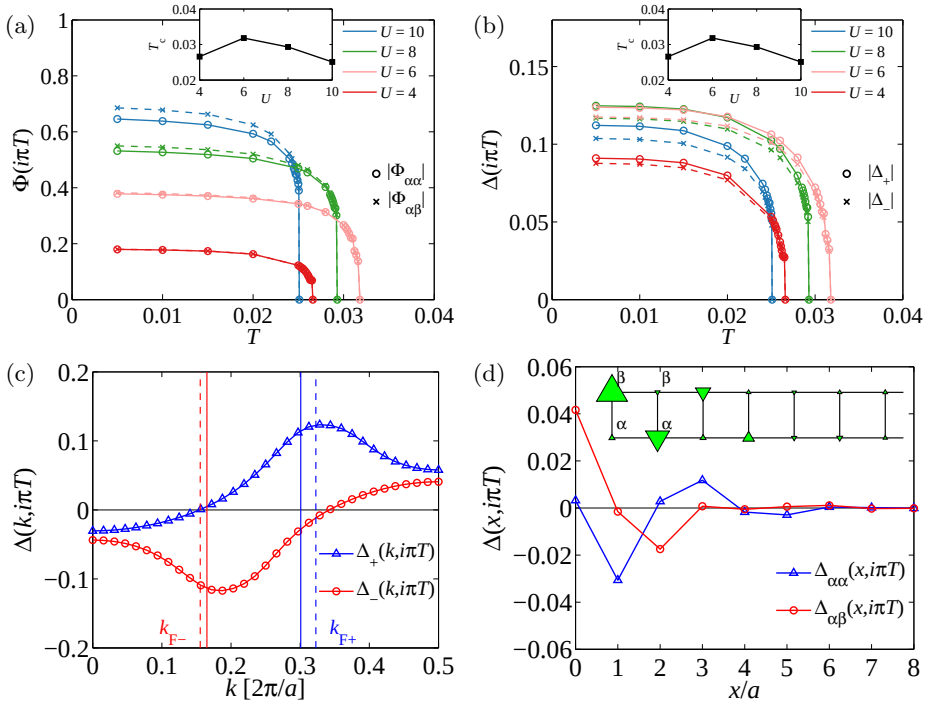

FIG. 13. (a) Anomalous self-energy in orbital space $\max_{\mathbf{k}\in \mathrm{BZ}} |\Phi(\mathbf{k}, i\pi T)|$ vs T, for different values of U, at a filling $n = 0.95$. (b) Superconducting gap function in band space $\max_{\mathbf{k}\in \mathrm{BZ}} |\Delta(\mathbf{k}, i\pi T)|$ vs T, for different values of U, at a filling $n = 0.95$. (c) Superconducting gap function in the band and momentum space for $U = 6$ and $T = 0.01$. The vertical lines show the noninteracting Fermi surface (dashed lines) and interacting Fermi surface (solid lines), respectively. Blue: bonding band; red: antibonding band. (d) Superconducting gap function in the orbital and real space (only the first nine lattice sites are shown) for $U = 6$ and $T = 0.01$. The inset is a pictorial representation of the pairing gap Δ_{ij} in the ladder system (only a part of full system is shown), where $i = 0$ and on the α-leg and j is on different lattice sites and ladder legs. The size of the triangle is proportional to $|\Delta_{ij}|$, while upward triangle means a positive gap and downward triangle means a negative gap.

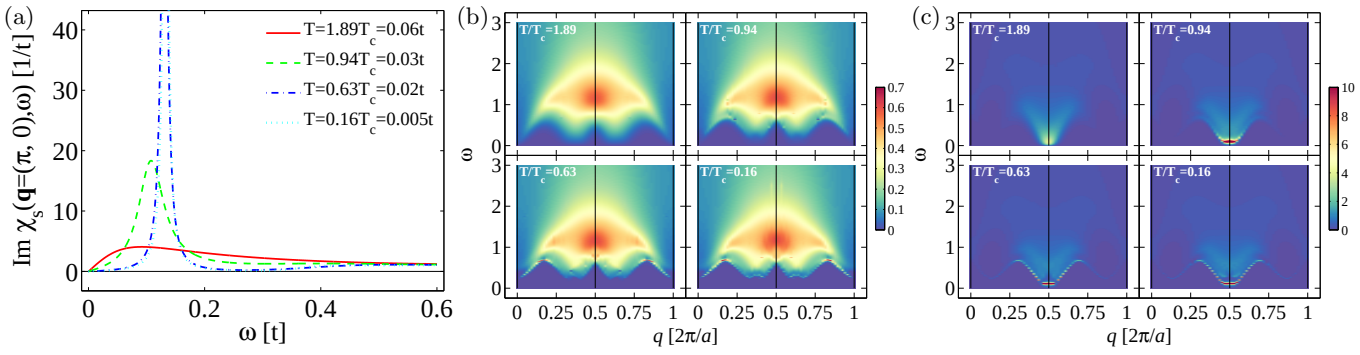

FIG. 14. (a) The RPA spin susceptibility $\chi^s_+(\mathbf{q}, \omega) + \chi^s_-(\mathbf{q}, \omega)$ at different temperatures in the normal and superconducting states at $\mathbf{q} = (\pi)$ point for $n = 0.95$ and $U = 6$. (b) and (c): RPA spin susceptibility $\chi^s_+(\mathbf{q}, \omega)$ (bonding band) and $\chi^s_-(\mathbf{q}, \omega)$ (antibonding band) along a path $\mathbf{q} = (q)$ for $n = 0.95$ and $U = 6$.

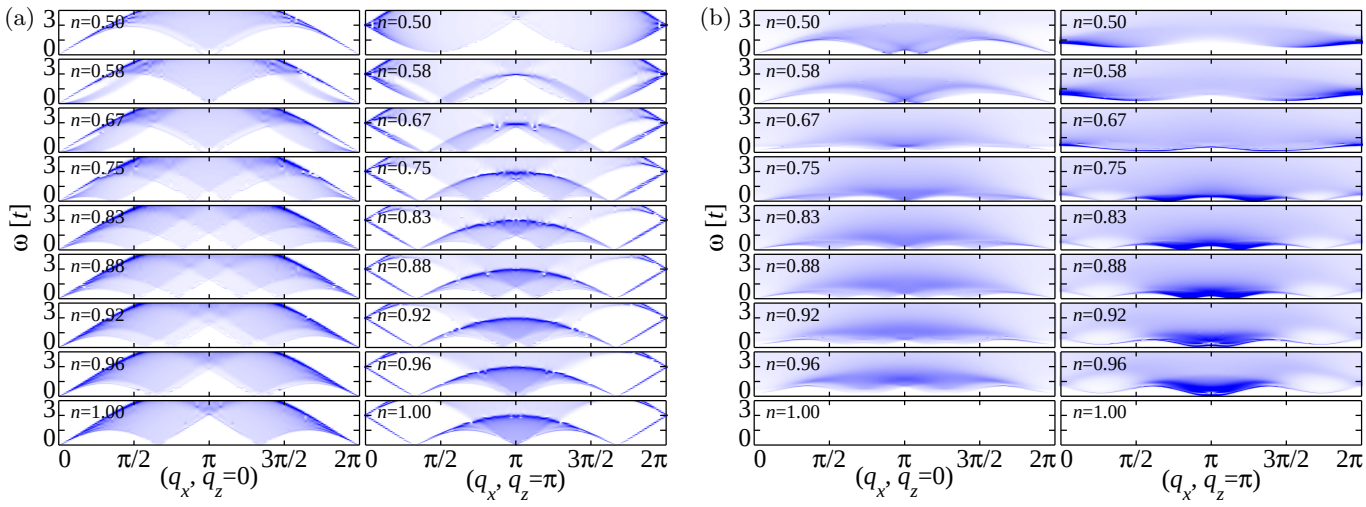

FIG. 15. RPA spin susceptibility for a single ladder system at $T = 0.01$ and different fillings n. (a) $U = 0$; (b) $U = 6$. $q_z = 0$ denotes $\chi^s_+(\mathbf{q},\omega)$ (bonding band) and $q_z = \pi$ denotes $\chi^s_-(\mathbf{q},\omega)$ (antibonding band). In (a) for $U = 0$, the RPA spin susceptibility is also the irreducible spin susceptibility. In (b), at the half filling $n = 1$, no data is plotted because the system reaches the magnetic instability at $T = 0.01$.

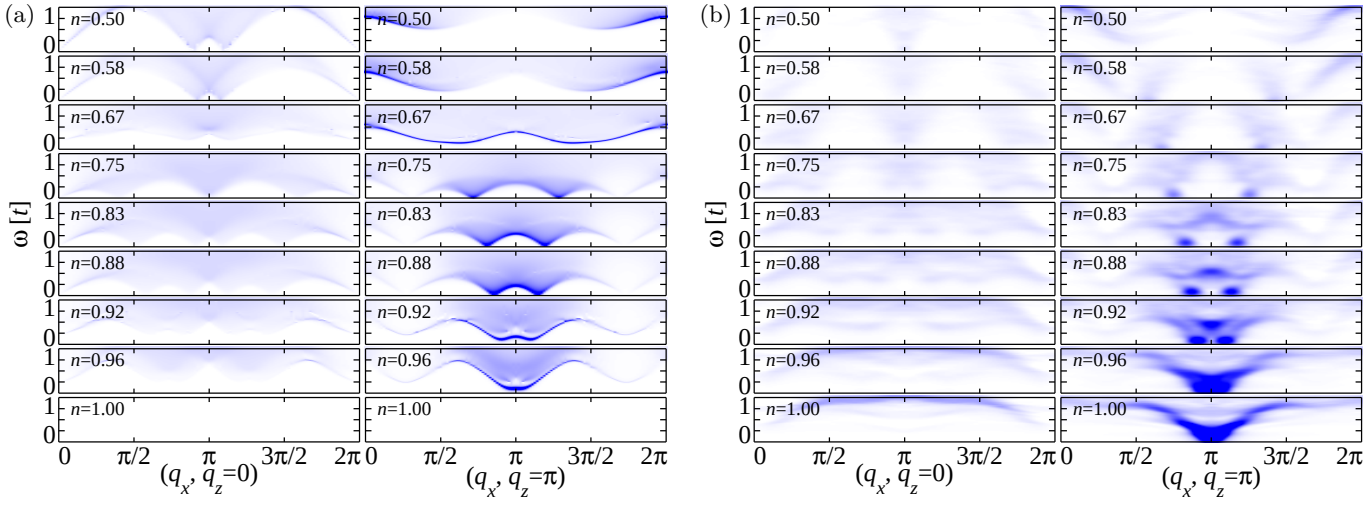

FIG. 16. RPA spin susceptibility for a single ladder system at $T = 0.01$, $U = 6$, and different fillings n. (a) FLEX results; (b) DMRG results. $q_z = 0$ denotes $\chi^s_+(\mathbf{q},\omega)$ (bonding band) and $q_z = \pi$ denotes $\chi^s_-(\mathbf{q},\omega)$ (antibonding band). In (a), at the half filling $n = 1$, no data is plotted because the system reaches the magnetic instability at $T = 0.01$ where FLEX in the current form does not give a converged result.

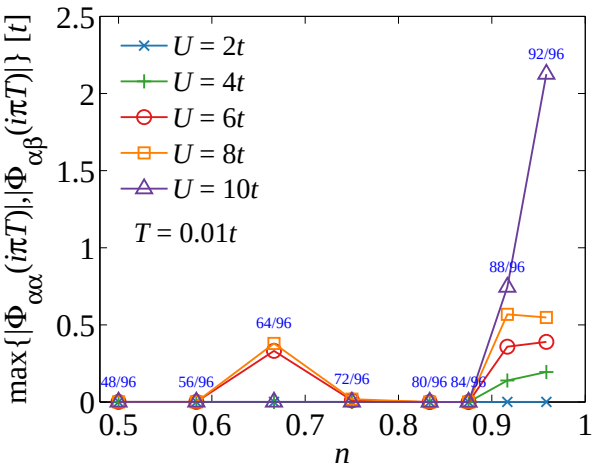

FIG. 17. The maximal anomalous self-energy at $T = 0.01$ vs filling n for various U. The blue numerals indicate a half of the total number of electrons in the 2×48 lattice system used in DMRG calculation.

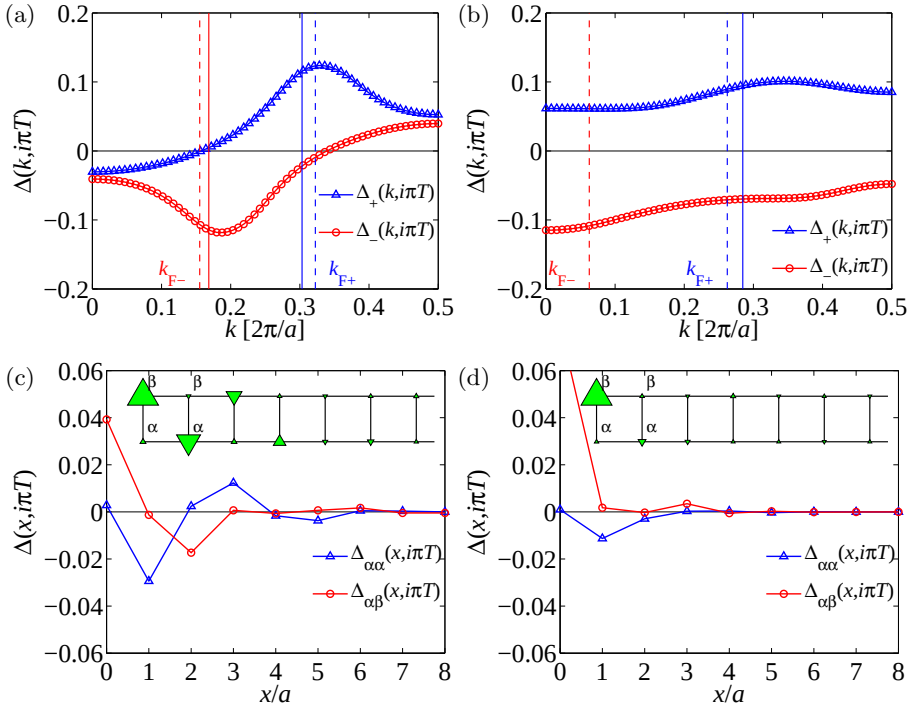

FIG. 18. Gap function in the band and momentum space for (a) $n = 0.96$ and (b) $n = 0.67$ and gap function in the orbital and real space for (c) $n = 0.96$ and (d) $n = 0.67$. $T = 0.01$ and $U = 6$.

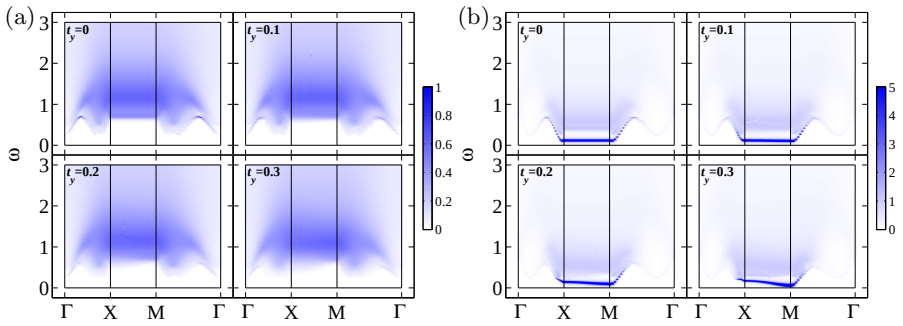

FIG. 19. RPA spin susceptibility (a) $\chi^s_+(\mathbf{q},\omega)$ (bonding band) and (b) $\chi^s_-(\mathbf{q},\omega)$ (antibonding band) along a high symmetry path for $n = 0.95$, $U = 6$, $T = 0.01$, and different values of t_y.

Appendix A: Aliasing correction to FFT computing Fourier integrals

The general problem arises from evaluating an integral with the integrand being a product of two function, one of which is highly oscillatory such as $\sin x$, $\cos x$, or e^{ix} as in the integral

$$f(i\omega_n) = \int_0^\beta e^{i\omega_n \tau} f(\tau) d\tau. \tag{A1}$$

The modern day method is Clenshaw-Curtis quadrature but the classical Filon's method[36] is suitable for our FFT algorithm. The key idea of Filon's method is to approximate $f(\tau)$ by a piecewise polynomial $g(\tau)$, either a Lagrange polynomial or a spline, and then integrate $e^{i\omega_n \tau} g(\tau)$ analytically; see Chap. 2.10.2 in Ref. 37.

We first discuss the use of Lagrange polynomial interpolation and the resulted Filon's integration formulae are analogous to Newton-Cotes formulae. For every order of Newton-Cotes formula (trapezoidal, quadratic, cubic, and so on), there is a corresponding Filon's formula. The implementation for trapezoidal order and cubic order is described in Chap. 13.9 in Press *et al.*[38] Ref. 13 uses trapezoidal order, which I find not satisfying in accuracy at low temperature. I have derived a quadratic order formula and implemented it. A side note: Press *et al.* and others believed a quadratic order formula requires two FFTs, which is not true, and thus they did not give a quadratic order formula. Sprung *et al.*[39] gave a more general derivation of the Filon's method so that a formula of arbitrary order can be obtained. In *Abramowitz & Stegun*,[40] Eq. (25.4.47) gives a quadratic order Filon's integration formula,[41] but it requires three FFTs. Nevertheless, nowhere in literature can I find the quadratic order formula I'll give below, so it needs to be triple-checked, if possible. [I will add the derivation of this formula later when I have time.]

Divide the interval $\tau \in [0, \beta]$ uniformly into N parts (even number preferred). Denote $\delta = \beta/N$, $\tau_l = (l-1)\delta$, where $1 \le l \le N+1$, and $\tilde{f}_l = e^{i\omega_n \tau_l} f(\tau_l)$. The Fourier integral $f(i\omega_n) = \int_0^\beta e^{i\omega_n \tau} f(\tau) d\tau$ can be calculated in quadratic order as

$$\begin{aligned} f(i\omega_n) =& (c_1 + c_2 + c_3) \sum_{l=1}^{N} \tilde{f}_l - (p_3 + c_3) V \\ &+ (s_1 - c_2 + p_3)\tilde{f}_1 + (s_2 - c_3)\tilde{f}_2 + s_3 \tilde{f}_3 + p_1 \tilde{f}_{N-1} + (p_2 - c_1)\tilde{f}_N, \end{aligned} \tag{A2}$$

where

$$\begin{aligned} V &= f(\tau = 0^+) - f(\tau = 0^-) = \tilde{f}_1 - \tilde{f}_{N+1}, \\ s_1 &= \frac{\delta}{4}[I_2(\delta) - 3I_1(\delta) + 2I_0(\delta)], \\ s_2 &= -\frac{\delta e^{-i\omega_n \delta}}{2}[I_2(\delta) - 2I_1(\delta)], \\ s_3 &= \frac{\delta e^{-2i\omega_n \delta}}{4}[I_2(\delta) - I_1(\delta)], \\ c_1 &= \frac{\delta}{4}[I_2(2\delta) - 3I_1(2\delta) + 2I_0(2\delta)], \\ c_2 &= -\frac{\delta e^{-i\omega_n \delta}}{2}[I_2(2\delta) - 2I_1(2\delta)], \\ c_3 &= \frac{\delta e^{-2i\omega_n \delta}}{4}[I_2(2\delta) - I_1(2\delta)], \\ p_1 &= \frac{\delta e^{i\omega_n \delta}}{4}[I_2(\delta) - I_1(\delta)], \\ p_2 &= -\frac{\delta}{2}[I_2(\delta) - I_0(\delta)], \\ p_3 &= \frac{\delta e^{-i\omega_n \delta}}{4}[I_2(\delta) + I_1(\delta)], \end{aligned}$$

where

$$\begin{aligned} I_0(u\delta) &= \int_0^{u\delta} e^{i\omega_n x} \frac{dx}{\delta} = \frac{e^{u\alpha} - 1}{\alpha}, \\ I_1(u\delta) &= \int_0^{u\delta} e^{i\omega_n x} \frac{x dx}{\delta^2} = \frac{u e^{u\alpha}}{\alpha} - \frac{e^{u\alpha} - 1}{\alpha^2}, \end{aligned}$$

$$I_3(u\delta) = \int_0^{u\delta} e^{i\omega_n x} \frac{x^2 dx}{\delta^3} = \frac{u^2 e^{u\alpha}}{\alpha} - \frac{2ue^{u\alpha}}{\alpha^2} + \frac{2(e^{u\alpha}-1)}{\alpha^3},$$
$$\alpha = i\omega_n \delta.$$

For a full frequency grid, the term $\sum_{l=1}^{N} \tilde{f}_l$ can be computed with one FFT (in $O(N \ln N)$ time), while other terms are easy to compute (in $O(N)$ time). This algorithm takes $O(N \ln N) + O(N)$ time, much faster than the brutal force that takes $O(N^2)$ time if N is large (i.e., low temperature).

Now, we discuss the use of spline interpolation, (called Filon-spline rule in Ref. 37). The use of cubic spline is discussed in detail in Ref. 42. It might be a better method than using a Lagrange polynomial in terms of numerical accuracy. Furthermore, according to Ref. 42, it is possible to choose the derivatives (spline interpolation requires derivatives be continuous) according to the rigrious sum rules for various quantities (Green's function and susceptibility) for Hubbard model. [More contents to be added.]

Appendix B: Derivations of other equations

1. Derivation of the solution to matrix Dyson's equation

We show some detailed derivation of the solution Eq. (58) to matrix Dyson's equation, Eq. (57). From Eq. (57), we find

$$\underline{F} = \underline{G}_0\underline{\Sigma}\underline{F} - \underline{G}_0\underline{\Phi}\underline{G}^* \Longrightarrow \underline{G}_0^{-1}\underline{F} = \underline{\Sigma}\underline{F} - \underline{\Phi}\underline{G}^* \Longrightarrow (\underline{G}_0^{-1} - \underline{\Sigma})\underline{F} = -\underline{\Phi}\underline{G}^* \Longrightarrow \underline{F} = -(\underline{G}_0^{-1} - \underline{\Sigma})^{-1}\underline{\Phi}\underline{G}^*.$$
$$\underline{G} = \underline{G}_0 + \underline{G}_0\underline{\Sigma}\underline{G} + \underline{G}_0\underline{\Phi}\underline{F}^* \Longrightarrow \underline{G}_0^{-1}\underline{G} = \mathbb{I} + \underline{\Sigma}\underline{G} + \underline{\Phi}(-\underline{G}_0^{*,-1} + \underline{\Sigma}^*)^{-1}\underline{\Phi}^*\underline{G} \Longrightarrow$$
$$[\underline{G}_0^{-1} - \underline{\Sigma} - \underline{\Phi}(-\underline{G}_0^{*,-1} + \underline{\Sigma}^*)^{-1}\underline{\Phi}^*]\underline{G} = \mathbb{I} \Longrightarrow \underline{G} = [\underline{G}_0^{-1} - \underline{\Sigma} - \underline{\Phi}(-\underline{G}_0^{*,-1} + \underline{\Sigma}^*)^{-1}\underline{\Phi}^*]^{-1}.$$

Next, plug the expression for $\underline{G}$ back into $\underline{F}$, and then use the identity $A^{-1}B^{-1} = (BA)^{-1}$ for two square matrices A and B, we find

$$\begin{aligned}
\underline{F} &= -(\underline{G}_0^{-1} - \underline{\Sigma})^{-1}\underline{\Phi}\underline{G}^* \\
&= -(\underline{G}_0^{-1} - \underline{\Sigma})^{-1}\underline{\Phi}[\underline{G}_0^{*,-1} - \underline{\Sigma}^* - \underline{\Phi}^*(-\underline{G}_0^{-1} + \underline{\Sigma})^{-1}\underline{\Phi}]^{-1} \\
&= -[(\underline{G}_0^{*,-1} - \underline{\Sigma}^*)\underline{\Phi}^{-1}(\underline{G}_0^{-1} - \underline{\Sigma}) - \underline{\Phi}^*(-\underline{G}_0^{-1} + \underline{\Sigma})^{-1}\underline{\Phi}\underline{\Phi}^{-1}(\underline{G}_0^{-1} - \underline{\Sigma})]^{-1} \\
&= -[(\underline{G}_0^{*,-1} - \underline{\Sigma}^*)\underline{\Phi}^{-1}(\underline{G}_0^{-1} - \underline{\Sigma}) + \underline{\Phi}^*]^{-1}.
\end{aligned}$$

Since $\underline{\Phi}$ is near singular near T_c for $T < T_c$ ($\underline{\Phi} = \mathbb{O}$ for $T > T_c$), one should avoid evaluating $\underline{\Phi}^{-1}$. Therefore, $\underline{F} = -(\underline{G}_0^{-1} - \underline{\Sigma})^{-1}\underline{\Phi}\underline{G}^*$ is recommended. Alternatively, using the Dyson's equation in the following form

$$\hat{\underline{G}}(k) = \hat{\underline{G}}_0(k) + \hat{\underline{G}}(k)\hat{\underline{\Sigma}}(k)\hat{\underline{G}}_0(k),$$

we find

$$\underline{F} = -\underline{G}\underline{\Phi}(\underline{G}_0^{*,-1} - \underline{\Sigma}^*)^{-1}.$$

We further discuss the symmetry of these matrices ($\underline{G}$, $\underline{F}$, $\underline{\Sigma}$, $\underline{\Phi}$) in orbital space. As shown before, for a system with time-reversal symmetry, inversion symmetry,[43] and for singlet pairing state, $\underline{G}(\mathbf{k}, i\omega_n)$ is symmetric and $\underline{F}(\mathbf{k}, i\omega_n)$ is hermitian. That is,

$$\underline{G}(\mathbf{k}, i\omega_n) = \underline{G}^t(\mathbf{k}, i\omega_n) \Longleftrightarrow G_{ab}(\mathbf{k}, i\omega_n) = G_{ba}(\mathbf{k}, i\omega_n) \Longleftrightarrow \underline{G}^*(\mathbf{k}, i\omega_n) = \underline{G}^\dagger(\mathbf{k}, i\omega_n),$$
$$\underline{F}(\mathbf{k}, i\omega_n) = \underline{F}^\dagger(\mathbf{k}, i\omega_n) \Longleftrightarrow F_{ab}(\mathbf{k}, i\omega_n) = F^*_{ba}(\mathbf{k}, i\omega_n) \Longleftrightarrow \underline{F}^*(\mathbf{k}, i\omega_n) = \underline{F}^t(\mathbf{k}, i\omega_n).$$

Therefore, $\underline{\Sigma}(\mathbf{k}, i\omega_n)$ is symmetric and $\underline{\Phi}(\mathbf{k}, i\omega_n)$ is hermitian as well. This can be shown by solving $\underline{\Sigma}(\mathbf{k}, i\omega_n)$ and $\underline{\Phi}(\mathbf{k}, i\omega_n)$ from $\underline{G}(\mathbf{k}, i\omega_n)$ and $\underline{F}(\mathbf{k}, i\omega_n)$.

$$\left.\begin{aligned}
\underline{F} = \underline{G}_0\underline{\Sigma}\underline{F} - \underline{G}_0\underline{\Phi}\underline{G}^* \Longrightarrow \underline{G}_0\underline{\Phi} = (\underline{G}_0\underline{\Sigma} - \mathbb{I})\underline{F}\underline{G}^{*,-1} \\
\underline{G} = \underline{G}_0 + \underline{G}_0\underline{\Sigma}\underline{G} + \underline{G}_0\underline{\Phi}\underline{F}^*
\end{aligned}\right\}$$
$$\Longrightarrow \underline{G} = \underline{G}_0 + \underline{G}_0\underline{\Sigma}\underline{G} + (\underline{G}_0\underline{\Sigma} - \mathbb{I})\underline{F}\underline{G}^{*,-1}\underline{F}^*$$
$$\Longrightarrow \underline{G} + \underline{F}\underline{G}^{*,-1}\underline{F}^* - \underline{G}_0 = \underline{G}_0\underline{\Sigma}(\underline{G} + \underline{F}\underline{G}^{*,-1}\underline{F}^*)$$
$$\Longrightarrow \underline{\Sigma} = \underline{G}_0^{-1} - (\underline{G} + \underline{F}\underline{G}^{*,-1}\underline{F}^*)^{-1}.$$

For $\underline{G} + \underline{F}\underline{G}^{*,-1}\underline{F}^*$ to be invertible, $\det(\underline{G} + \underline{F}\underline{G}^{*,-1}\underline{F}^*) \neq 0 \Longleftrightarrow \det(\mathbb{I} + \underline{G}^{-1}\underline{F}\underline{G}^{*,-1}\underline{F}^*) \neq 0$. Similarly, we find

$$\underline{\Phi} = (\underline{\Sigma} - \underline{G}_0^{-1})\underline{F}\underline{G}^{*,-1} = -(\underline{G} + \underline{F}\underline{G}^{*,-1}\underline{F}^*)^{-1}\underline{F}\underline{G}^{*,-1}.$$

Now, we show $\underline{\Sigma}(\mathbf{k}, i\omega_n)$ is symmetric and $\underline{\Phi}(\mathbf{k}, i\omega_n)$ is hermitian. For $\underline{\Sigma}(\mathbf{k}, i\omega_n)$,

$$\begin{aligned}
\underline{\Sigma} &= \underline{G}_0^{-1} - (\underline{G} + \underline{F}\underline{G}^{*,-1}\underline{F}^*)^{-1} \Longrightarrow \\
\underline{\Sigma}^t &= \underline{G}_0^{t,-1} - (\underline{G}^t + \underline{F}^\dagger\underline{G}^{\dagger,-1}\underline{F}^t)^{-1} \\
&= \underline{G}_0^{-1} - (\underline{G} + \underline{F}\underline{G}^{*,-1}\underline{F}^*)^{-1} = \underline{\Sigma}.
\end{aligned}$$

For $\underline{\Phi}(\mathbf{k}, i\omega_n)$,

$$\underline{\Phi} = -(\underline{G} + \underline{F}\underline{G}^{*,-1}\underline{F}^*)^{-1}\underline{F}\underline{G}^{*,-1} \Longrightarrow$$

$$
\begin{aligned}
\underline{\Phi}^\dagger &= -\underline{G}^{t,-1}\underline{F}^\dagger(\underline{G}^\dagger + \underline{F}^t\underline{G}^{t,-1}\underline{F}^\dagger)^{-1} \\
&= -\underline{G}^{-1}\underline{F}(\underline{G}^* + \underline{F}^*\underline{G}^{-1}\underline{F})^{-1} \\
&= -(\underline{G} + \underline{F}\underline{G}^{*,-1}\underline{F}^*)^{-1}(\underline{G} + \underline{F}\underline{G}^{*,-1}\underline{F}^*)\underline{G}^{-1}\underline{F}(\underline{G}^* + \underline{F}^*\underline{G}^{-1}\underline{F})^{-1} \\
&= -(\underline{G} + \underline{F}\underline{G}^{*,-1}\underline{F}^*)^{-1}(\underline{F} + \underline{F}\underline{G}^{*,-1}\underline{F}^*\underline{G}^{-1}\underline{F})(\underline{G}^* + \underline{F}^*\underline{G}^{-1}\underline{F})^{-1} \\
&= -(\underline{G} + \underline{F}\underline{G}^{*,-1}\underline{F}^*)^{-1}\underline{F}\underline{G}^{*,-1}(\underline{G}^* + \underline{F}^*\underline{G}^{-1}\underline{F})(\underline{G}^* + \underline{F}^*\underline{G}^{-1}\underline{F})^{-1} \\
&= -(\underline{G} + \underline{F}\underline{G}^{*,-1}\underline{F}^*)^{-1}\underline{F}\underline{G}^{*,-1} = \underline{\Phi}.
\end{aligned}
$$

2. Index symmetry of RPA susceptibility matrix

We prove the symmetry relation

$$\chi^s_{l_1l_2,l_3l_4}(q) = \chi^s_{l_4l_3,l_2l_1}(-q),$$

for RPA spin susceptibility $\underline{\chi}^s = (\mathbb{I} - \underline{\chi}^{0,s}\underline{U}^s)^{-1}\underline{\chi}^{0,s}$. A similar relation $\chi^c_{l_1l_2,l_3l_4}(q) = \chi^c_{l_4l_3,l_2l_1}(-q)$ holds for charge susceptibility $\underline{\chi}^c = (\mathbb{I} + \underline{\chi}^{0,c}\underline{U}^c)^{-1}\underline{\chi}^{0,c}$.

First, we show the irreducible susceptibility $\chi^{0,s}_{l_1l_2,l_3l_4}(q) = \chi^{0,s}_{l_4l_3,l_2l_1}(-q)$.

$$
\begin{aligned}
\chi^{0,s}_{l_1l_2,l_3l_4}(\mathbf{r},\tau) &= G_{l_1l_3}(\mathbf{r},\tau)G_{l_4l_2}(\mathbf{r},\beta-\tau) - F_{l_1l_4}(\mathbf{r},\tau)F_{l_3l_2}(\mathbf{r},\tau) \Longrightarrow \\
\chi^{0,s}_{l_4l_3,l_2l_1}(-\mathbf{r},-\tau) &= G_{l_4l_2}(-\mathbf{r},-\tau)G_{l_1l_3}(-\mathbf{r},\beta+\tau) - F_{l_4l_1}(-\mathbf{r},-\tau)F_{l_2l_3}(-\mathbf{r},-\tau) \\
&= G_{l_1l_3}(\mathbf{r},\tau)G_{l_4l_2}(\mathbf{r},\beta-\tau) - F_{l_1l_4}(\mathbf{r},\tau)F_{l_3l_2}(\mathbf{r},\tau) \\
&= \chi^{0,s}_{l_1l_2,l_3l_4}(\mathbf{r},\tau) \Longrightarrow \\
\chi^{0,s}_{l_1l_2,l_3l_4}(q) &= \chi^{0,s}_{l_4l_3,l_2l_1}(-q).
\end{aligned}
$$

Next, we write

$$
\begin{aligned}
\underline{\chi}^s = (\mathbb{I} - \underline{\chi}^{0,s}\underline{U}^s)^{-1}\underline{\chi}^{0,s} &= \sum_{n=0}^{\infty}\underline{\chi}^{n,s} \\
\underline{\chi}^{n,s} = \underline{\chi}^{n-1,s}\underline{U}^s\underline{\chi}^{0,s} &= \underline{\chi}^{0,s}\underline{U}^s\underline{\chi}^{n-1,s} \quad (\text{for } n \geq 1).
\end{aligned}
$$

To prove $\chi^s_{l_1l_2,l_3l_4}(q) = \chi^s_{l_4l_3,l_2l_1}(-q)$, we show

$$\chi^{n,s}_{l_1l_2,l_3l_4}(q) = \chi^{n,s}_{l_4l_3,l_2l_1}(-q) \quad (\text{for } n \geq 0).$$

This can be done with the method of mathematical induction. For $n = 0$, the above is true. Assume $n-1$ is true, then

$$
\begin{aligned}
\chi^{n,s}_{l_1l_2,l_3l_4}(q) &= \sum_{l_{1'},l_{2'},l_{3'},l_{4'}} \chi^{n-1,s}_{l_1l_2,l_{1'}l_{2'}}(q)U^s_{l_{1'}l_{2'},l_{3'}l_{4'}}\chi^{0,s}_{l_{3'}l_{4'},l_3l_4}(q) \\
&= \sum_{l_{1'},l_{2'},l_{3'},l_{4'}} \chi^{n-1,s}_{l_{2'}l_{1'},l_2l_1}(-q)U^s_{l_{4'}l_{3'},l_{2'}l_{1'}}\chi^{0,s}_{l_4l_3,l_4'l_{3'},}(-q) \\
&= \sum_{l_{1'},l_{2'},l_{3'},l_{4'}} \chi^{0,s}_{l_4l_3,l_4'l_{3'},}(-q)U^s_{l_{4'}l_{3'},l_{2'}l_{1'}}\chi^{n-1,s}_{l_{2'}l_{1'},l_2l_1}(-q) = \chi^{n,s}_{l_4l_3,l_2l_1}(-q).
\end{aligned}
$$

Therefore, we have proved $\chi^s_{l_1l_2,l_3l_4}(q) = \chi^s_{l_4l_3,l_2l_1}(-q)$. It is easy to see that the effective interaction follows the same symmetry. This symmetry is not used in the calculation but they can be used to check the results. The symmetry $\chi^{s/c}_{l_1l_2,l_3l_4}(q) = \chi^{s/c}_{l_3l_4,l_1l_2}(q)$, i.e., that the susceptibility matrix is symmetric $\underline{\chi}^{s/c}_{A,B} = \underline{\chi}^{s/c}_{B,A}$, where $A = (l_1l_2)$ and $B = (l_3l_4)$, is used in the calculation.

Appendix C: Calculation of filling and Hartree-Fock self-energy

The calculations of filling and (intra-orbital) Hartree-Fock self-energy need to be dealt with care using the Green's function in frequency space because of the long tail that decays as $(i\omega_n)^{-1}$ that needs some regulation to obtain the

correct convergent sum over the frequencies (or, equivalently, one can consider that it is due to the discontinuity of Green's function in imaginary time τ space at $\tau = 0$, a consequence of the fundamental commutation relation of the fermion operators).

The formulae to calculate the filling (two spins) for each orbital (n_a) and for the total (n) are

$$n_a = \frac{2}{N}\sum_{\mathbf{k}} G_{aa}(\mathbf{k}, \tau = 0^-) = \frac{2T}{N}\sum_{\mathbf{k},n} G_{aa}(\mathbf{k}, i\omega_n)e^{-i\omega_n 0^-} = \frac{2T}{N}\sum_{\mathbf{k},n} G_{aa}(\mathbf{k}, i\omega_n)e^{i\omega_n 0^+}, \tag{C1a}$$

$$n = \sum_a n_a. \tag{C1b}$$

The formulae to calculate the Hartree-Fock self-energy are

$$\Sigma^{\mathrm{HF}}_{ab} = \frac{T}{N}\sum_{a'b'}\sum_{\mathbf{k},n}\left(\frac{3}{2}U^s_{aa',bb'} - \frac{1}{2}U^c_{aa',bb'}\right) G_{a'b'}(\mathbf{k}, i\omega_n)e^{i\omega_n 0^+}, \tag{C2a}$$

$$\Phi^{\mathrm{HF}}_{ab} = \frac{T}{N}\sum_{a'b'}\sum_{\mathbf{k},n}\left(\frac{1}{2}U^s_{aa',b'b} + \frac{1}{2}U^c_{aa',b'b}\right) F_{a'b'}(\mathbf{k}, i\omega_n)e^{i\omega_n 0^+}. \tag{C2b}$$

The above equations all involve calculating the frequency sum $S(\tau = 0^-) = \lim_{\tau\to 0^-} T\sum_{n=-\infty}^{\infty} g(i\omega_n)e^{-i\omega_n\tau}$. If $S(\tau = 0^-) \neq S(\tau = 0^+)$, (i) the order of $\lim_{\tau\to 0^-}$ and $\sum_{n=-\infty}^{\infty}$ cannot be interchanged and (ii) $\sum_{n=-\infty}^{\infty}$ cannot be replaced by a sum $\sum_{n=-N_c}^{N_c-1}$ with a finite cut-off N_c. (i) and (ii) can be easily proved by the method of *reductio ad absurdum*: (i) We interchange the order of the sum and limit, and take the limit first, then both $S(\tau = 0^-) = S(\tau = 0^+) = T\sum_{n=-\infty}^{\infty} g(i\omega_n)$; (ii) We cut-off the sum with N_c, then the limit and the finite sum can be interchanged, again, this leads to $S(\tau = 0^-) = S(\tau = 0^+) = T\sum_{n=-N_c}^{N_c-1} g(i\omega_n)$.

Therefore, to deal with the limit, we use a theorem for Fourier transform, that is, $[S(\tau = 0^-) + S(\tau = 0^+)]/2 = S(0) \equiv T\sum_{n=-\infty}^{\infty} g(i\omega_n)$. Then, we calculate $S(0)$ with a finite cut-off N_c. Furthermore, since $S(\tau = 0^-) - S(\tau = 0^+)$ can be found using the fundamental commutation relation of the fermion operators, $S(\tau = 0^-)$ can be solved. Note that, contradict to the usual claim, the sum $\sum_{n=-\infty}^{\infty} g(i\omega_n)$ does converge in the sense that the limit $\lim_{N_c\to\infty}\sum_{n=-N_c}^{N_c-1} g(i\omega_n)$ exists [the logarithmic divergence due to $(i\omega_n)^{-1}$ cancels out from the sum over $\omega_n < 0$ and $\omega_n > 0$]; however, the convergence is slow. Another method showing better convergence is to subtract the high frequency pole from the sum:

$$\begin{aligned} S(\tau = 0^-) &= \lim_{\tau\to 0^-} T\sum_{n=-\infty}^{\infty}\left[g(i\omega_n) - \frac{g^\infty}{i\omega_n - \xi}\right]e^{-i\omega_n\tau} + \lim_{\tau\to 0^-} T\sum_{n=-\infty}^{\infty}\frac{g^\infty}{i\omega_n - \xi}e^{-i\omega_n\tau} \\ &= T\sum_{n=-\infty}^{\infty}\lim_{\tau\to 0^-}\left[g(i\omega_n) - \frac{g^\infty}{i\omega_n - \xi}\right]e^{-i\omega_n\tau} + g^\infty n_{\mathrm{F}}(\xi) \\ &= T\sum_{n=-N_c}^{N_c-1}\left[g(i\omega_n) - \frac{g^\infty}{i\omega_n - \xi}\right] + g^\infty n_{\mathrm{F}}(\xi). \end{aligned} \tag{C3}$$

The interchange of the limit and the sum in the first term is because it converges faster after the subtraction (this proof given here is not rigorous). The Fermi distribution function $n_{\mathrm{F}}(\xi)$ in the second term is obtained by first completing the sum with the method of contour integral then taking the limit $\tau \to 0^-$ (the calculation of the contour integral also involve a limit that requires the convergence factor $e^{-z\tau}$).

Now we investigate which term in the formulae for calculating the filling or the Hartree-Fock self-energy has the discontinuity at $\tau = 0$ so that we must do the subtraction trick. First, we consider the *orbital occupancy factors*

$$n^\sigma_{ab}(\mathbf{k}) = G^\sigma_{ab}(\mathbf{k}, \tau = 0^-) = -\lim_{\tau\to 0^-}\langle T_\tau c_{\mathbf{k}a\sigma}(\tau)c^\dagger_{\mathbf{k}b\sigma}(0)\rangle = +\lim_{\tau\to 0^-}\langle c^\dagger_{\mathbf{k}b\sigma}(0)c_{\mathbf{k}a\sigma}(\tau)\rangle = \langle c^\dagger_{\mathbf{k}b\sigma}c_{\mathbf{k}a\sigma}\rangle.$$

In the last step, we have used $c_{\mathbf{k}a\sigma}(\tau) = e^{\mathcal{H}\tau}c_{\mathbf{k}a\sigma}e^{-\mathcal{H}\tau}$ and

$$\lim_{\tau\to 0^-} c_{\mathbf{k}a\sigma}(\tau) = \lim_{\tau\to 0^-}\left(e^{\mathcal{H}\tau}c_{\mathbf{k}a\sigma}e^{-\mathcal{H}\tau}\right) = \left(\lim_{\tau\to 0^-} e^{\mathcal{H}\tau}\right)c_{\mathbf{k}a\sigma}\left(\lim_{\tau\to 0^-} e^{-\mathcal{H}\tau}\right) = c_{\mathbf{k}a\sigma},$$

where $\lim_{\tau\to 0^-} e^{\pm\mathcal{H}\tau}$ equals the identity operator. Similarly, we find

$$G^\sigma_{ab}(\mathbf{k}, \tau = 0^+) = -\lim_{\tau\to 0^+}\langle T_\tau c_{\mathbf{k}a\sigma}(\tau)c^\dagger_{\mathbf{k}b\sigma}(0)\rangle = -\lim_{\tau\to 0^+}\langle c_{\mathbf{k}a\sigma}(\tau)c^\dagger_{\mathbf{k}b\sigma}(0)\rangle = -\langle c_{\mathbf{k}a\sigma}c^\dagger_{\mathbf{k}b\sigma}\rangle.$$

Since the operators satisfy the fundamental commutation relation

$$[c^\dagger_{\mathbf{k}b\sigma}, c_{\mathbf{k}a\sigma}]_+ = c^\dagger_{\mathbf{k}b\sigma} c_{\mathbf{k}a\sigma} + c_{\mathbf{k}a\sigma} c^\dagger_{\mathbf{k}b\sigma} = \delta_{ab},$$

we find

$$G^\sigma_{ab}(\mathbf{k}, \tau = 0^-) - G^\sigma_{ab}(\mathbf{k}, \tau = 0^+) = \delta_{ab}. \tag{C4}$$

Furthermore, we define

$$G^\sigma_{ab}(\mathbf{k}, \tau = 0) \equiv \sum_{n=-\infty}^{\infty} G^\sigma_{ab}(\mathbf{k}, i\omega_n) = \frac{1}{2}[G^\sigma_{ab}(\mathbf{k}, \tau = 0^-) + G^\sigma_{ab}(\mathbf{k}, \tau = 0^+)] = n^\sigma_{ab}(\mathbf{k}) - \frac{1}{2}\delta_{ab}. \tag{C5}$$

Or, after a summation of spin index,

$$\sum_\sigma G^\sigma_{ab}(\mathbf{k}, \tau = 0) = n_{ab}(\mathbf{k}) - \delta_{ab}, \tag{C6}$$

where $n_{ab}(\mathbf{k}) = n^\sigma_{ab}(\mathbf{k}) + n^{\bar{\sigma}}_{ab}(\mathbf{k})$.

For the anomalous Green's function, we find

$$F^{\sigma\sigma'}_{ab}(\mathbf{k}, 0^-) = -\lim_{\tau\to 0^-} \langle T_\tau c_{\mathbf{k}a\sigma}(\tau) c_{-\mathbf{k}b\sigma'}(0)\rangle = +\lim_{\tau\to 0^-} \langle c_{-\mathbf{k}b\sigma'}(0) c_{\mathbf{k}a\sigma}(\tau)\rangle = \langle c_{-\mathbf{k}b\sigma'} c_{\mathbf{k}a\sigma}\rangle,$$

and

$$F^{\sigma\sigma'}_{ab}(\mathbf{k}, 0^+) = -\lim_{\tau\to 0^+} \langle T_\tau c_{\mathbf{k}a\sigma}(\tau) c_{-\mathbf{k}b\sigma'}(0)\rangle = -\lim_{\tau\to 0^+} \langle c_{\mathbf{k}a\sigma}(\tau) c_{-\mathbf{k}b\sigma'}(0)\rangle = -\langle c_{\mathbf{k}a\sigma} c_{-\mathbf{k}b\sigma'}\rangle.$$

Because of the fundamental commutation relation

$$[c_{\mathbf{k}a\sigma}, c_{\mathbf{k}'a'\sigma'}]_+ = c_{\mathbf{k}a\sigma} c_{\mathbf{k}'a'\sigma'} + c_{\mathbf{k}'a'\sigma'} c_{\mathbf{k}a\sigma} = 0,$$

we find

$$F^{\sigma\sigma'}_{ab}(\mathbf{k}, 0^-) = F^{\sigma\sigma'}_{ab}(\mathbf{k}, 0^+), \tag{C7}$$

and naturally we have

$$F^{\sigma\sigma'}_{ab}(\mathbf{k}, 0) = F^{\sigma\sigma'}_{ab}(\mathbf{k}, 0^-) = F^{\sigma\sigma'}_{ab}(\mathbf{k}, 0^+) = \sum_{n=-\infty}^{\infty} F^{\sigma\sigma'}_{ab}(\mathbf{k}, i\omega_n) \equiv n^{\mathrm{F},\sigma\sigma'}_{ab}(\mathbf{k}). \tag{C8}$$

To sum up,

$$G^\sigma_{ab}(\mathbf{k}, \tau = 0^-) = n^\sigma_{ab}(\mathbf{k}) = \frac{1}{2} n_{ab}(\mathbf{k}), \tag{C9a}$$

$$G^\sigma_{ab}(\mathbf{k}, \tau = 0^+) = n^\sigma_{ab}(\mathbf{k}) - \delta_{ab}, \tag{C9b}$$

$$G^\sigma_{ab}(\mathbf{k}, \tau = 0) \equiv n^\sigma_{ab}(\mathbf{k}) - \frac{1}{2}\delta_{ab} = \frac{1}{2}\left[n_{ab}(\mathbf{k}) - \delta_{ab}\right]. \tag{C9c}$$

$$F^{\sigma\bar{\sigma}}_{ab}(\mathbf{k}, \tau = 0^-) = F^{\sigma\bar{\sigma}}_{ab}(\mathbf{k}, \tau = 0^+) \equiv n^{F,\sigma}_{ab}(\mathbf{k}), \tag{C9d}$$

$$F^{\sigma\bar{\sigma}}_{ab}(\mathbf{k}, \tau = 0) \equiv n^{F,\sigma}_{ab}(\mathbf{k}). \tag{C9e}$$

In Eq. (C9c) and Eq. (C9e), the Fourier sum with $\tau = 0$ in the convergence factor $e^{-i\omega_n\tau}$ can be used to calculate orbital occupancy number $\underline{n}^\sigma(\mathbf{k})$, $\underline{n}^{F,\sigma}(\mathbf{k})$, the filling matrix in orbital space $\underline{n} \equiv \frac{2}{N}\sum_{\mathbf{k}} \underline{n}^\sigma(\mathbf{k})$, and the total filling

$$n = \frac{2}{N}\sum_{\mathbf{k}} \mathrm{Tr}\, \underline{n}^\sigma(\mathbf{k}) = \frac{2}{N}\sum_{\mathbf{k},l} n^\sigma_{ll}(\mathbf{k}) = 2\sum_l n^\sigma_{ll}, \tag{C10}$$

albeit the slow convergence with respect to the cut-off N_c. The subtraction technique with better convergence becomes very complicated in orbital space and with anomalous self-energy; we describe this method below although we don't use it currently in the computing code.

First, we simplify the Hartree-Fock self-energy using the definition of the interaction matrix Eq. (65)

$$U^s_{aa,aa} = U, \quad U^s_{ab,ab} = U', \quad U^s_{aa,bb} = J, \quad U^s_{ab,ba} = J';$$

$$U^c_{aa,aa} = U, \quad U^c_{ab,ab} = 2J - U', \quad U^c_{aa,bb} = 2U' - J, \quad U^c_{ab,ba} = J',$$

where $a \neq b$. Plug it in the formulae for the Hartree-Fock self-energy

$$\begin{aligned}
\Sigma^{\mathrm{HF}}_{ab} &= \frac{T}{N}\sum_{a'b'}\sum_{\mathbf{k},n}\left(\frac{3}{2}U^s_{aa',bb'} - \frac{1}{2}U^c_{aa',bb'}\right) G_{a'b'}(\mathbf{k}, i\omega_n)e^{i\omega_n 0^+}, \\
&= \sum_{a'b'}\left(\frac{3}{2}U^s_{aa',bb'} - \frac{1}{2}U^c_{aa',bb'}\right) n^{\sigma}_{a'b'} \\
\Phi^{\mathrm{HF}}_{ab} &= \frac{T}{N}\sum_{a'b'}\sum_{\mathbf{k},n}\left(\frac{1}{2}U^s_{aa',b'b} + \frac{1}{2}U^c_{aa',b'b}\right) F_{a'b'}(\mathbf{k}, i\omega_n)e^{i\omega_n 0^+} \\
&= \sum_{a'b'}\left(\frac{1}{2}U^s_{aa',b'b} + \frac{1}{2}U^c_{aa',b'b}\right) n^{F,\sigma}_{a'b'},
\end{aligned}$$

and then we find

$$\Sigma^{\mathrm{HF}}_{aa} = (2U' - J)\frac{n}{2} + (U - 2U' + J)n^{\sigma}_{aa}, \tag{C11a}$$

$$\Sigma^{\mathrm{HF}}_{ab} = (2J - U')n^{\sigma}_{ab} + J'n^{\sigma}_{ba} = (2J - U' + J')n^{\sigma}_{ab} = \Sigma^{\mathrm{HF}}_{ba}; \tag{C11b}$$

$$\Phi^{\mathrm{HF}}_{aa} = Jn^{F,\sigma} + (U - J)n^{F,\sigma}_{aa}, \tag{C11c}$$

$$\Phi^{\mathrm{HF}}_{ab} = U'n^{F,\sigma}_{ab} + J'n^{F,\sigma}_{ba} = (U' + J')n^{F,\sigma}_{ab} = \Phi^{\mathrm{HF}}_{ba}, \tag{C11d}$$

where $a \neq b$. We have used the fact that the occupancy matrix are real and symmetric, resulting from the symmetry of the Green's function $\underline{G}(\mathbf{k}, \tau)$ and $\underline{F}(\mathbf{k}, \tau)$. Here, $n^{F,\sigma}$ and $n^{F,\sigma}_{ll'}$ is defined in a similar way as the total filling n and momentum averaged orbital occupancy $n^{\sigma}_{ll'}$.

$$n^{F,\sigma} = \frac{1}{N}\sum_{\mathbf{k},l} n^{F,\sigma}_{ll}(\mathbf{k}) = \sum_{l} n^{F,\sigma}_{ll}. \tag{C12}$$

Next, using the above self-energy $\underline{\Sigma}^{\mathrm{HF}} = \underline{\Sigma}^{\mathrm{HF}}[\underline{n}^{\sigma}]$ and $\underline{\Phi}^{\mathrm{HF}} = \underline{\Phi}^{\mathrm{HF}}[\underline{n}^{F,\sigma}]$ and the Dyson's equation we define the Hartree-Fock Green's function

$$\underline{G}^{\mathrm{HF}}(\mathbf{k}, i\omega_n) = \left\{\left[i\omega_n\mathbb{I} - (\underline{\varepsilon}_{\mathbf{k}} - \mu\mathbb{I}) - \underline{\Sigma}^{\mathrm{HF}}[\underline{n}^{\sigma}]\right] - \underline{\Phi}^{\mathrm{HF}}[\underline{n}^{F,\sigma}]\left[i\omega_n\mathbb{I} + (\underline{\varepsilon}_{\mathbf{k}} - \mu\mathbb{I}) + \underline{\Sigma}^{\mathrm{HF}}[\underline{n}^{\sigma}]\right]^{-1}\underline{\Phi}^{\mathrm{HF}}[\underline{n}^{F,\sigma}]\right\}^{-1}.$$

The subtraction trick gives the self-consistent equation for occupancy matrix $\underline{n}^{\sigma}$ and the chemical potential μ (total $M^2 + 1$ parameters and equations)

$$\underline{n}^{\sigma} = \frac{T}{N}\sum_{\mathbf{k}}\sum_{n=-N_c}^{N_c-1}\left[\underline{G}(\mathbf{k}, i\omega_n) - \underline{G}^{\mathrm{HF}}(\mathbf{k}, i\omega_n; [\underline{n}^{\sigma}, \underline{n}^{F,\sigma}])\right] + \underline{n}^{\sigma,\mathrm{HF}}, \tag{C13a}$$

$$n = 2\sum_{l} n^{\sigma}_{ll}, \tag{C13b}$$

where n is a fixed value for the total filling. Here, $\underline{G}$ is the Green's function from the previous iteration in FLEX calculation and $\underline{n}^{F,\sigma}$ is calculated by the Fourier sum without subtraction. The filling $\underline{n}^{\sigma,\mathrm{HF}}$ can be calculated analytically using Hartree-Fock Green's function. Once the new chemical potential and the Hartree-Fock self-energy is determined, we go to next iteration using $\underline{G}$ to calculate new FLEX self-energy (higher order term), update the FLEX Green's function $\underline{G}$, compare it with the old one, and determine whether the iteration is converged.

The above procedure is very complicated: first, the occupancy matrix and the chemical potential μ are determined by a set of coupled equations; second, to calculate $\underline{n}^{\sigma,\mathrm{HF}}$ analytically using the method of contour integral, one needs to find the poles of Green's function $\underline{G}^{\mathrm{HF}}(\mathbf{k}, i\omega_n)$ at every $\mathbf{k}$ point (i.e., to diagonalize the Hartree-Fock band and it is even more difficulty in the superconducting state). This method is used in Ref. 44. A simpler method[45] is to subtract the $\underline{G}_0$ instead of $\underline{G}^{\mathrm{HF}}$, which is what I have done for one band case.

$$n^{\sigma}_{ll} = \frac{T}{N}\sum_{\mathbf{k}}\sum_{n=-N_c}^{N_c-1}\left[G_{ll}(\mathbf{k}, i\omega_n) - G_{0,ll}(\mathbf{k}, i\omega_n)\right] + n^{\sigma}_{0,ll}, \tag{C14}$$

$$n = 2\sum_{l} n^{\sigma}_{ll}, \tag{C15}$$

The calculation can be simplified with the unitary matrix $u^{\mathbf{k}}_{ln}$ diagonalizing the dispersion $\varepsilon_{\mathbf{k}} = [\varepsilon^{\mathbf{k}}]_{ll'}$. For a unitary matrix $u^{\mathbf{k}}_{ln}$, we have $\sum_n u^{\mathbf{k}}_{ln} u^{*,\mathbf{k}}_{l'n} = \delta_{ll'}$ and $\sum_l u^{*,\mathbf{k}}_{ln'} u^{\mathbf{k}}_{ln} = \delta_{nn'}$. From the diagonalization $\sum_{ll'} u^{*,\mathbf{k}}_{ln} \varepsilon^{\mathbf{k}}_{ll'} u^{\mathbf{k}}_{l'n'} = \xi^{\mathbf{k}}_n \delta_{nn'}$, we find the inverse transformation $\varepsilon^{\mathbf{k}}_{ll'} = \sum_n u^{\mathbf{k}}_{ln} u^{*,\mathbf{k}}_{l'n} \xi^{\mathbf{k}}_n$, and, similarly, the Green's function and orbital occupancy

$$n^{\sigma}_{0,ll'} = \frac{1}{N} \sum_{\mathbf{k}} \sum_n u^{\mathbf{k}}_{ln} u^{*,\mathbf{k}}_{l'n} n_{\mathrm{F}}(\xi^{\mathbf{k}}_n - \mu), \tag{C16}$$

$$G_{0,ll'}(\mathbf{k}, i\omega_n) = \sum_m \frac{u^{\mathbf{k}}_{lm} u^{*,\mathbf{k}}_{l'm}}{i\omega_n - (\xi^{\mathbf{k}}_m - \mu)}, \tag{C17}$$

where $n_{\mathrm{F}}(x) = \frac{1}{e^{x/T}+1}$ is the Fermi distribution function. (Finding the poles of the Hartree-Fock Green's function in normal state is similar to the diagonalization technique used here.) Using the identity $\sum_l |u^{\mathbf{k}}_{ln}|^2 = 1$ for the matrix elements of a unitary matrix, we have the final equation for the chemical potential,

$$n = \frac{2T}{N} \sum_{\mathbf{k}} \sum_{n=-N_c}^{N_c-1} \sum_l \left[G_{ll}(\mathbf{k}, i\omega_n) - \sum_m \frac{|u^{\mathbf{k}}_{lm}|^2}{i\omega_n - (\xi^{\mathbf{k}}_m - \mu)} \right] + \frac{2}{N} \sum_{\mathbf{k}} \sum_l n_{\mathrm{F}}(\xi^{\mathbf{k}}_l - \mu). \tag{C18}$$

The above is the equation used in Ref. 45. The actual unitary matrix is not needed to determine the chemical potential; it is only needed if one wants to also use subtraction method to determine the orbital occupancy for Hartree-Fock self-energy calculation. Interestingly, the only terms in the Hartree-Fock self-energy that cannot be calculated with a simple sum of Green's function with a relatively slower convergence are the terms $\Sigma^{\mathrm{HF}}_{aa} = (2U'-J)\frac{n}{2} + (U-2U'+J) n^{\sigma}_{aa}$. If we make a shift in chemical potential $\mu - \frac{n}{2}(2U'-J) - \frac{1}{2}(U-2U'+J) \to \mu$ and, accordingly, a shift in the Hartree-Fock self-energy $\Sigma^{\mathrm{HF}}_{aa} - \frac{n}{2}(2U'-J) - \frac{1}{2}(U-2U'+J) \to \tilde{\Sigma}^{\mathrm{HF}}_{aa} = (U-2U'+J)(n^{\sigma}_{aa} - \frac{1}{2}) = (U-2U'+J)\frac{T}{N}\sum_{\mathbf{k},n} G_{aa}(\mathbf{k}, i\omega_n)$, which now can be calculated with a simple sum of Green's function, albeit a slower convergence.

A further simplification can be done from Eq. (C18). We replace μ in the term $(\xi^{\mathbf{k}}_l - \mu)$ with a constant μ_0 so that $n = \frac{2}{N}\sum_{\mathbf{k}} \sum_l n_{\mathrm{F}}(\xi^{\mathbf{k}}_l - \mu_0)$. Then the equation for the chemical potential becomes

$$\frac{2T}{N} \sum_{\mathbf{k}} \sum_{n=-N_c}^{N_c-1} \sum_l \left[G_{ll}(\mathbf{k}, i\omega_n; \mu) - \sum_m \frac{|u^{\mathbf{k}}_{lm}|^2}{i\omega_n - (\xi^{\mathbf{k}}_m - \mu_0)} \right] = 0. \tag{C19}$$

Note that only the FLEX Green's function $G_{ll'}(\mathbf{k}, i\omega_n; \mu)$ depends on the chemical potential. The above equation is used Ref. 42. However, we will use a even more simplified form (to avoid diagonalizing the non-interacting band and find the eigen-energies $\xi^{\mathbf{k}}_l$). We replace $(\xi^{\mathbf{k}}_l - \mu)$ with a constant ξ so that $n = \frac{2}{N}\sum_{\mathbf{k}} \sum_l n_{\mathrm{F}}(\xi) = \frac{2M}{e^{\xi/T}+1}$, which gives

$$\xi = T \ln\left(\frac{2M}{n} - 1 \right), \tag{C20}$$

where M is the total number of orbitals. Then the equation for the chemical potential becomes

$$\frac{2T}{N} \sum_{\mathbf{k}} \sum_{n=-N_c}^{N_c-1} \sum_l \left[G_{ll}(\mathbf{k}, i\omega_n; \mu) - \frac{1}{i\omega_n - \xi} \right] = 0. \tag{C21}$$

The above is used by Zhang *et al.* in Ref. 13 and possibly in Ref. 26 and 27 as well. We will use Eq. (C21) in our current code. If needed, the diagonal elements of the orbital occupancy matrix can be calculated using this subtracting method

$$n^{\sigma}_{aa} = \frac{T}{N} \sum_{\mathbf{k}} \sum_{n=-N_c}^{N_c-1} \left[G_{aa}(\mathbf{k}, i\omega_n; \mu) - \frac{1}{i\omega_n - \xi} \right] + n_{\mathrm{F}}(\xi). \tag{C22}$$

We could plug the above into the Hartree-Fock self-energy $\Sigma^{\mathrm{HF}}_{aa} = (2U'-J)\frac{n}{2} + (U-2U'+J) n^{\sigma}_{aa}$; however, since any constant can be shifted into the chemical potential for the diagonal (intra-orbital) Hartree-Fock self-energy, giving a modified Hartree-Fock self-energy $\tilde{\Sigma}^{\mathrm{HF}}_{ab} \to \Sigma^{\mathrm{HF}}_{ab} - c\delta_{ab}$, we can calculate the $\tilde{\Sigma}^{\mathrm{HF}}_{aa} = (U-2U'+J)\frac{T}{N}\sum_{\mathbf{k}} \sum_{n=-N_c}^{N_c-1} G_{aa}(\mathbf{k}, i\omega_n)$ by a simple sum with a finite cut-off N_c, the same as stated before.

Because the term in the intra-orbital Hartree-Fock self-energy due to the discontinuity of the Green's function at $\tau = 0$ is exactly the same for different orbitals [only true for the subtraction scheme in Eq. (C21), not for the subtraction scheme in Eq. (C13), (C18), (C19)] and can be absorbed into the chemical potential, we don't need to

deal with the subtraction to the FLEX Green's function explicitly when calculating the Hartree-Fock self-energy. The subtraction, however, has to be included in the filling calculation. Furthermore, when we forward Fourier transform the Green's function $G_{l_1l_2}:(\mathbf{k},i\omega_n)\to(\mathbf{r},\tau)$ and backward Fourier transform the irreducible susceptibility $\chi^{0,s/c}_{l_1l_2,l_3l_4}:(\mathbf{r},\tau)\to(\mathbf{q},i\nu_m)$ and the self-energy $\Sigma_{l_1l_2}:(\mathbf{r},\tau)\to(\mathbf{k},i\omega_n)$, we need to consider this subtraction carefully so that it gives the required discontinuity at $\tau=0$ for Green's function. (We assume the effective interaction $V^{n/a}_{l_1l_2,l_3l_4}$ excluding the first order Hartree-Fock part has no discontinuity at $\tau=0$.) This issue is discussed in the Appendix D.

Appendix D: Technical details for solving the Eliashberg equation in real space

The advantages of solving the Eliashberg equation in real space $x=(\mathbf{r},\tau)$ are: (i) fast because the FFT (fast Fourier transform) can be used to compute the convolution or cross-correlation over the 4-momentum $k=(\mathbf{k},i\omega_n)$ [or $q=(\mathbf{q},i\nu_m)$] in these equations; (ii) as shown for the singlet state, all propagators are real valued, thus we deal with real signals (in the sense of FFT); (iii) physically, this might be the easiest way to deal with the high frequency tail in the propagators and essentially *eliminate* the high-energy cut-off (strictly speaking, to make the result much less sensitive to the high-energy cut-off since, in reality, a constant high-energy cut-off is still present in the calculation).

As discussed in Appendix C, by a subtraction, the Green's function $\tilde{G}_{l_1l_2}(\mathbf{k},i\omega_n)$ is

$$\tilde{G}_{l_1l_2}(\mathbf{k},i\omega_n)=G_{l_1l_2}(\mathbf{k},i\omega_n)-G^{\xi}_0(\mathbf{k},i\omega_n)\delta_{l_1l_2}=G_{l_1l_2}(\mathbf{k},i\omega_n)-\frac{\delta_{l_1l_2}}{i\omega_n-\xi}, \tag{D1}$$

where $\xi=T\ln\left(\frac{2M}{n}-1\right)$, $\omega_n=(2n+1)\pi T$, $n\in\{-N_c,-N_c+1,\ldots,N_c-1\}$, and $G^{\xi}_0(\mathbf{k},i\omega_n)=(i\omega_n-\xi)^{-1}$. The frequency Fourier transform of $G^{\xi}_0(\mathbf{k},i\omega_n)$ is

$$G^{\xi}_0(\mathbf{k},\tau)=T\sum_{n=-\infty}^{\infty}G^{\xi}_0(\mathbf{k},i\omega_n)e^{-i\omega_n\tau}=T\sum_{n=-\infty}^{\infty}\frac{e^{-i\omega_n\tau}}{i\omega_n-\xi} \tag{D2}$$

$$=-e^{-\tau\xi}[\theta(\tau)-n_{\mathrm{F}}(\xi)] \tag{D3}$$

$$=\begin{cases}-\frac{e^{(\beta-\tau)\xi}}{e^{\beta\xi}+1}, & (\tau>0),\\ n_{\mathrm{F}}(\xi)-\frac{1}{2}, & (\tau=0),\\ \frac{e^{-\tau\xi}}{e^{\beta\xi}+1}. & (\tau<0),\end{cases} \tag{D4}$$

Here $\beta=1/T$. Since any Greens's function satisfies the relation $G(\mathbf{k},\tau)=-G(\mathbf{k},\tau+\beta)$ for $\beta<\tau<0$, we only discuss $G(\mathbf{k},\tau>0)$ from now on. The momentum Fourier transform of $G^{\xi}_0(\mathbf{k},\tau>0)$ is

$$G^{\xi}_0(\mathbf{r},\tau>0)=\frac{1}{N}\sum_{\mathbf{k}}G^{\xi}_0(\mathbf{k},\tau>0)e^{-i\mathbf{k}\cdot\mathbf{r}}=-\frac{e^{(\beta-\tau)\xi}}{e^{\beta\xi}+1}\delta_{\mathbf{r},\mathbf{0}}. \tag{D5}$$

Therefore, the Fourier transform of FLEX Green's function is

$$G_{l_1l_2}(\mathbf{r},\tau>0)=\frac{T}{N}\sum_{\mathbf{k}}\sum_{n=N_c}^{N_c-1}\tilde{G}_{l_1l_2}(\mathbf{k},i\omega_n)e^{-i(\mathbf{k}\cdot\mathbf{r}+\omega_n\tau)}-\frac{e^{(\beta-\tau)\xi}}{e^{\beta\xi}+1}\delta_{\mathbf{r},\mathbf{0}}\delta_{l_1l_2}. \tag{D6}$$

Apparently, we have

$$G_{l_1l_2}(\mathbf{r},\tau=0^+)-G_{l_1l_2}(\mathbf{r},\tau=0^-)=-\delta_{\mathbf{r},\mathbf{0}}\delta_{l_1l_2}. \tag{D7}$$

In numerical calculations, the interval $0<\tau<\beta$ is discretized as $\tau_n=(n-1)\frac{\beta}{2N_c}+0^+\delta_{n,1}$ for $n\in\{1,2,\ldots,2N_c\}$, where the first term is understood as $\tau_1=0^+$. All $N\times(2N_c)$ data points on the space-time grid $(\mathbf{r},\tau_n)$ can be found using the FFT algorithm twice (one for space and the other for time). Since $G_{l_2l_1}=G_{l_1l_2}$, we only need to do this for $M(M+1)/2$ matrix elements in orbital space (in fact, we only store this many matrix elements). Since $\underline{G}(\mathbf{r},\tau)$ is real, all imaginary part due to numerical accuracy in the FFT will be removed before we calculate the susceptibilities. Similarly, $\underline{F}(\mathbf{r},\tau)$ is also obtained by the FFT and no subtraction is needed.

The irreducible spin and charge susceptibilities

$$\chi^{0,s}_{l_1l_2,l_3l_4}(q)=-\frac{T}{N}\sum_k[G_{l_1l_3}(k+q)G_{l_4l_2}(k)+F_{l_1l_4}(k+q)F^*_{l_3l_2}(k)],$$

$$\chi^{0,c}_{l_1l_2,l_3l_4}(q)=-\frac{T}{N}\sum_k[G_{l_1l_3}(k+q)G_{l_4l_2}(k)-F_{l_1l_4}(k+q)F^*_{l_3l_2}(k)],$$

can now be calculated in real space using $\underline{G}(\mathbf{r},\tau)$ and $\underline{F}(\mathbf{r},\tau)$ as follows

$$\begin{aligned}\chi^{0,s}_{l_1l_2,l_3l_4}(\mathbf{r},\tau) &= -G_{l_1l_3}(\mathbf{r},\tau)G_{l_4l_2}(\mathbf{r},-\tau) - F_{l_1l_4}(\mathbf{r},\tau)F_{l_3l_2}(\mathbf{r},\tau)\\ &= G_{l_1l_3}(\mathbf{r},\tau)G_{l_4l_2}(\mathbf{r},\beta-\tau) - F_{l_1l_4}(\mathbf{r},\tau)F_{l_3l_2}(\mathbf{r},\tau), \quad \text{(D9a)}\\ \chi^{0,c}_{l_1l_2,l_3l_4}(\mathbf{r},\tau) &= -G_{l_1l_3}(\mathbf{r},\tau)G_{l_4l_2}(\mathbf{r},-\tau) + F_{l_1l_4}(\mathbf{r},\tau)F_{l_3l_2}(\mathbf{r},\tau)\\ &= G_{l_1l_3}(\mathbf{r},\tau)G_{l_4l_2}(\mathbf{r},\beta-\tau) + F_{l_1l_4}(\mathbf{r},\tau)F_{l_3l_2}(\mathbf{r},\tau). \quad \text{(D9b)}\end{aligned}$$

We change the variable $-\tau \to \beta-\tau$ because we only store the data on the time grid $0 < \tau_n = (n-1)\frac{\beta}{2N_c} + 0^+\delta_{n,1} < \beta$ for $n \in \{1,2,\ldots,2N_c\}$. The inversion symmetry $G_{l_1l_2}(-\mathbf{r},\tau) = G_{l_1l_2}(\mathbf{r},\tau)$ and the property that $\underline{G}(\mathbf{r},\tau)$ and $\underline{F}(\mathbf{r},\tau)$ are real have been used to obtain the above equations. Furthermore, at $\tau_{n=1} = 0^+$, the above formulae use the term $G_{l_1l_2}(\mathbf{r},\beta^-)$ not included in the FFT grid, which can be obtained from the relation

$$G_{l_1l_2}(\mathbf{r},\beta^-) = -G_{l_1l_2}(\mathbf{r},0^-) = -G_{l_1l_2}(\mathbf{r},0^+) - \delta_{\mathbf{r},\mathbf{0}}\delta_{l_1l_2}. \quad \text{(D10)}$$

Since $G_{l_1l_2}(\mathbf{r},\tau) = G_{l_2l_1}(\mathbf{r},\tau)$, we can easily show that

$$\chi^{0,s}_{l_1l_2,l_3l_4}(\mathbf{r},\tau) = \chi^{0,s}_{l_3l_4,l_1l_2}(\mathbf{r},\tau), \quad \text{(D11a)}$$
$$\chi^{0,c}_{l_1l_2,l_3l_4}(\mathbf{r},\tau) = \chi^{0,c}_{l_3l_4,l_1l_2}(\mathbf{r},\tau). \quad \text{(D11b)}$$

Therefore, we only store $M^2(M^2+1)/2$ matrix elements of the $M^2\times M^2$-dimension matrix $\chi^{0,s/c}_{l_1l_2,l_3l_4}(\mathbf{r},\tau)$. Furthermore, $F_{l_1l_2}(\mathbf{r},\tau) = F_{l_2l_1}(\mathbf{r},-\tau) = F_{l_1l_2}(-\mathbf{r},-\tau)$, we can easily show that

$$\chi^{0,s}_{l_1l_2,l_3l_4}(\mathbf{r},\tau) = \chi^{0,s}_{l_4l_3,l_2l_1}(-\mathbf{r},-\tau), \quad \text{(D12a)}$$
$$\chi^{0,c}_{l_1l_2,l_3l_4}(\mathbf{r},\tau) = \chi^{0,c}_{l_4l_3,l_2l_1}(-\mathbf{r},-\tau). \quad \text{(D12b)}$$

The above relations, together with $U^{s/c}_{l_1l_2,l_3l_4} = U^{s/c}_{l_3l_4,l_1l_2} = U^{s/c}_{l_4l_3,l_2l_1}$, indicate that

$$\chi^{p}_{l_1l_2,l_3l_4}(q) = \chi^{p}_{l_3l_4,l_1l_2}(q), \quad \text{(D13a)}$$
$$\chi^{p}_{l_1l_2,l_3l_4}(q) = \chi^{p}_{l_4l_3,l_2l_1}(-q), \quad \text{(D13b)}$$
$$V^{p}_{l_1l_2,l_3l_4}(q) = V^{p}_{l_3l_4,l_1l_2}(q), \quad \text{(D13c)}$$
$$V^{p}_{l_1l_2,l_3l_4}(q) = V^{p}_{l_4l_3,l_2l_1}(-q), \quad \text{(D13d)}$$

where $p = 0, s$ $(0, c)$ for irreducible spin (charge) susceptibility, $p = s$ (c) for RPA spin (charge) susceptibility, and $p = n$ (a) for the effective interaction for the normal (anomalous) self-energy. Here, $q = (\mathbf{q}, i\nu_m)$. We show the proof of the relation for RPA spin (charge) susceptibility $\chi^{s/c}_{l_1l_2,l_3l_4}(q) = \chi^{s/c}_{l_4l_3,l_2l_1}(-q)$ in the appendix. The last two equations lead to

$$V^{p}_{l_1l_2,l_3l_4}(x) = V^{p}_{l_3l_4,l_1l_2}(x), \quad \text{(D14a)}$$
$$V^{p}_{l_1l_2,l_3l_4}(x) = V^{p}_{l_4l_3,l_2l_1}(-x), \quad \text{(D14b)}$$

where $x = (\mathbf{r},\tau)$. Both $\underline{G}(\mathbf{r},\tau)$ and $\underline{F}(\mathbf{r},\tau)$ being real leads to

$$[\underline{\chi}^p(q)]^* = \underline{\chi}^p(-q), \quad \text{(D15a)}$$
$$[\underline{V}^p(q)]^* = \underline{V}^p(-q). \quad \text{(D15b)}$$

The last equation leads to $\underline{V}^p(x) \in \mathbb{R}$.

The RPA susceptibilities takes a simple form only in $(\mathbf{q}, i\nu_m)$ space ($\nu_m = 2m\pi T$, $m \in \{-N_c, -N_c+1, \ldots, N_c-1\}$), so we first backward Fourier transform the irreducible spin and charge susceptibilities from $(\mathbf{r},\tau)$ to $(\mathbf{q}, i\nu_m)$ space using the Eq. (A2) from Appendix A. To use this formula (works for both fermionic and bosonic Matsubara frequencies), we need the difference $\chi^{0,s/c}_{l_1l_2,l_3l_4}(\mathbf{r},0^+) - \chi^{0,s/c}_{l_1l_2,l_3l_4}(\mathbf{r},0^-)$. It is easy to show that

$$\begin{aligned}V^{\chi}_{l_1l_2,l_3l_4} &= \chi^{0,s}_{l_1l_2,l_3l_4}(\mathbf{r},0^+) - \chi^{0,s}_{l_1l_2,l_3l_4}(\mathbf{r},0^-)\\ &= \chi^{0,c}_{l_1l_2,l_3l_4}(\mathbf{r},0^+) - \chi^{0,c}_{l_1l_2,l_3l_4}(\mathbf{r},0^-)\\ &= \delta_{\mathbf{r},\mathbf{0}}\left[-G_{l_1l_3}(\mathbf{0},0^+)\delta_{l_4l_2} + \delta_{l_1l_3}G_{l_4l_2}(\mathbf{0},0^+)\right]. \quad \text{(D16)}\end{aligned}$$

After $\chi^{0,s/c}_{l_1l_2,l_3l_4}(q)$ are calculated by the backward FFT of $\chi^{0,s/c}_{l_1l_2,l_3l_4}(\mathbf{r},\tau)$, the effective interactions are calculated from Eq. (78) (excluding the Hartree-Fock part that has already been calculated). Then, self-energies are given by Eq. (79)

$$\Sigma_{lm}(k) = \frac{T}{N}\sum_q \sum_{l'm'} V^n_{ll',mm'}(q) G_{l'm'}(k-q),$$
$$\Phi_{lm}(k) = \frac{T}{N}\sum_q \sum_{l'm'} V^a_{ll',m'm}(q) F_{l'm'}(k-q),$$

which can again be calculated in real space using as follows

$$\Sigma_{lm}(\mathbf{r},\tau) = \sum_{l'm'} V^n_{ll',mm'}(\mathbf{r},\tau) G_{l'm'}(\mathbf{r},\tau), \tag{D18a}$$
$$\Phi_{lm}(\mathbf{r},\tau) = \sum_{l'm'} V^a_{ll',m'm}(\mathbf{r},\tau) F_{l'm'}(\mathbf{r},\tau), \tag{D18b}$$

where $V^n_{l_1l_2,l_3l_4}(\mathbf{r},\tau)$ and $V^a_{l_1l_2,l_3l_4}(\mathbf{r},\tau)$ are obtained by the forward Fourier transform of $V^n_{l_1l_2,l_3l_4}(q)$ and $V^a_{l_1l_2,l_3l_4}(q)$ (excluding the Hartree-Fock part), unlike that of Green's function $G_{l_1l_2}(k)$, with out any subtraction. It is easy to show $\underline{\Sigma}^t(x) = \underline{\Sigma}(x)$ and $\underline{\Phi}^t(x) = \underline{\Phi}(-x)$ using the relations $\underline{G}^t(x) = \underline{G}(x)$, $\underline{F}^t(x) = \underline{F}(-x)$, and $V^p_{l_1l_2,l_3l_4}(x) = V^p_{l_3l_4,l_1l_2}(x) = V^p_{l_4l_3,l_2l_1}(-x)$; as a result, $\underline{\Sigma}^t(k) = \underline{\Sigma}(k)$ and $\underline{\Phi}^\dagger(k) = \underline{\Phi}(k)$. This is consistent with the result from Dyson's equation. Therefore, these symmetry relations persist in every iteration of the calculation and we only need to store a half of the matrix elements of the self-energies in the orbital space.

The final step is to backward Fourier transform Σ_{lm} and Φ_{lm} from $(\mathbf{r},\tau)$ to $(\mathbf{k},i\omega_n)$ and add in the corresponding Hartree-Fock terms. We need the difference $\Sigma_{lm}(\mathbf{r},0^+) - \Sigma_{lm}(\mathbf{r},0^+)$.

$$\begin{aligned} V^\Sigma_{lm} &= \Sigma_{lm}(\mathbf{r},0^+) - \Sigma_{lm}(\mathbf{r},0^+) \\ &= \sum_{l'm'} V^n_{ll',mm'}(\mathbf{r},0)[G_{l'm'}(\mathbf{r},0^+) - G_{l'm'}(\mathbf{r},0^-)] \\ &= -\sum_{l'm'} V^n_{ll',mm'}(\mathbf{r},0)\delta_{\mathbf{r},\mathbf{0}}\delta_{l'm'} \\ &= -\delta_{\mathbf{r},\mathbf{0}} \sum_j V^n_{lj,mj}(\mathbf{0},0). \end{aligned} \tag{D19}$$

Last, use $\underline{\Sigma}(k) + \underline{\Sigma}^{\mathrm{HF}}(k)$ and $\underline{\Phi}(k) + \underline{\Phi}^{\mathrm{HF}}(k)$ and the Dyson's equation to find the new Green's function and a new chemical potential. Note that the Dyson's equation has to be solved for every trial chemical potential until Eq. (C21) for a fixed filling is satisfied. Then, we repeat until the difference of self-energies between consecutive iterations is smaller than an error threshold. A flowchart for the FLEX calculation procedures is shown in Fig. 20.

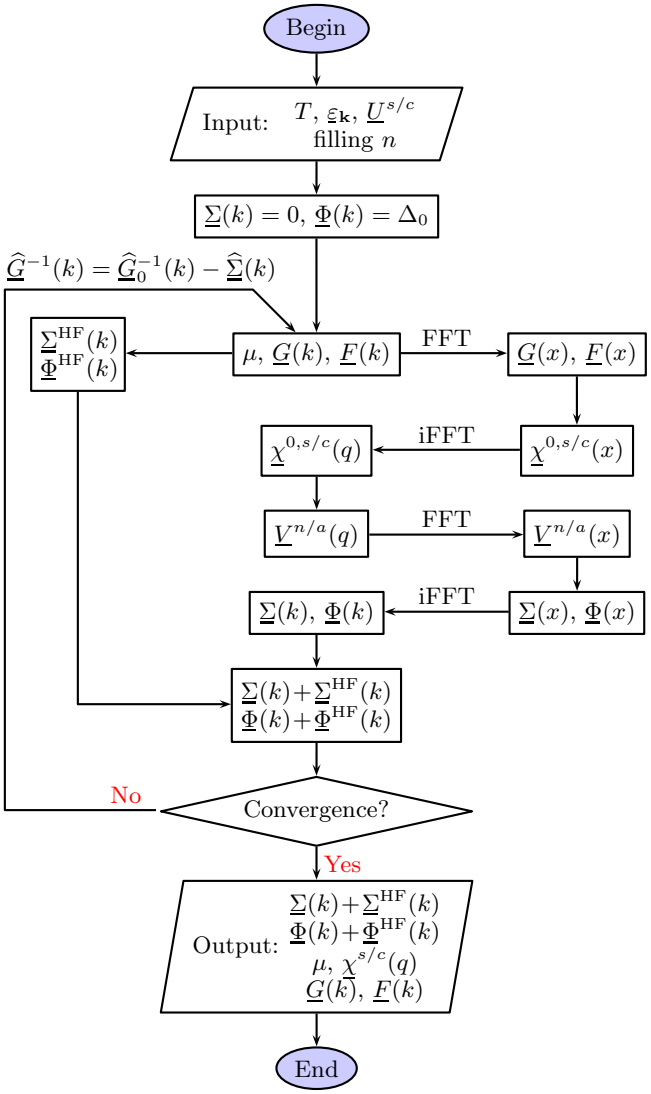

FIG. 20. A flowchart for the FLEX calculation procedures. The underscore $\underline{\ }$ denotes the whole matrix in the orbital space. The caret $\widehat{\ }$ denotes the whole matrix in the Nambu space. The Dyson's equation $\widehat{\underline{G}}^{-1}(k)=\widehat{\underline{G}}_0^{-1}(k)-\widehat{\underline{\Sigma}}(k)$ must be solved in product space. The momentum $k=(\mathbf{k},i\omega_n)$ and $q=(\mathbf{q},i\omega_n)$ and the coordinate $x=(\mathbf{r},\tau)$. The fast Fourier transform (FFT, forward) and the inverse FFT (iFFT, backward) are used to speed up the whole calculation. Note that the forward and backward Fourier transforms are defined in an opposite way that is used in signal analysis.

[1] N. E. Bickers, D. J. Scalapino, and S. R. White, Phys. Rev. Lett. **62**, 961 (1989).
[2] N. Bickers and D. Scalapino, Ann. Phys. **193**, 206 (1989).
[3] J. W. Serene and D. W. Hess, Phys. Rev. B **44**, 3391 (1991).
[4] N. E. Bickers and S. R. White, Phys. Rev. B **43**, 8044 (1991).
[5] C.-H. Pao and N. E. Bickers, Phys. Rev. Lett. **72**, 1870 (1994).
[6] P. Monthoux and D. J. Scalapino, Phys. Rev. Lett. **72**, 1874 (1994).
[7] J. Schmalian, Phys. Rev. Lett. **81**, 4232 (1998).
[8] T. Takimoto, T. Hotta, and K. Ueda, Phys. Rev. B **69**, 104504 (2004).
[9] K. Kubo, Phys. Rev. B **75**, 224509 (2007).
[10] J. W. Serene and D. W. Hess, "Massively-parallel realizations of self-consistent perturbation theories," in *Recent Progress in Many-Body Theories: Volume 3*, edited by T. L. Ainsworth, C. E. Campbell, B. E. Clements, and E. Krotscheck (Springer US, Boston, MA, 1992) pp. 469–479.
[11] J. J. Deisz, D. W. Hess, and J. W. Serene, "Improved treatment of frequency sums in propagator-renormalized perturbation theories," in *Recent Progress in Many-Body Theories: Volume 4*, edited by E. Schachinger, H. Mitter, and H. Sormann (Springer US, Boston, MA, 1995) pp. 433–441.
[12] J. Schmalian, M. Langer, S. Grabowski, and K. Bennemann, Comput. Phys. Commun. **93**, 141 (1996).
[13] J. Zhang, *Theory of spin-fluctuation induced superconductivity in iron-based superconductors*, Ph.D. thesis, Iowa State University (2011).
[14] H. J. Vidberg and J. W. Serene, J. Low Temp. Phys. **29**, 179 (1977).
[15] N. Bulut and D. J. Scalapino, Phys. Rev. B **45**, 2371 (1992).
[16] N. Bulut and D. J. Scalapino, Phys. Rev. B **47**, 3419 (1993).
[17] N. Bulut and D. J. Scalapino, Phys. Rev. B **50**, 16078 (1994).
[18] H.-R. Fang and Y. Saad, Numer. Linear Algebra Appl. **16**, 197 (2009).
[19] H. F. Walker and P. Ni, SIAM J. Numer. Anal. **49**, 1715 (2011).
[20] N. Bulut, D. W. Hone, D. J. Scalapino, and N. E. Bickers, Phys. Rev. B **41**, 1797 (1990).
[21] Y. Vilk and A.-M. Tremblay, J. Phys. I France **7**, 1309 (1997).
[22] A.-M. S. Tremblay, in *Strongly Correlated Systems: Theoretical Methods* (Springer, 2012) pp. 409–453.
[23] J. M. Tranquada, in *Handbook of High-Temperature Superconductivity: Theory and Experiment*, edited by J. R. Schrieffer and J. S. Brooks (Springer New York, New York, NY, 2007) pp. 257–298.
[24] N. B. Christensen, D. F. McMorrow, H. M. Rønnow, B. Lake, S. M. Hayden, G. Aeppli, T. G. Perring, M. Mangkorntong, M. Nohara, and H. Takagi, Phys. Rev. Lett. **93**, 147002 (2004).
[25] K. Yada and H. Kontani, J. Phys. Soc. Jpn. **74**, 2161 (2005).
[26] J. Zhang, R. Sknepnek, R. M. Fernandes, and J. Schmalian, Phys. Rev. B **79**, 220502 (2009).
[27] J. Zhang, R. Sknepnek, and J. Schmalian, Phys. Rev. B **82**, 134527 (2010).
[28] Typos in these references I have found: (i) Ref. 8, Eq. (40) and (41), U and χ switch order in the brackets; Eq. (35) and (36), $k-q \to k+q$. (ii) Ref. 25, Eq. (4) and (5), S/C and χ switch order in the brackets; Eq. (6), it should be $G_{l_1 l_3} G_{l_4 l_2}$. (iii) Ref. 27, Eq. (4) $\chi^{ab,a'b'} \to \chi^{ba,a'b'}$.
[29] This is the completeness relation of Pauli matrices, which can be verified directly for all of the 16 components. Alternatively, it can be proved using the *great orthogonality theorem* in group theory because $\{\pm\sigma_0, \pm i\sigma_1, \pm i\sigma_2, \pm i\sigma_3\}$ is the two-dimensional irreducible representation of the quaternion group.
[30] K. Kuroki, S. Onari, R. Arita, H. Usui, Y. Tanaka, H. Kontani, and H. Aoki, Phys. Rev. Lett. **101**, 087004 (2008).
[31] S. Graser, T. A. Maier, P. J. Hirschfeld, and D. J. Scalapino, New J. Phys. **11**, 025016 (2009).
[32] K. Kuroki and R. Arita, Phys. Rev. B **64**, 024501 (2001).
[33] D. J. Scalapino, Rev. Mod. Phys. **84**, 1383 (2012).
[34] K. Kuroki, T. Kimura, and R. Arita, Phys. Rev. B **66**, 184508 (2002).
[35] W. Lv, A. Moreo, and E. Dagotto, Phys. Rev. B **88**, 094508 (2013).
[36] L. Filon, Proc. Roy. Soc. Edinburgh Sect. A **49**, 38 (1928).
[37] P. J. Davis and P. Rabinowitz, *Methods of Numerical Integration*, 2nd ed. (Dover, 2007).
[38] W. Press, S. Teukolsky, W. Vetterling, and B. Flannery, *Numerical Recipes in Fortran* (Cambridge U. P., 1992).
[39] D. Sprung, M. Betti, and W. van Dijk, Comput. Phys. Commun. **184**, 607 (2013).
[40] M. Abramowitz and I. A. Stegun, eds., *Handbook of Mathematical Functions with Formulas, Graphs, and Mathematical Tables*, 10th ed., Applied Mathematics Series 55 (National Bureau of Standards, 1972).
[41] The formula given in *Abramowitz & Stegun* has an interesting footnote that says "For certain difficulties associated with this formula, see the article by J. W. Tukey.[46]" On the referenced page in John Tukey's article is a discussion on *aliasing*.
[42] D. Bergeron, V. Hankevych, B. Kyung, and A.-M. S. Tremblay, Phys. Rev. B **84**, 085128 (2011).
[43] For a unit cell with a basis, to assure each element in the orbital space is even under the inversion, it also requires that each orbital is mapped to itself under the inversion. Otherwise, the use of inversion symmetry is more complicated. Also, we assume that only the hoppings between orbitals of the same parity are allowed.
[44] G. Esirgen and N. E. Bickers, Phys. Rev. B **55**, 2122 (1997).
[45] H. Ikeda, R. Arita, and J. Kuneš, Phys. Rev. B **81**, 054502 (2010).
[46] J. W. Tukey, in *On Numerical Approximation*, edited by R. E. Langer (Univ. Wisconsin Press, Madison, 1959).